CRANFIELD UNIVERSITY

NIGEL A. LEGRAVE

Deposition onto Heat Exchanger Surfaces from the Co-firing of Coal & Biomass

SCHOOL OF APPLIED SCIENCES

MSc (By Research) THESIS

CRANFIELD UNIVERSITY

SCHOOL OF APPLIED SCIENCES

MSc (By Research) THESIS

Academic Year 2011-2012

NIGEL A. LEGRAVE

Deposition onto Heat Exchanger Surfaces from the Co-firing of Coal & Biomass

Supervisors **Dr Nigel J Simms**
Dr Paul Kilgallon
Subject Advisor **Dr Raffaella Villa**

December 2011

This thesis is submitted in partial fulfilment of the requirements for the degree of Master of Science

Executive summary

In the latter part of the 20th century, there has been a continuing global concern of the consumption of fossil fuels used in power production. There is further concern of the gaseous emissions that are created from this consumption and an awareness of climbing carbon dioxide (CO_2) levels that are exhausted into the atmosphere.

The concept of co-firing fossil fuel with varying levels of biomass species is not new but there is a requirement to explore its applications further in the interests of both the environment and power production. With dwindling fossil fuel resources, co-firing with biomass is a logical step forward as biomass is a generally a renewable product – whereas fossil fuels are not. More importantly, the study of effects of burning higher biomass percentages on the heat exchanger matrix of power plants requires more attention. This has been explored before in other studies that have resulted in inefficiencies within the power generation plant.

The main of objectives of this research were to: co-fire coal with biomass over a wide range of mixes within a combustion environment; monitor the gaseous emissions and capture and analyse the deposits that are formed on deposit capture probes.

The analysis of data obtained will enabled further research to be carried out and model deposit flux behaviour of simulated heat exchanger models and materials in the future.

Acknowledgements

I wish to express my sincere thanks and appreciation to the following people who have given me assistance, having the faith in me and who have been a source of inspiration throughout this period of my research:

Dr Nigel Simms – Principle Research Fellow and Supervisor (Centre for Energy & Resource Technology, Cranfield University)

Dr Paul Kilgallon – Senior Engineer, Doosan Babcock (former Research Fellow and Supervisor at Cranfield University)

Dr Raffaella Villa – Lecturer in Bioprocess Technology – Subject Advisor

Dr Kate Coleman – former Centre for Energy & Resource Technology's PhD student for giving me guidance in certain aspects of my research.

Brian Carpenter (BSc) – the centre's engineering contractor for reaching parts that other technicians' cannot reach regarding the 'black arts' of electronics.

Dr Ala Khodier - a former Centre for Energy & Resource Technology's PhD student , work colleague and a good friend who spent many hours with me by carrying trial work on the Combustion Rig experiments and having our in-depth conversations pondering the mysteries life, the universe and everything.

My family who has been a source of support and understanding- especially my dear partner, Ruth.

In honour of David Clarke, former engineering teacher (1988), Homefield School, Christchurch, Dorset, – a major influence on my career .

In memory of my late father, Raymond.

Nigel Alec Legrave (aka: Buzz)
Senior Technical Officer
Centre for Energy & Resource Technology
Cranfield University

December 2011

"Scientists explore nature in order to discover general principles.

Engineers apply established principles drawn from mathematics and science in order to develop economical solutions to technical problems"

Samuel Florman – "The Civilized Engineer"

"Engineering isn't about perfect solutions; its doing the best you can with limited resources."

Dr Randy Pausch- "The Last Lecture"

Ex hypothesi et ex mea sentential.....

Per Ardua ad Astra

Contents ***Page no***

NOTATION

The following abbreviations have been used throughout this work. All have relevance in both the engineering and scientific community:

ar	as received
CAD	Computer Aided Design
CCP	Cereal Co-product
CERT	Centre for Energy and Research Technology
daf	Dry ash free
Dims	dimensions
FBC	Fluidised Bed Combustion
FTIR	Fourier Transform Infrared Spectroscopy
G A	General Assembly (refers to engineering assembly drawings)
HHV	High Heating Value
ID	Internal diameter (can be designated as IØ)
IPCC	Intergovernmental Panel on Climate Change
LHV	Low Heating Value
Lim	detection Limit
Msr	Measured
NB	Nominal Bore
ND	Not determined
OD	Outside diameter (can be designated as OØ)
Pa	Proximate analysis
PF	Pulverised Fuel
SEM	Scanning Electron Microscope
SRF	Short-rotation energy forest
SS	stainless steel
ua	Ultimate analysis
SI	Standard Units

1 Introduction

1.1 Background

Since the conception of the Industrial Revolution of the 18th century, the use of fossil fuels have been exploited at an alarming rate. In the late 20th and early 21st centuries, that there is a realisation that these resources are dwindling and being exploited further with the rapid expansion of developing industrialised countries like China and India. To this end, there are concerns that the once plentiful supplies in certain parts of the globe are drying up and more difficult and challenging reserves are having to be procured.

The rate of consumption of fossil fuels has been further emphasised with major environmental concerns of the emissions they produce that are exhausted into the atmosphere.. Environmental studies show the continuing use of fossil fuels are contributing to the increase of carbon dioxide (CO_2) levels in the atmosphere. This then drives the continuing debate relating to Global Warming. Other gaseous emissions also contribute towards these levels, eg: methane and nitrous oxide species.

The use of biomass has accelerated over the last 10 to 20 years. The main issues being increased energy requirements accompanying the constant need to drive down the CO_2 emissions that have been alleged to increase global warming. As biomass is CO_2 neutral and renewable, the energy in some species can be used as an on its own or alongside to fossil fuels.

However, the use of biomass fuels has its own issues from a mechanical perspective. It have been proved in other research eg: Coleman (2008) that various parts of the combustion plant can suffer from corrosion; eg: the heat

exchanger matrixes. Fouling of the units can also lead to inefficiencies, which can lead onto further failures of materials and plant. By monitoring the deposits that are formed on such surfaces, the levels of deposition can be measured and calculations of possible failure and inefficiency can be modelled. This information can be passed on to other levels of research in this field.

Other issues relating to the use of biomass that have to be taken into consideration are, for example, the use of land that is employed to grow such energy crops instead of food. The continued emission targets that are set by the EU and the UK's fulfilment of the Kyoto Protocol are driving this type of research and use of biomass fuels forward.

1.2 Aims

The overall aim of this MSc is to generate data from the co-firing of coal and a biomass (as a single fuel and at varying blends). This will include, deposit structure, gas emissions and the calculation of deposition flux data that will be used with future studies.

1.3 Objectives

The specific objectives for this work will include:

- Carry out the studies utilising the pilot scale combustion unit – known as a Multi-fuel combustion rig at the Centre of Energy and Resource Technology (CERT), Cranfield University.
- Investigate the optimum feed system for delivery of the coal and biomass blends into the Multi-fuel combustion rig.

- Combust fuel blends in the Multi-fuel combustion rig aiming for an overall temperature of ~ 800 °C.
- Collect deposits on three, air cooled deposition probes that will have surface temperatures of ~500, 600 and 700 °C respectively. (This is to simulate conditions within a heat exchanger fuel fired boiler environments).
- Record gas emissions data during an experimental run data utilising a Fourier Transform Infra-Red (FTIR) gas analyser unit. The data will include CO, CO_2, O_2, H_2O, SO_2 NO_x and HCl.
- Observe and record the deposit formation on the air cooled deposition probes following the experimental runs.
- From each experimental run, remove the resultant deposits from specific areas of each probe, weigh and analyse utilising Scanning Electron Microscope (SEM) Energy Dispersive X-Ray (EDX).
- Calculate deposition fluxes for each test so that this data may be used in future work .
- Report on further recommendations for future work

This research work has been funded by a number of projects that have included Supergen Bio Energy, Supergen Plant Life Extension and a part of DTI Corrosion Modelling contract (now know as DBEER).

2. Literature Review

2.1 Introduction

This Literature Review summarises current knowledge in the distinct topics covered during the course of this thesis :

- Fuel characterisation
- Coal formation and classifications
- Biomass structures, applications and analysis
- Ash structure and analysis
- Deposit formation mechanisms
- Application of industrial and research deposit probes
- Heat Transfer calculations
- Deposit probes utilised in other industrial research

2.2 Fuel characterisation

The Energy Centre of the Netherlands (ECN) are one of the many providers of information to a wide range of fuels. This information is provided on the 'Phyllis' database. The information is provided is a number of forms. This information for the coal and biomass fuels is produced in the following way; calorific value (CV), ash content, moisture, chemical composition and volatiles. There are two ways in which this is carried out:

- Proximate analysis
- Ultimate analysis

2.2.1 Proximate analysis

Proximate analysis from ECN provides the ash and moisture content, volatiles and fixed carbon. The ash content is expressed in weight (wt %) on a dry basis and on a as received (ar) material. The ash content of a fuel is derived from the moisture content.

Therefore, ECN states that:

Ash content (wt %) dry =

ash content (wt % ar) x 100/100 – moisture content (wt%) [1]

The moisture content in expressed in (wt %) on a wet basis (ar). ECN state that there can be a large difference between the fuel as it is available and at the moment of its analysis.

The volatiles and fixed carbon levels are determined via standard methods (see Appendix). The volatiles is expressed in (wt %) - dry material, ar , dry and dry ash free (daf). The fixed carbon levels are calculated in the remaining part via the same standardised method. The formula used is:

dry: fixed C* = 100 – ash(dry)-volatiles (dry) [2]

daf : fixed C* = 100-volatiles (DAF) [3]

ar : fixed C *= 100-ash-$H_20^{\#}$ – volatiles [4]

(C* - carbon; $H_2O^{\#}$ – water)

Tables 2.3 and 2.5 give examples of Proximate Analysis that has been carried out on both coal and biomass feedstocks.

2.2.2 Ultimate Analysis

ECN present this information from the chemical composition and CV. The major elements are given as well as information previously found via proximate analysis. The elements presented are carbon (C), hydrogen (H), oxygen (O), nitrogen (N), sulphur (S), chlorine (Cl), fluorine (F) and bromine (Br). The other definitions remain the same; ie: ar, dry, daf and are all expressed as (wt %).

The formula that ECN utilise are:

dry : $C + H + O + N + S + Cl + F + Br + ash = 100$ [5]

daf: $C + H + O + N + S + Cl + F + Br = 100$ [6]

ar: $C + H + O + N + S + Cl + F + Br + ash + H_20 = 100$ [7]

ECN state that in some examples, the oxygen content is not a measured parameter. This is due experimental errors in the analysis. It is also stated in the analysis whether each chemical element is measured or calculated.

2.2.3 Calorific value

The units for Calorific value (CV) are kJ/kg. It is expressed as a Higher Heating Value (HHV) and a Lower Heating Value (LHV). The difference is caused by heat applied for the evaporation of water from the hydrogen in the material and the moisture.

It is determined that the CV gives the result of the HHV. A comparison is also calculated from the elemental composition:

$$HHV_{Milne} = 0.341 \cdot C + 1.322 \cdot H - 0.12 \cdot O - 0.12 \cdot N + 0.0686 \cdot S - 0.0153 \cdot ash \quad [8]$$

Tables 2.4 and 2.6 give examples of Ultimate Analysis that has been carried out on Daw Mill and Miscanthus (*Giganteus*) feedstock.

2.3 Coal formation

Coal is a fuel that society has utilised for thousands of years. Salway (2001) identifies its first uses as far back as the Bronze Age. This type of coal was known as 'outcrop' coal. However, coal formation began during the Carboniferous Period, approximately 360BC to 290BC million years ago. Jones *et.al,* (1964) identifies coal as a naturally occurring substance that is the fossilised remains of plant matter from the Carboniferous Period that has undergone various chemical and physical changes. Figure 2.1 illustrates these changes.

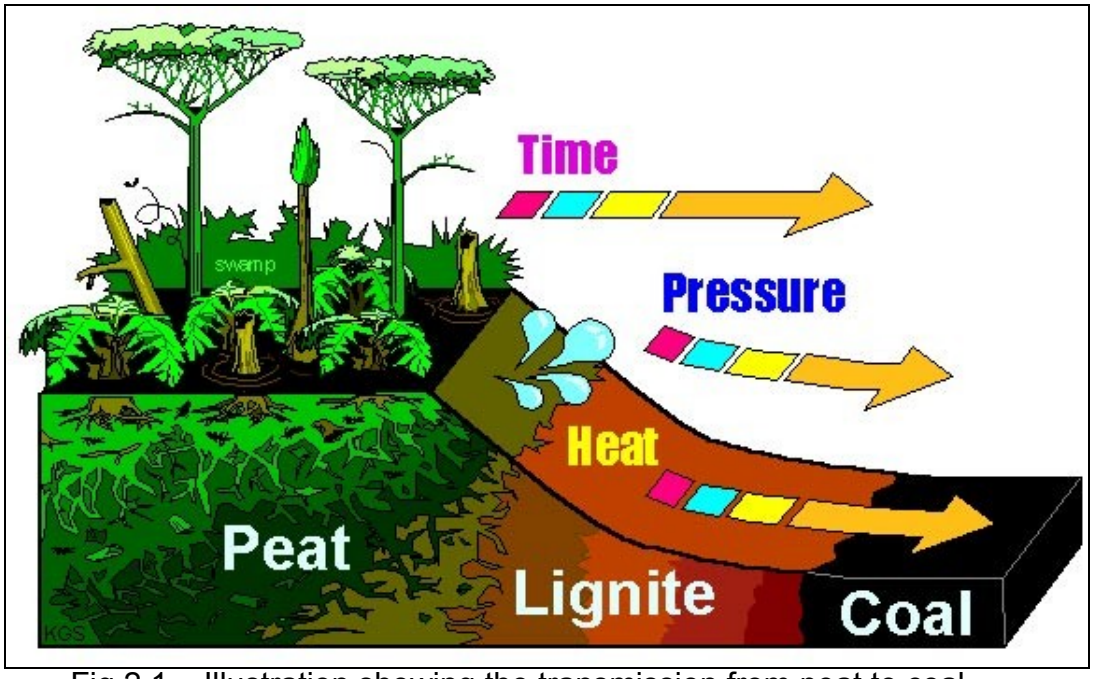

Fig 2.1 – Illustration showing the transmission from peat to coal

ucsusa.org/clean_energy/impacts

Venables (2008) explains that the quality of each coal deposit is determined by pressure and temperature and the length of time spent in its formation. It is also dependant on the geographical location. Tomeczek (1994) goes on further by identifying certain differences between the original plants and their stages of decomposition. The time spent during its formation is referred to it as its 'organic maturity' . Peat has the lowest maturity which is converted with further pressure and time into Lignite or 'brown coal'.

2.4 Coal Classification

An example of coal classification comes from the The American Society Testing Materials (ASTM). ASTM D388-05 refers to this range of classification. These methods were developed in 1936. ASTM – D388-05 identifies four basic classes:

- Lignite: Contains the highest amount of moisture and the the lowest amount of carbon. Table 2.1 refers to two types of Lignite (ie: A and B). It is also known as brown coal and is used mainly in electricity generation plants. (Figure 2.2)

Fig 2.2 – Lignite or 'brown coal'

(Illustration from the University of Kentucky – Centre of Applied Energy Research)

- Sub bituminous: This species of coal has less of a moisture content than Lignite and is spilt into three separate classes. (Table 2.1 refers) This is generally used in electricity generation to produce steam. (Figure 2.3)

Fig 2.3 – Sub Bituminous coal
(illustration from Kaltimprimacoal.wordpress.com)

- Bituminous: This type contains very little moisture and has a high heating valve (HHV) Table 2.1 refers to six different types. Apart from electricity generation, it is used to produce coke as employed in the steel industry. (Figure 2.4)

Fig 2.4 – Bituminous coal
(Illustration from the University of Kentucky – Centre of Applied Energy Research)

- Anthracite: This species has a very high carbon content with very little moisture and ash content. It burns slowly and is an excellent heating fuel for homes. (Figure 2.5)

Fig 2.5 – Anthracite coal
(Illustration from Newark-Ohio State Education)

ASTM- D388-05 expands these types of coal further expanded to identify other characteristics within each of these four groups.

Table 2.1 is an extract from ASTM –D388-05 illustrates these groups to further define sub-groups with their characteristics. Table 2.2 are notes that relate to Table 2.1.

Classification of Coals by Rank

Class or Rank	Group	Fixed Carbon [b] (wt % dry mmf)		Volatile Matter [b] (wt % dry mmf)		Gross Heating Value [c] (MJ/kg moist mmf)	
		Equal or greater than	Less than	Greater than	Equal or less than	Equal or greater than	Less than
Anthracitic	Metaanthracite [d]	98			2		
	Anthracite [d]	92	98	2	8		
	Semianthracite [d]	86	92	8	14		
Bituminous	Low-volatile bituminous [d]	78	86	14	22		
	Medium-volatile bituminous [d]	69	78	22	31		
	High-volatile A bituminous		69	31		32.55	
	High-volatile B bituminous					30.23	32.55
	High-volatile C bituminous [e]					26.74	30.23
	High-volatile C bituminous [f]					24.41	26.74
Subbituminous	Subbituminous A					24.41	26.74
	Subbituminous B					22.09	24.41
	Subbituminous C					19.30	22.09
Lignite	Lignite A					14.65	19.30
	Lignite B						14.65

Table 2.1 – Coal Classification (ASTM- D388-05)

a) This classification does not include a few coals (referred to as unbanded coals) having unusual physical and chemical properties falling within the fixed carbon and heating value ranges of the high-volatile bituminous and subbituminous ranks.

(b) Percentage by weight on a dry and mineral matter free basis (mmf).

(c) Gross Heating Value on a moist and mineral matter free basis. Moist refers to the natural inherent water contained in a coal but does not include visible water (if any) on the surface of the coal. Multiply MJ/kg by 430.11 to convert to Btu/lb.

(d) Coals containing 69 wt % or more fixed carbon on a dry mmf basis are ranked according to their fixed carbon contentregardless of their Gross Heating Value.

(e) A high-volatile C bituminous coal that may be agglomerating or non-agglomerating.[1][5]

(f) A high-volatile C bituminous coal that is an agglomerating coal, which means that it tends to become sticky and to *cake*when heated. The agglomerating character of a coal is determined by heating a sample to 950 °C under certain conditions. If the residue is coherent and supports a weight of 500g without pulverizing, the coal is classified as being agglomerating

Table 2.2 – Associated notes for Table 2.1.

The material composition of a coal is then analysed further by the methods previously stated in section 2.3.

The Table 2.3 shows an example of four typical coal types that have undergone proximate analysis to determine their properties. Included in Table 2.3 is Daw Mill - one of the primary coals that is utilised in the power stations of the United Kingdom. This coal will be discussed further during the course of this research.

Table 2.4 illustrates the Ultimate Analysis of Daw Mill at an elemental level.

Material composition of typical coals

(Proximate Analysis, wt %)

Coal (location)	Daw Mill	El Cerrejon [2]	Douglas	Illinois No 6
Element → / Analysis area ↓	dry (UK)[1]	daf (S/American)	ar Premium (S/Africa)[1]	(USA)[3]
C	69.3	79.5	67.1	Msr
H	4.3	4.9	4.2	Msr
O	10.7	12.2	10.3	Msr
N	1.2	1.38	1.16	Msr
S	1.48	1.7	1.43	Msr
Cl	0.241	0.276	0.233	Msr
F	0.016	0,018	0.015	ND
Moisture, % total	12.4	8.5	0.4	2.0
Ash, % ar	11.4	10.5	14.3	12.9
Volatile matter, % ar	31.3	30.7	31.4	33.1
CV, kJ/kg ar Gross	25260	24568	27685	25594
Net	24107	23293	26845	24647
Br	-	-	-	ND
Sulphur, % ar	1.86	0.79	0.54	2.84
Chlorine, % daf	0.23	ND	0.01	0.11
Volatile matter, % daf	41.1	38	36.8	30088
CV, kJ/kg daf Gross	33150	30442	32488	29032

Table 2.3 – Proximate analysis of typical coals used in power generation

Notes:: [1] EoN - Radcliffe-on-Soar Power Station

'Phyllis' Database for the following, [2]University of North Dakota,

[3]VTT Publication 287,

Further analysis is then carried out on an Ultimate Analysis lto determine an elemental level of the fuel. Table 2.4 illustrates the Ultimate analysis of Daw Mill Coal.

Material composition of a typical Coal species

***Daw Mill- Ultimate Analysis (wt %)**

Table 2.4 – Ultimate analysis of Daw Mill coal (UK)

Notes: Details extracted from 'Phyllis' Database via the following :

* ECN Laboratories,

ND – Not determined; Msr – Measured

ar – 'as received', daf – dry ash free

2.5 Biomass

Since prehistoric ages, humans have been using biomass in its various forms for shelter, warmth and food. It has played a major role as an energy resource up until the beginning of the nineteenth century.

Authors such as Doshi (2009), Wigley (2007) and Robinson (2001) all agree that the use of sustainable, renewable biomass is a way forward to reduce the dependency on fossil fuels and the impact that they are considered to have on the environment. Therefore, this part of the investigation has commenced with the understanding of the fundamentals of the biomass crops – i.e. plant cell compositions, crop rotation, and cultivation.

El Bassam (1998) has identified four basic groups of plant species suitable for solid biomass conversion that are rich in the lignin and cellulose compounds that is required for combustion of plant matter:

- Annual plant species – e.g: hemp, reed canary grass, rape-seed
- Perennial species – e.g: annual harvest miscanthus
- Fast growing tree varieties e.g.: popular and willow
- Other tree varieties with a long rotation cycle

Baxter (2005) further identifies other inexpensive sources of biomass materials that are residues from both forestry and farming products. These represent a more socially and environmentally beneficial resource. He further suggests that as long as these residues are produced (ie: from forestry and farming products) and they are conducted in a sustainable application, the growing of new plant species at either an equal or greater rate than the harvest rate, there would be no increase in the overall CO_2 . A product that is associated with the use of harvest machinery fuel.

Sims (2002) describes short-rotation energy crop plantations as sustainable sources of renewable energy. The particular example that is written is concerning the *Eucalyptus Brookeriana*. This crop (and other derivatives of this species) undergoes the practice of 'coppicing'. This involves the harvesting of trees a few years after planting them and then allowing the plants to sprout again from the stumps. This would then be followed by subsequent harvesting of the regrowth some years later. This is usually on a 2 –10 year period or 'rotation'. Several rotations are possible before replanting is required.

Gifford *et al* (2000) explains the questions regarding fertilising land that woody biomass species are grown on. A large proportion of a forest's nutrients are provided in the leaves through the natural cycle of the growing season; ie: deciduous species in the autumn. During harvest, very few of these nutrients are removed from site. As carbon (C), hydrogen (H) and oxygen (O_2) are consumed during a combustion process, these are easily replenished from water (H_2O) and carbon dioxide (CO_2). Nitrogen (N) may well need to be replaced as this can be lost through transition with nitrogen oxides (NO_x) during the combustion process. Therefore, it is certainly possible to return the trace elements and nutrients through the ash and hence producing a sustainable production system. Therefore, Gifford *et al* (2000) suggests that if certain species are carefully managed and the soil has the correct nutritional characteristics, short rotation growing regimes with minimal artificial fertiliser inputs are possible. He concludes by suggesting that the optimum length of a growing rotation is dependant on the following:

- Plant species
- Soil type

- Wildlife management (eg: protection from the UK's native, free-roaming wildlife)
- Harvesting machinery availability
- Planting density
- Geographical areas where wind damage is possible.

2.5.1 Basic chemical compositions in biomass

The chemical composition of the biomass is the key to the combustibility of the plant matter. This is achieved by two important compounds in the material.

2.5.2. Lignin

Lignin is one of the basic compounds that is required for the combustion of biomass. Schultz *et al* (1989) explain that the substance is derived from wood species which are found in the cell walls of plants. Figure 2.6 illustrates the structure of Lignin.

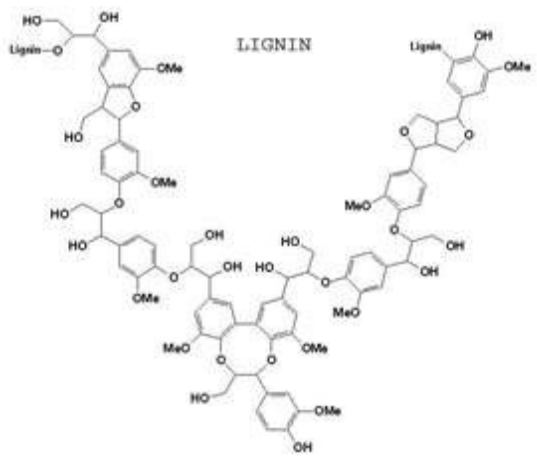

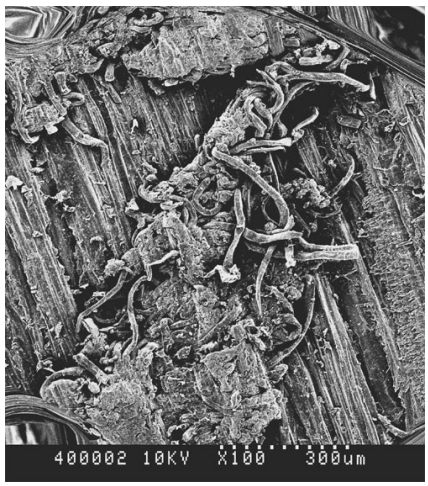

Fig 2.6 - A chemical schematic and illustration of the Lignin structure (Princeton.edu).

Higgins (2002) defines Lignin as a 'glue' that binds that natural occurring cells together in the structure on the wood species and can, therefore, be defined as the material that is a naturally occurring composite.

2.5.3 . Cellulose

All woody plants form cellulose in the same structural way. Hall & Kitani (1989) define the substance as a fibrous structure that forms threadlike structures called 'microfibrils'. (Figure 2.7).These are then connected together with many intra- and intermolecular hydrogen bonds.

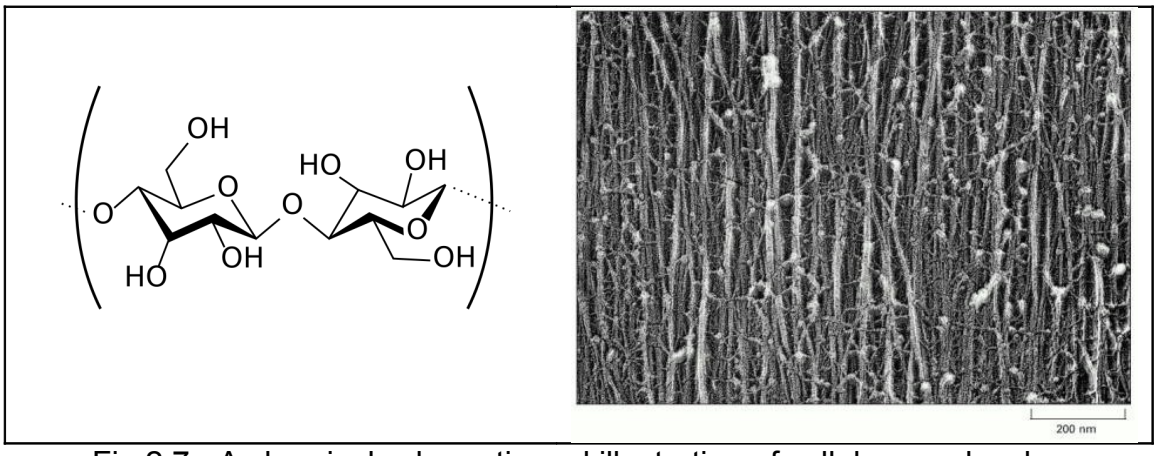

Fig 2.7- A chemical schematic and illustration of cellulose molecules

(Illustration from 'Molecular Biology of the Cell' Alberts B, Johnson A, Lewis J, et al 2002)

2.6 Analysis of biomass species

As with the analysis of coal species (section 2.3 of this chapter) the same analysis techniques are applied via Proximate Analysis. Table 2.5 illustrates the material compositions of some typical biomass species.

Material composition of typical biomass species-

Proximate Analysis, wt %

Crop type → / Analysis area ↓	Miscanthus[1] (*Giganteus*)	Straw (stalk,cob & ear mix)[2]	Summer Swtichgrass[3]
Moisture, % total	10.8	14	13.3
Ash, % ar	4.8	3.9	2.3
Volatile matter, % ar	71.2	67.1	71.9
CV, kJ/kg ar Gross	17270	16383	16096
Net	15914	14934	14675
Sulphur, % ar	0.11	0.13	0.04
Chlorine, % daf	0.09	0.34	ND
Volatile matter, % daf	84.2	81.7	85.2
CV, kJ/kg daf Gross	20414	19949	19072

Table 2.5 – Proximate analysis of typical biomass species

Notes: Details extracted from 'Phyllis' Database via the following :

(1)Supplied by EoN, Nottingham, UK

(2)Danish Cereal Straw

(3)T. R. Miles, T. R. Miles,Jr, L. Baxter, R. W. Bryers, B. M. Jenkins and L. L. Oden: Alkali deposits found in biomass power plants. A preliminary investigation of their extend and nature, NREL/TP-433-8142, 82 p. (1995).

ND – Not determined, ar – 'as received', daf – dry ash free

Cl	0.13	0.132	0.112	Msr
F	-	-	-	ND
Br	-	-	-	ND

Material composition of a typical biomass species

*Miscanthus (*Giganteus* variety)- Ultimate Analysis (wt %)

Table 2.6 – Ultimate analysis of Miscanthus (Giganteus)

Notes: Details extracted from 'Phyllis' Database via the following :

* J. B. Illerup and O. Rathmann: CO2 gasification of wheat straw, barley straw, willow and giganteus, Rosoe, Denmark, Risoe-R-873(EN), 32 p. (1996).

ND – Not determined; Msr – Measured; Cal – Calculated;

ar – 'as received', daf – dry ash free

2.7 Utilisation of biomass in society

The continued use of biomass is a subject that has not been without controversy. This has been expressed in a number of texts with the continuing debate that the various energy crisis's are still very much. Opinions have been expressed in the following:

- Oil price market (Pagnamenta 2008);
- Governmental taxation issues (Webster 2007)
- Alternative, inventive ideas to produce fuels with RDF (Aryers 2008).

Further examples have come from Sims (2002) who looked into a particular quote that came from a British environmentalist - Jonathan Porritt in 2000. He explained that the politicians perceive environmental issues as a series of obstacles in a drive to create more wealth and consumer goods. It is then argued that the ignorance of these issues is symptomatic of a non-sustainable system that has "ignored the fundamental principles relating to the undisputed laws of conservation of energy and matter". This is further argued that these laws have been ignored in order to pursue the materialistic progress of society and we are now faced with the very real threat of a system that cannot function for ever.

Nathan (2007) reported on the production and use of bio ethanol in Brazil. Up till the 1970's, Brazil was importing 75% of its oil. At the time, the OPEC cartel oil embargo very nearly crippled the nation's economy but the then dictator, General Ernesto Geisel decided to curtail Brazil's oil habit by not having the yoke of OPEC hanging around its neck. Instead, they heavily

financed a research and build program into bio ethanol plants. The result is that by the mid-1980's, nearly all cars sold in Brazil ran exclusively on ethanol.

However, the production of ethanol is a 'dirty' production process and the exploitation of workers are separate issues

Cassedy (2005) goes onto explain that even after these various problems, less than 3% of the primary energy output comes from biomass (source: US Dept of Energy). What is realised in all areas of research that new, large and diverse ideas for biomass fuel sources have to be considered. One of the leading arguments that has been raised is that energy crops are also food crops. Cassedy (2005) goes onto explain that the EC agricultural polices are in a constant state of dispute and this is indeed backed up by the news items that appear on a weekly basis – especially where third-world countries are concerned.

Our way of life has depended on cheap fossil fuels. Therefore, it can be argued that we have come a full circle by going back to utilising biomass fuels.

2.8 Ash

The fly ash that is produced from burning pulverised fuel is fine-grain. In a conventional combustion environment i.e. a power station facility, the ash is carried out via flue gases or collected in the various areas of the plant e.g. a bag house filter system or a collection cyclone.

There are two types of 'ash' that is of interest during this research:

- Ash analysis – produced from fuel analysis, eg: carried out under laboratory conditions
- Fly Ash – produced from burning fuel feedstock of one species or more of each other.

2.8.1 Ash analysis

ECN carry out ash analysis by heating the material to a level determined by the feedstock type. For example, Miscanthus (*Giganteus* variety) is ashed at 500 °C in a reducing atmosphere. The chemical compounds are presented in Table 2.7. It represents the normal range of a chemical analysis of fly ash and are represented in terms of oxides.

Ashed Composition of Miscanthus (wt % ash)
500 °C in a reducing atmosphere

Chemical Symbol	Components	Miscanthus
$Al_2 O_3$	Aluminium Oxide	1.6
Ca O	Calcium Oxide	8.6
Cl	Chlorine	3.5
$Fe_2 O_3$	Iron Oxide	1.1
K_2O	Potassium Oxide	27.0
MgO	Magnesium Oxide	5.9
$Na_2 O$	Sodium Oxide	2.2
$Si O_2$	Silicone Oxide	39.0
SO_3	Sulphur Oxide	4.9
TiO_2	Titanium Oxide	-

Table 2.7 – Ashed analysis of Miscanthus
(ECN Denmark, Risoe-R-873(EN), . (1996).

2.8.2 Fly ash

Fly ash is the resultant of burning a feedstock until no further heat energy can be expelled. Tomeczek & Palugniok (2002) have identified the mechanism employed in the breakdown of the fuel when exposed in a combustion environment Figure 2.8 The particular chemical elements are also identified depending on the nature of the combustion and the particular fuel used, i.e: its geographical area.

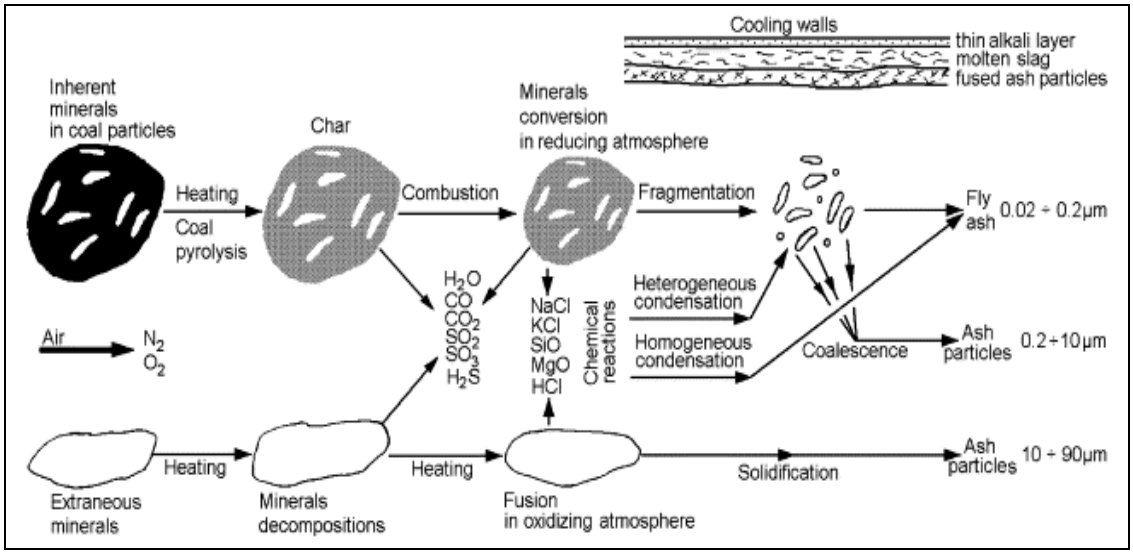

Fig 2.8 – Mineral matter transformation mechanism

(Tomeczek & Polugniok 2002) 'Fuel' Vol 81

During the course of this research, ash analysis was carried out utilising SEM (Scanning Electron Microscope) techniques. This will be discussed further in Chapter 4.

Table 2.8 shows the normal composition of fly ash produced from Daw Mill.

Daw Mill fly ash analysis

Chemical Component	Weight (%)
$Si\ O_2$	41.8
$Al_2\ O_3$	21.3
$Fe_2\ O_3$	14.1
Ca O	6.35
Mg O	2.47
SO_3	7.99
Na_2 O	0.85
K_2O	2.03

Table 2.8– The composition of Daw coal fly ash .

(Analysis carried out 7th March, 2008 – EoN)

Table 2.9 illustrates the normal composition of fly ash produced from various types of biomass

Biomass species (Expressed as % wt)

Chemical Component	Miscanthus[1] (*Giganteus*)	Cereal Co-Product[1]	Summer Swtichgrass[2]
SiO_2	55.85	40.2	61.6
Al_2O_3	3.14	2.5	1.3
Fe_2O_3	2.12	2.2	1.1
Ca O	8.77	7.0	11.1
Mg O	3.79	3.5	ND
SO_3	ND	5.3	0.8
Na_2O	0.5	0.3	0.6
K_2O	12.69	22.4	8.2

Table 2.9– The composition of biomass fly ash .

Notes: Details extracted from 'Phyllis' Database via the following :

[1]Supplied by EoN, Nottingham, UK. Analysis carried out 7th May, 2007

[2]T. R. Miles, *et.al* "Alkali deposits found in biomass power plants." investigation of their extend and nature, NREL/TP-433-8142, 82 p. (1995).

2.9 Deposition Mechanisms

2.9.1. Introduction

The combustion of coal and biomass blends the hot combusted gas that passes the heat exchanger and results in deposit formation on the tube surfaces.

Figure 2.9 illustrates an example of this is (Huang *et al* 1996).

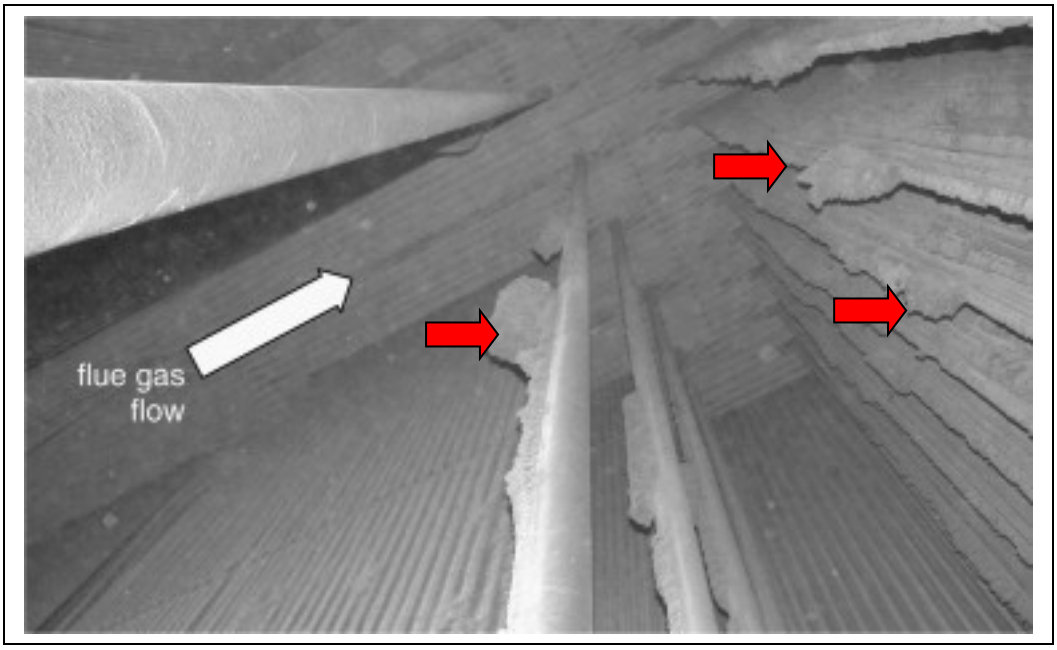

Fig 2.9 – Deposit growth in a super heater section of a coal fired power station (Huang *et al* 1996) – Fuel, Vol 75

Huang *et al* (1996) explains that in Figure 2.9, the resultant deposits are created from months of continuous operation. The direction of the flue gas flow has resulted in deposits forming on the upstream side of the tubes (indicated by the red arrows).

Baxter & DeSollar (1992) and Tomeczek & Waclawiak (2009) both identify that there are five parallel processes that contribute to these resultant deposits.

The effect of these deposits causes heat transfer losses in heat exchanger tubing and loss of thermal efficiency that can bring about financial penalties with repairs and loss of production in power generation. The five processes identified are:

- Inertial impaction (direct)
- Eddy diffusion / impaction
- Thermophoresis
- Brownian & eddy diffusion
- Vapour deposition
- Heterogeneous chemical reactions

2.9.2 Inertial impaction (direct)

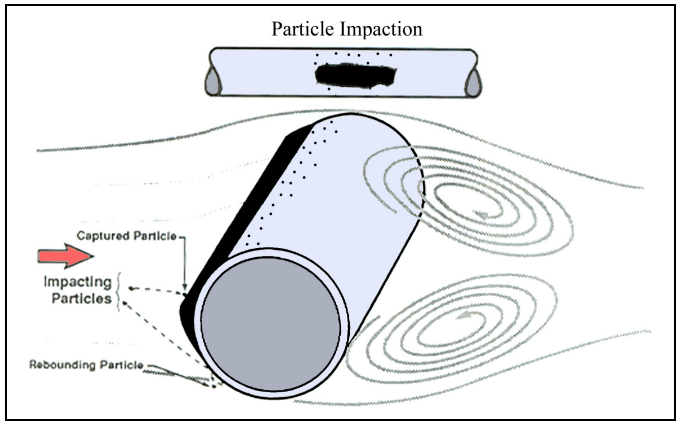

Fig 2.10– Inertial Impaction (Baxter & DeSollar, 1993) - Fuel , Vol 72

Tomeczek & Waclawiak (2009) consider this deposition mechanism the most important for the larger particles that are generally > 10 μm. It is dependent on the tube size, density, and concentration of the flue gas velocity and particle size. This mechanism takes place when the momentum of the particle travelling towards the tube is large enough to overcome drag forces produced by the flow which directs particles around the tube.

Figure 2.10 shows this mechanism where the particles that are in the gas stream and the trajectory of their impaction. Baxter & Desollar (1993) identified that as some particles are captured on the surface, others will impact and rebound to be carried into the recirculation area behind the capture area.

Tomeczek *et.al* (2002) have modelled inertial impaction on the following equation:

$$m_1 = B\, P_1 P_2\, C_{p,m}\, W \qquad [9]$$

Where:

B = constant

P_1 = probability of particle striking the surface

$P_1 = \frac{A - A_{free}}{A}$; where A_{free} = cross section of gas path, A = surface area of target

P_2 = probability of particle sticking to the surface

$P_2 = \frac{\eta_{ref}}{\eta}$ (for $\eta > \eta_{ref}$), P2 = 1 (for $\eta < \eta_{ref}$) where η is the particle velocity

C_{pm} = Concentration of particulate matter

W = Gas velocity

m_1 = rate of condensation of vapours forming a sticky layer

2.9.3 Thermophoresis

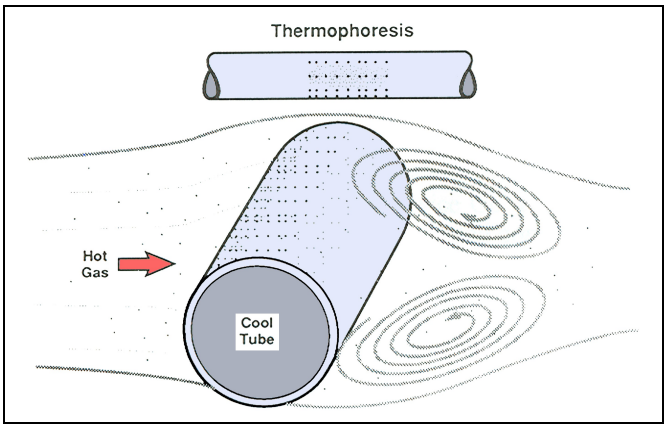

Fig 2.11 - Thermophoresis (Baxter & DeSollar, 1993) - Fuel , Vol 72

Baxter & Desollar (1993) and Tomeczek & Waclawiak (2009) both identify the practicality of Thermophoresis as a process of particle motion in a gas stream due to local temperature gradients. The particle size is generally sub-micron (< 1 μm) and are more evenly distributed over the tube surface (Figure 2.11). Kaufmann *et al* (2002) suggests that eddy impactions also contribute with this mechanisum.

Baxter & Desollar (1993) represents this action with the following equation:

$$F_T = 6\,\pi\mu_g\, d_p f\,(Kn)\ \ \nabla T_g \qquad [10]$$

This is defined as:

$f\,(Kn)$*= function of particle Ø with Knudsen* number
∇ = 'Nabla' – used in vector calculus (descriptions in fluid flow)
μ_g = dynamic viscosity of gas
T_g = gas temperature
F_T = Thermophoretic force
d_p = Diameter of tube

* Knudsen number – ratio of the gas mean free path to the particle diameter

2.9.4. Eddy diffusion / impaction

Kaufmann *et al* (2002) state that eddy diffusion / impaction is the random movement of particles suspended in a liquid or gas. Tomeczek & Waclawiak (2009) identifies a smaller particle size of < 10 μm reaching the tube surface. The tube surface is exposed to random impacts of particles and as the boundary layer becomes more turbulent, the particle diffusion increases. The 'eddies' that occur around the surface help mix the particles up. Thermophoresis assists in this mechanism. . Lokare (2008) further suggests that the process is the lesser understood than the other deposit mechanisms as it is based on empirical coefficients.

2.9.5. Vapour condensation

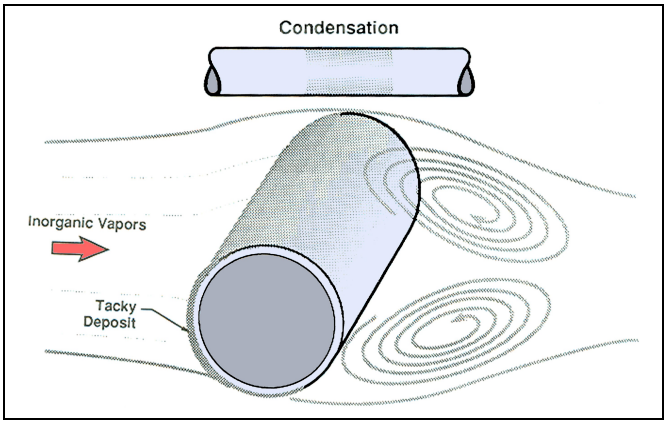

Fig 2.12 – Vapour condensation (Baxter & DeSollar, 1993) - Fuel , Vol 72

Tomeczek & Waclawiak (2009) states that vapour condensation is produced in the flame area during mineral matter and subsequent homogeneous reactions within the combustion environment add to the deposition rate. The condensation occurs either homogenously (deposits via thermophoresis) and heterogeneously onto the tube surface. Both Lokare (2008) and Tomeczek & Waclawiak (2009) concur that chemical

heterogeneous reactions of gases with the resultant deposit matter can also play a part in the deposit mass.

2.9.6. Heterogeneous chemical reactions

The heterogeneous reactions also contributes to the deposition rate. Lokare (2008) suggests that the conversion rate of the material can depend on the mass transfer rate to the surface and on the material kinetics of the heterogeneous reactions involved in the process. Baxter (2000), Huang *et al* (1996), Lokare (2008) and Tomeczek & Waclawiak (2009) all state that the most important reactions during this process are alkali absorption, oxidation and sulfation.

One possible reaction from sulfation is that they contain alkali metals eg: potassium and sodium. It is suggested by Lokare (2008) that these elements easily form hydroxides and sulphate in this environment. Silica (SiO_2) absorbs alkali material to form silicates (SiO_3). These in turn are more fluid and melt at lower temperatures than SiO_2. This transformation to SiO_3 can result in sintering and various changes in the deposit properties.

2.10. Practical application of deposition mechanisms

As stated in section 2.9.2, Tomeczek & Waclawiak (2009), consider that inertial impaction of particles is the most important aspects of deposit formation. Earlier work by Tomeczek (2004) also identified that the growth of such deposits are directly related to some of the following environments:

- Geometry of tubes and in relation to one another in the gas path.
- Combustion conditions within the geometry of the chamber design.
- Composition of the fuel species.
- Conditions on or near surfaces in the environment.

As well as these, hard deposits are created from the melted ash particles in the hot parts of the boiler or by the solid phase particles in the cooler regions of the boiler. The flue gases are cooled within the tube boundary layer which allows the condensing salts - potassium chloride (KCl), sodium chloride (NaCl),potassium sulfide (K_2SO_4) and sodium sulfide (Na_2SO_4) to defuse onto the tube surface and condense onto it which allows solid ash particles to start forming the deposit layers. Some particles may stick or others may rebound and adhere to another part of the tube.

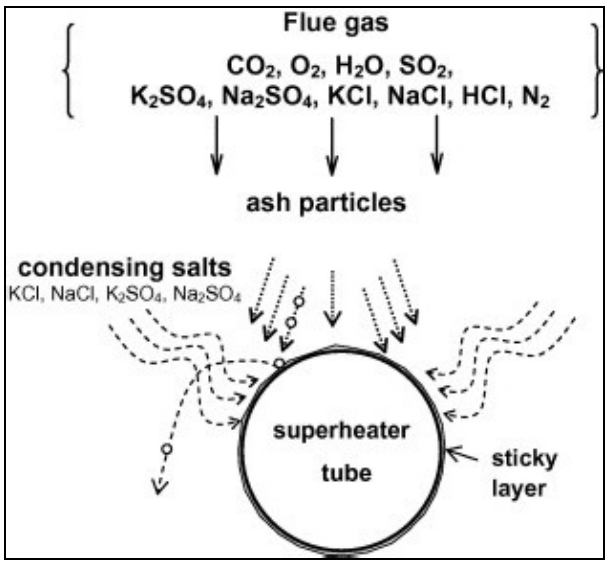

Fig 2.13 – Illustration showing the deposition of ash particles and other interactions during formation.
Tomeczek & Waclawiak (2009) Fuel, Vol 88

As illustrated in Figure 2.13, the presence of the sticky layer (as a result from the condensing salts) is essential for the particles to adhere to the surface. The ash particles that are transported in the flue gas hit the tube surface at varying

angles and therefore, the deposit is not uniform in appearance nor in growth. As the deposit thickens (and taking into account the other deposit mechanisms previously mentioned), the deposition rate slows and the condensation loses its efficiency

Allan *et al* (1996) have identified three classifications in respect to these deposits:

- Inner layer
- Upstream
- Downstream

With the inner layer forms on both the upstream and downtream surfaces acting as a sticky layer where these deposits can adhere . Upstream, the inner layer is formed via diffusion and thermophoresis and the downstream mechanism mainly consists of deposits formed by inertial impaction and other particles contained in the flow of the gas path.

2.11 Heat Transfer Calculations - Radial Systems

2.11.1 Introduction

The various formula that have been presented in the preceding sections are required for the calculation of heat transfer. These are based on a combination of various other equations that are used in heat transfer and fluid dynamics and play an active role in deposition theory. The theory only will be presented in this section.

Holman (1997) has produced several examples of methodology in calculating heat transfer rates and has taken both Newton's Law of cooling and Fourier's 2nd Law of heat conduction are applied to the overall solution.

The various sections that make up the overall solution will now be discussed in the following sections.

2.11.2 Newton's Law of Cooling

Generally, this is given as the rate of cooling of a hot surface which is losing heat both by radiation and natural convection which is proportional to the difference in temperature between the object and its surroundings. This can expressed as:

$$q = hA\ (T_w - T_\infty) \qquad [11]$$

where: A = surface area

h = convection heat transfer co-efficient

T_w = Temperature of surface of tube

T_∞ = Temperature of surrounding area

q = Thermal energy

2.11.3 Fourier's 2nd Law of Heat Conduction

Fourier's law is generally expressed by the following equation:

Heat flow = Thermal potential difference / Thermal resistance

$$q = kA\left(\frac{\partial T}{\partial x}\right) \qquad [12]$$

where:

k = thermal conductivity of the material

q = Heat Flux density

$A = 2\pi rl$

Taking a wall of uniform thickness Δx , Fourier's law can be applied as:

$$q = \frac{-kA}{\Delta x}(T_2 - T_1) \qquad [13]$$

where:

T_1 and T_2 are the wall face temperatures

Consideration is then applied to the geometry of the cylinder, the following are considered in the final application of the equation:

$r_{\text{(number designation)}}$ = inside / outside radius of the ceramic

l = length of cylinder

$T_2 - T_1$ = Temperature gradient

Therefore, with the application of these equations and the geometry of the various surfaces of the deposit capture probe (Figure 2.14), the expression to find q can be applied.

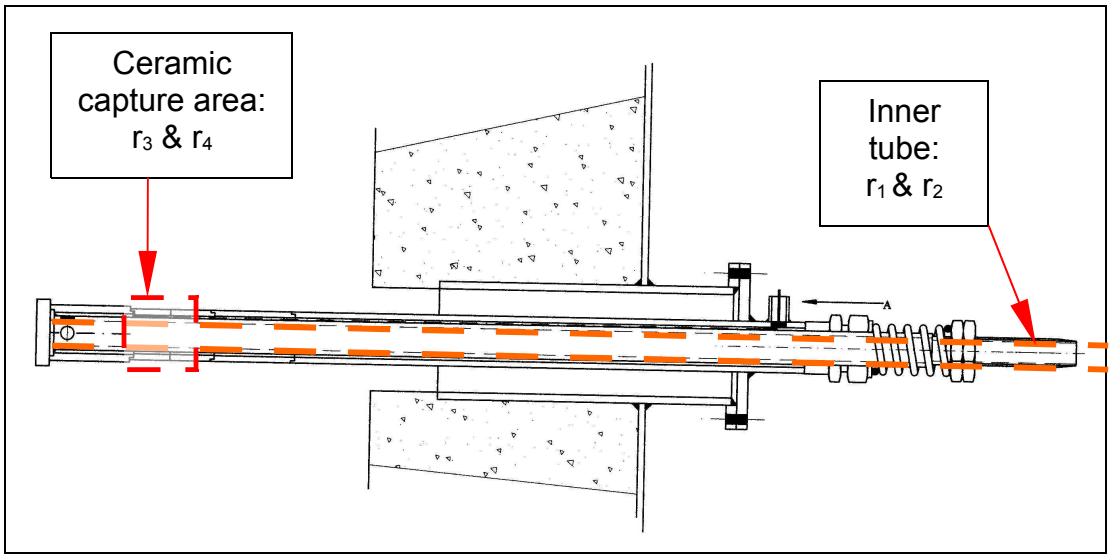

Fig 2.14 – Cross section of the deposit capture probe illustrating the inner tube (r_1 & r_2) and the ceramic capture area (r_3 & r_4)

The ceramic capture area (marked in red) forms part of the expression to find q. The parts r_3 and r_4 are added to the equation with the inner tube (marked in orange) applied to parts r_1 and r_2.

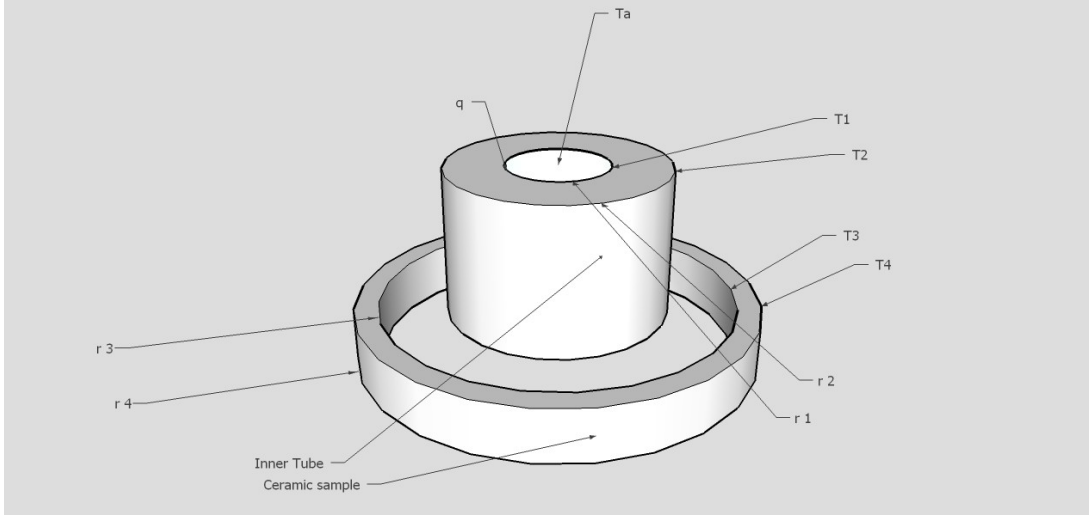

Fig 2.15 – Illustration showing the areas required in calculating the heat transfer in radial systems

[14]

$$q = \frac{T_2 - T_1}{\left[\frac{1}{h_4}\frac{1}{A_4} + \frac{In(r_4/r_3)}{2\pi k_c l} + \frac{1}{h_3 A_3} \right] + \left[\frac{1}{h_2 A_2} + \frac{In(r_2/r_1)}{2\pi k_m l} + \frac{1}{h_1 A_1} \right]}$$

Where:

r_1 = Inner radius of inner metal tube

r_2 = Outer radius of inner metal tube

r_3 = Inner radius of ceramic tube

r_4 = Outer radius of ceramic tube

A = 2 π r l

h_4 = Convection heat transfer co-efficient outside ceramic tube

h_3 = Convection heat transfer co-efficient of inside ceramic tube

h_2 = Convection heat transfer co-efficient of outside metal tube

h_1 = Convection heat transfer co-efficient of inside metal tube

k_m = Conductivity of metal tube

k_c = Conductivity of ceramic tube

In = Natural log

$T_2 \& T_1$ = Wall surface temperatures

q = Heat flux density

2.12 Deposition probes in other industrial applications

The deposit probes that are applied to this research are of a largely universal design. Some play differing roles in the investigation of deposit capture, corrosion monitoring and investigation of combustion environment behaviours eg: the modelling of heat dynamics within a heater matrix of a power station's generating plant. (Figure 2.16)

.

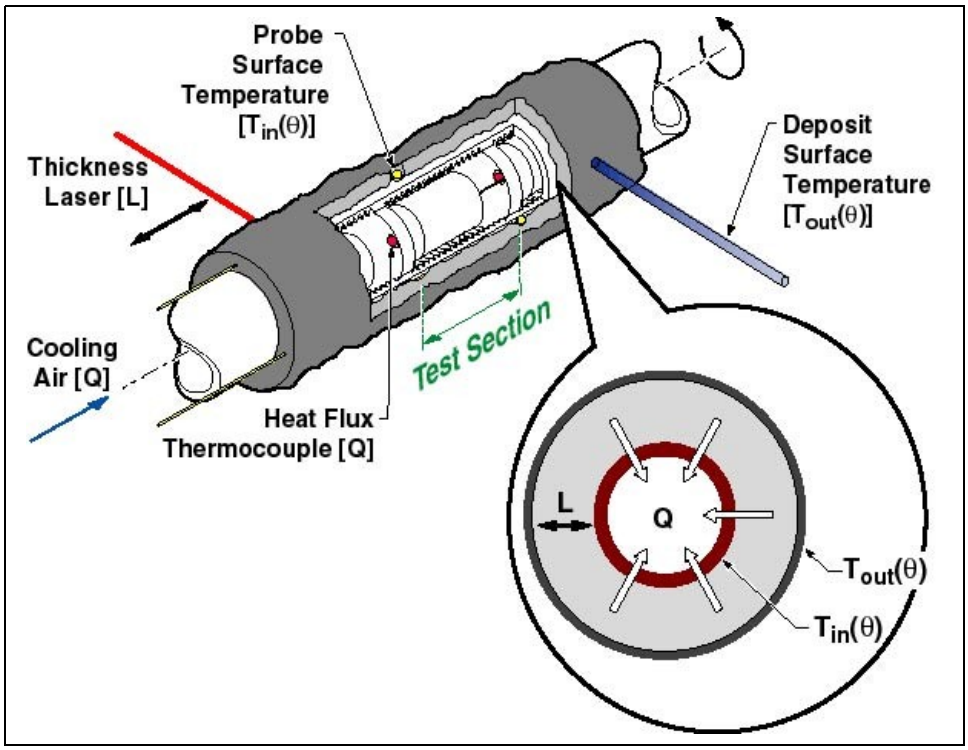

Fig .2.16 – Air cooled deposit probe
(http://www.et.byu.edu/~larryb/index.htm)

Their geometry varies greatly as does their cooling medium. Some are water cooled and others are inert gas / air cooled. One recent application has been at the RWE owned Tilbury Power Station. Doosan Babcock has created a deposit probe that has been designed to capture such deposit species but also

measures the rate of corrosion in various test sections that are attached to the probe unit. Figure 2.17 illustrates the probe unit with the various test sections attached.

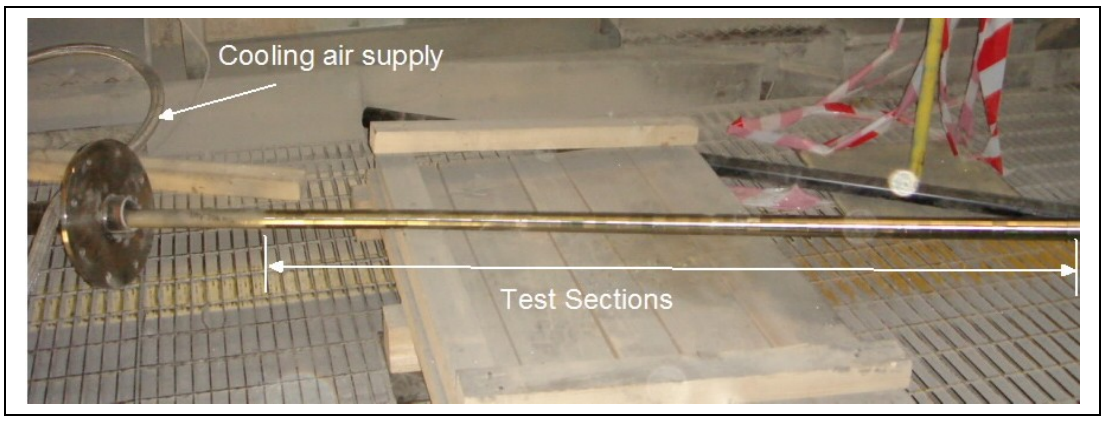

Fig 2.17 – Deposit probe employed at Tilbury Power Station (courtesy of Doosan Babcock)

The probe assembly is placed into the hot gas stream within the heat exchanger. The assembly is air cooled and has a number of thermocouples placed in varying areas to monitor temperature. (Figure 2.18)

Fig 2.18 – Deposit probe in situ in the heat exchanger bank at Tilbury Power Station.(courtesy of Doosan Babcock)

Other units have been designed to operate in small, laboratory-scale environments. ECN (Biomass, Coal and Environment Research) carry out a number of procedures utilising small 'drop- tube' furnaces with a deposit probe in the gas steam (Figure 2.19 illustrates).

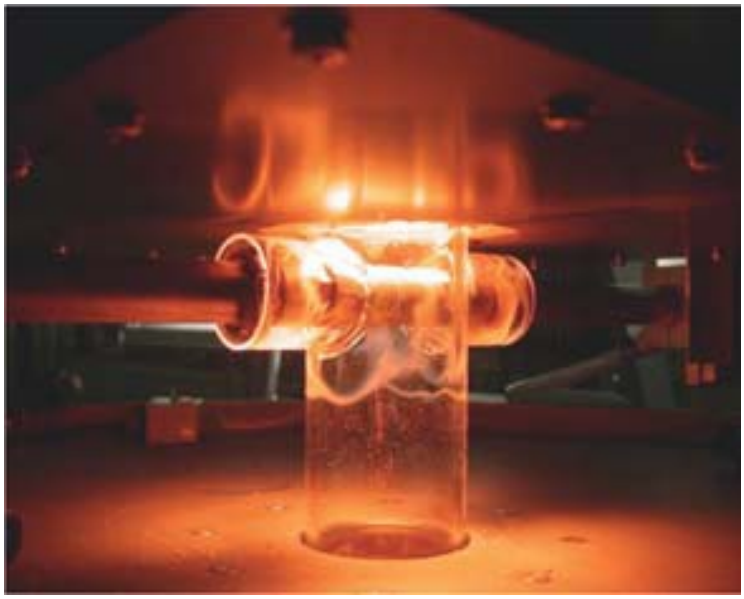

Fig 2.19 – Deposit probe in situ within a small, lab scale environment (ECN Biomass, Coal and Environment Research)

Following a deposit test, the various test sections are removed for analysis.

Fig 2.20 – Deposit probe removed for analysis
(ECN Biomass, Coal and Environment Research)

The main constituents of the Cranfield Probe will be explored in further detail in Chapter 3.

3. Methodology

3.1 Introduction

This chapter of the research describes the methodology in which the practical aspect was carried. It will cover the following areas:

- Fuel test schedule
- Combustion apparatus
- Fuel delivery systems
- Deposition probe
- Temperature logging
- Gas analysis
- Deposit collection
- Deposit Flux calculations
- Mould encapsulation of a deposition capture area

3.2 Fuel Test Schedule

Table 3.1 displays the test matrix of the various feedstocks that were employed in this research. It should be noted that miscanthus -*Giganteus* variety feedstock was a late addition to the test plan and therefore time did not allow it to be tested across both spectrums of Daw Mill and El Cerrejon coal.

Fuel type	Mix Ratio (wt %)	Fuel details
PF Coal	100	Daw Mill (United Kingdom coal)
PF Coal + CCP	80:20 60:40 40:60 20:80	Daw Mill & cereal co-product (CCP)
PF Coal	100	El Cerrejon (South American coal)
PF Coal + CCP	80:20 60:40 40:60 20:80	El Cerrejon & CCP
CCP	100	(Cereal co-product)
Miscanthus	100	Miscanthus crop (*Giganteus* variety)

Table 3.1 – Test matrix of fuels investigated

*CCP – Cereal co-product : see specifications in the Appendix

(All fuels were co-fired into the combustion rig facility)

PF = pulverised fuel

3.3 Combustion Apparatus

The experiments were carried out at the Centre for Energy and Resource Technology (CERT) - combustion rig facility. Figures 3.1 and 3.2 show the rig assembly as a multi-chambered unit. It is comprised of a fluidised bed combustor that is linked in series with a pulverised fuel combustor (PFC) chamber. Figure 3.2. illustrates the overall, external size of the PFC chamber and figure 3.3 illustrates the internal layout of the PFC chamber and the refractory lining. The internal dimensions 0.3m^2 . (Comprehensive drawings of the PFC chamber can be found in Appendix III)

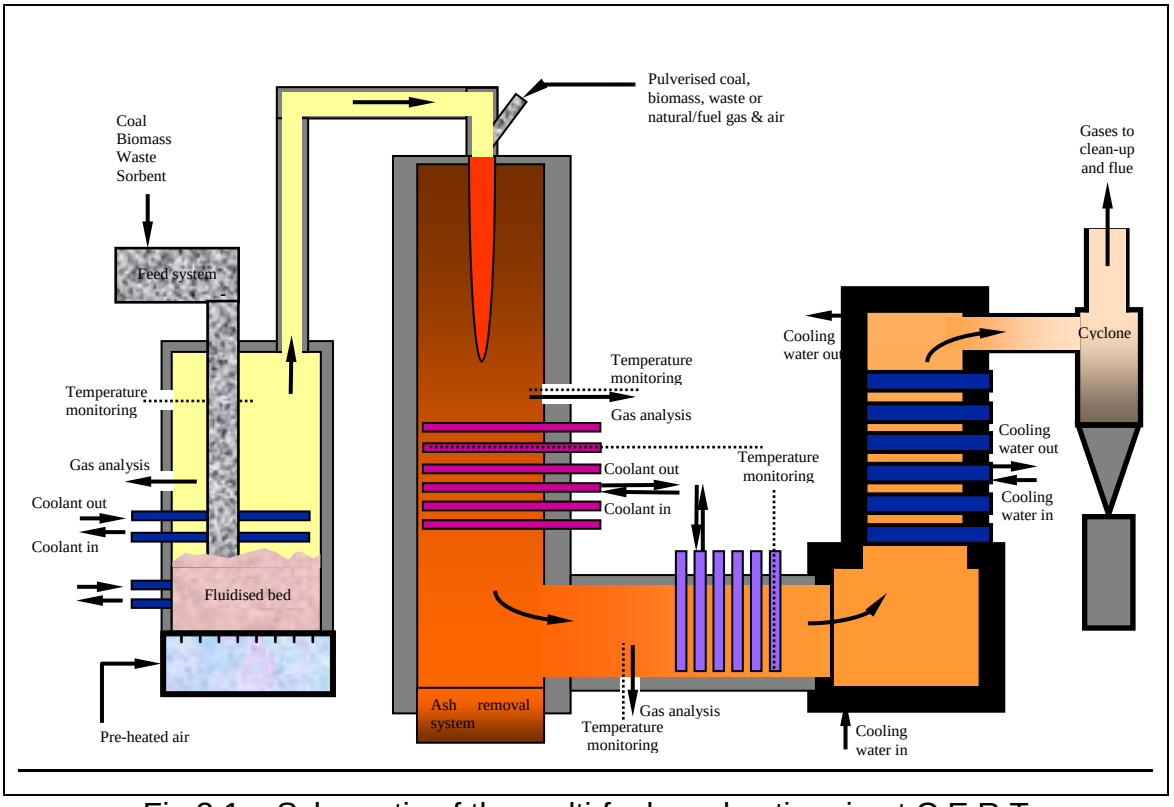

Fig 3.1 – Schematic of the multi-fuel combustion rig at C.E.R.T (Cranfield University)

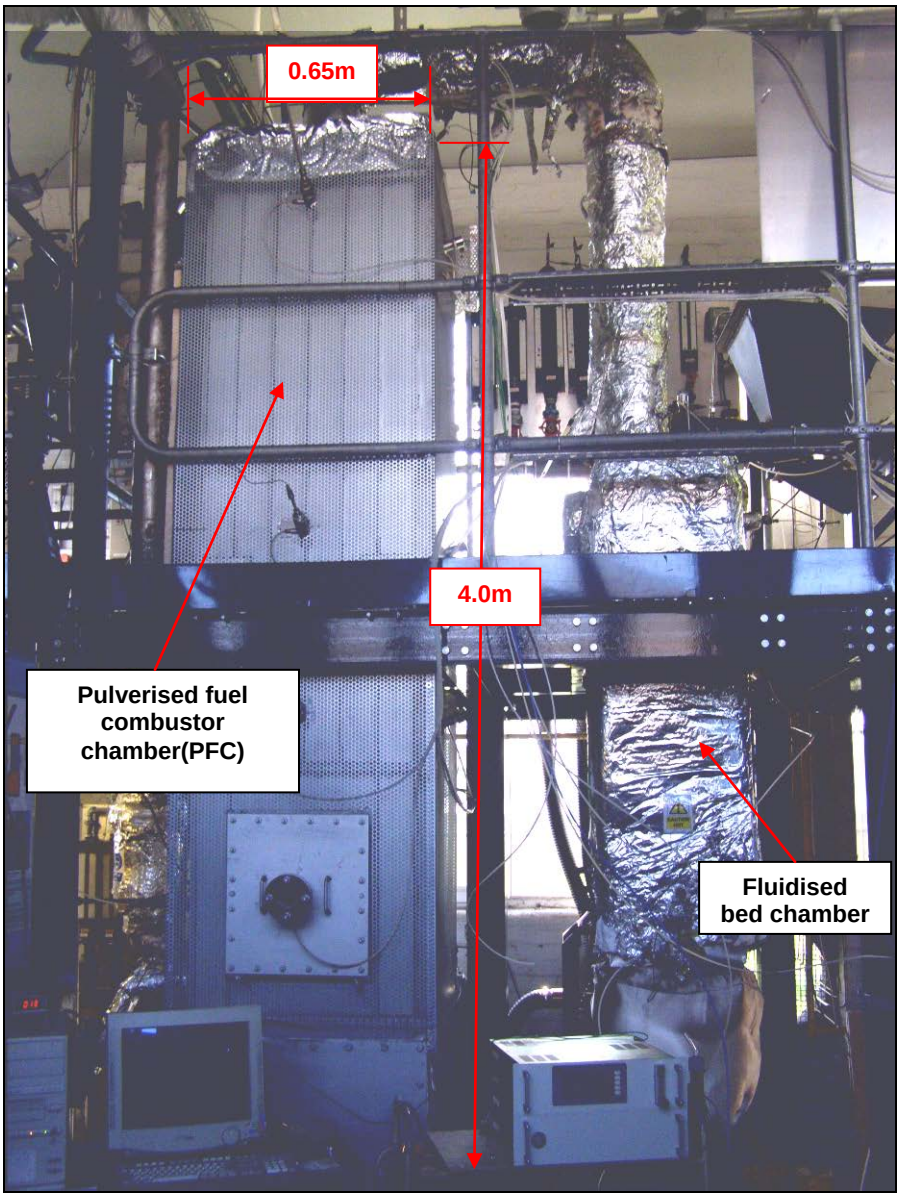

Fig 3.2 – The front view of the multi-fuel combustion rig (Cranfield University)

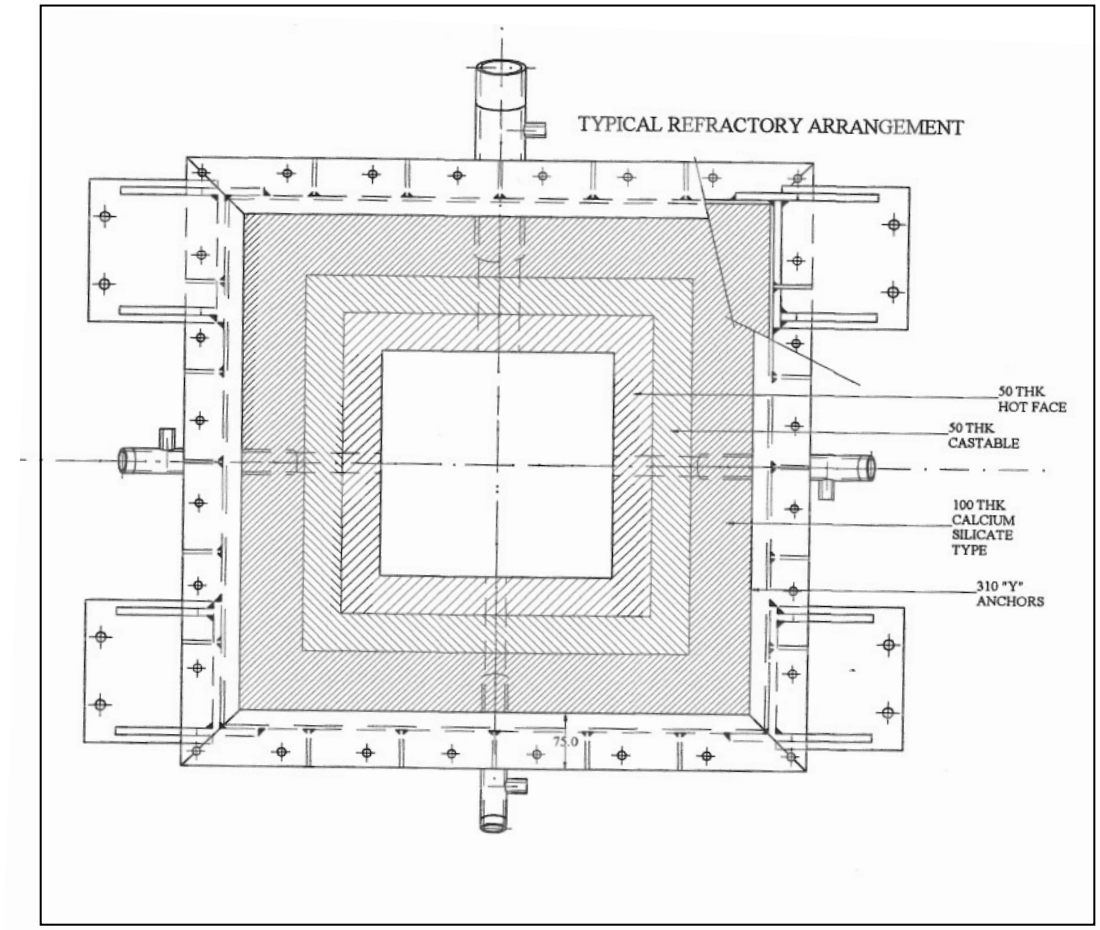

Fig 3.3 – Drawing illustrating the cross-section through the PFC chamber and the typical refractory arrangement.
(Energy Audit Services)

3.3.1 Control of combustion process

The combustion rig facility has the capability to simulate the conditions within a power generation environment by controlling the input of air, nitrogen, natural gas and / or fossil fuel, biomass and waste feedstocks.

However, before any experiment can proceed, certain conditions have to be met in obtaining the correct environment within the unit. For example, the system is designed in such a way that certain service conditions have to be met with the application of safety interlocks. These include :

- Cooling water flow for heat exchanger
- Compressed air (8 bar)
- Air flow from two fan units:
    - The inlet air fan supplies combustion air for the whole unit
    - The outlet air fan draws combusted gases from the rig to be exhausted via the chimney to atmosphere
- Gas pressure from mains supply

The combustor rig's control panel has interlocks contained within it. A series of lights indicate when the various interlocks are made. If any of the interlocks are not made then the rig will not start. Also, if any of the interlocks fail (eg: supply of compressed air), the rig will shut down and terminate all other supplies. In both instances, this is critical for safety reasons.

The sequence for start- up is :

- Water flow (coolant in /out of rig) - this goes to a heat exchanger that will expel waste heat
- Compressed air on
- Fan systems on
- Natural gas supply to rig

In Figure 3.1, the fluidised bed combustion chamber area of the rig has to be started first. The air and gas balance is controlled by a set of rotameters that are shown in Figure 3.3. Approximately, 1000 ltrs/min of air and 30 ltrs/min of natural gas is required for ignition. The temperature that is typically achieved during the heat up process is 400 °C, which takes approximately two hours.

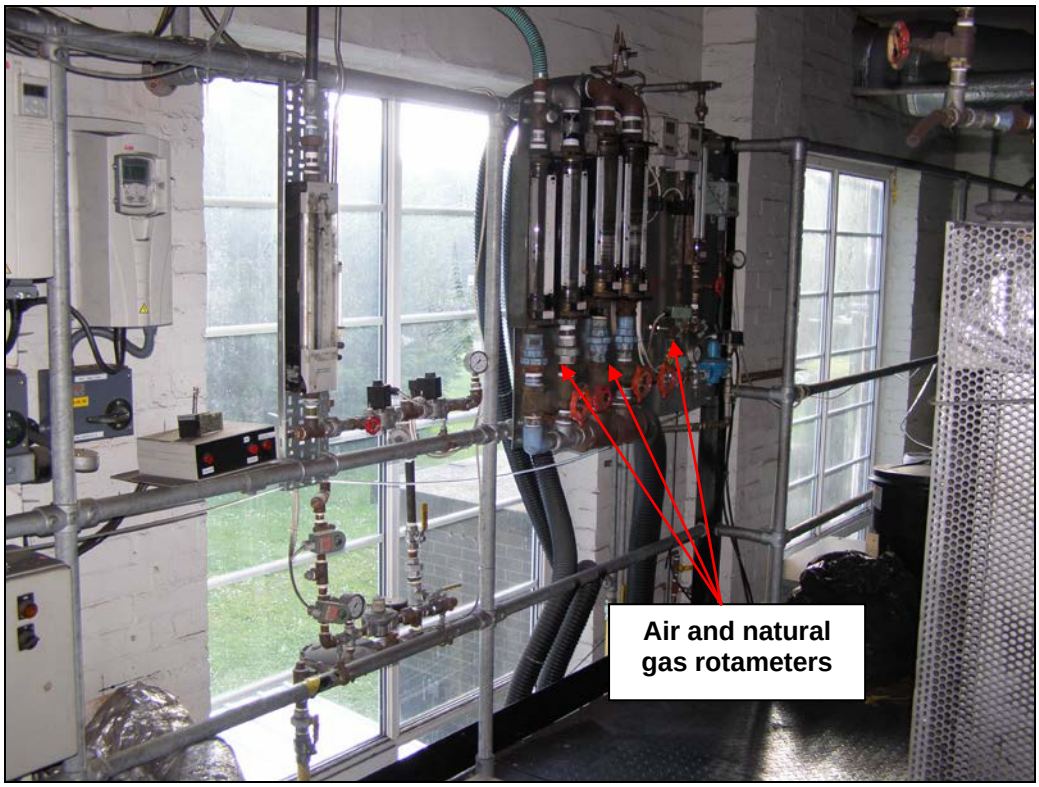

Fig 3.4. – Natural gas and air rotameters for the fluidised bed and pulverised fuel combustion chamber

The PFC chamber is then required to be pre-heated. This is achieved by two separate burner units – a pilot flame (to assist with the ignition of main burner unit) and the main burner itself.

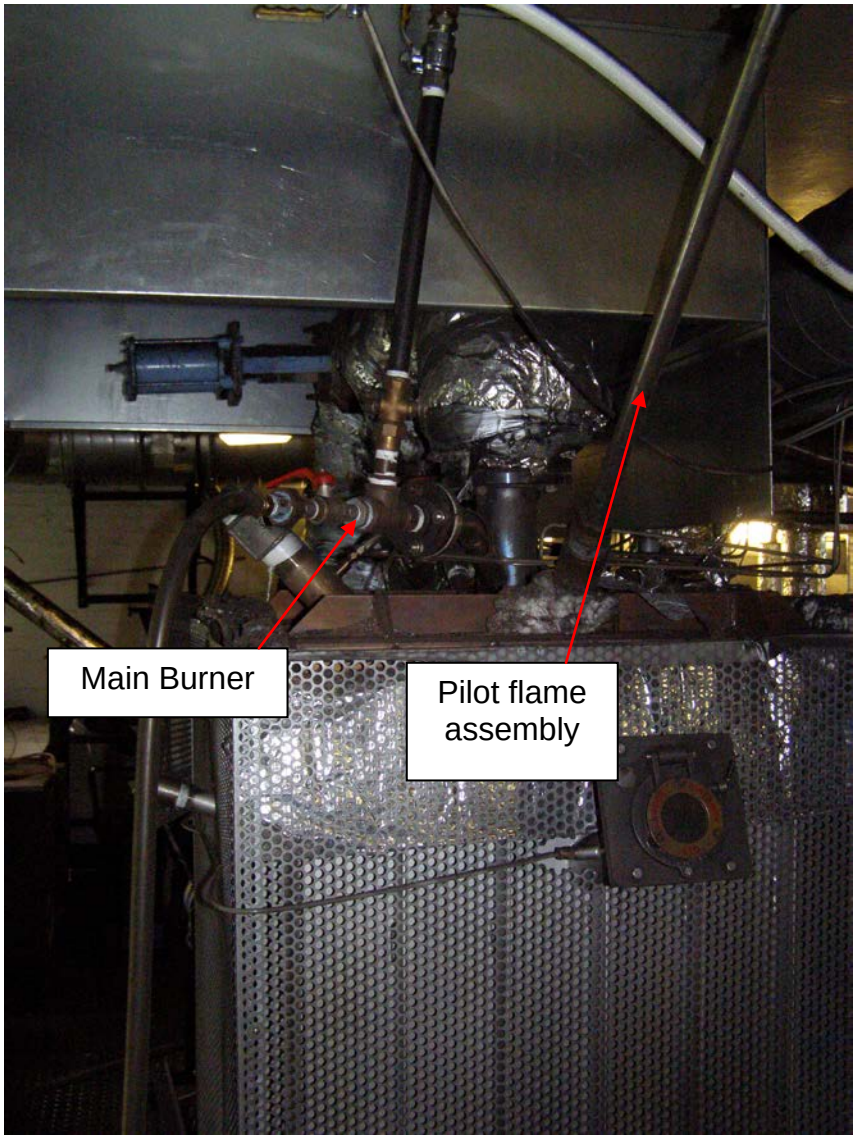

Fig 3.5 – View of top of the pulverised fuel combustion chamber

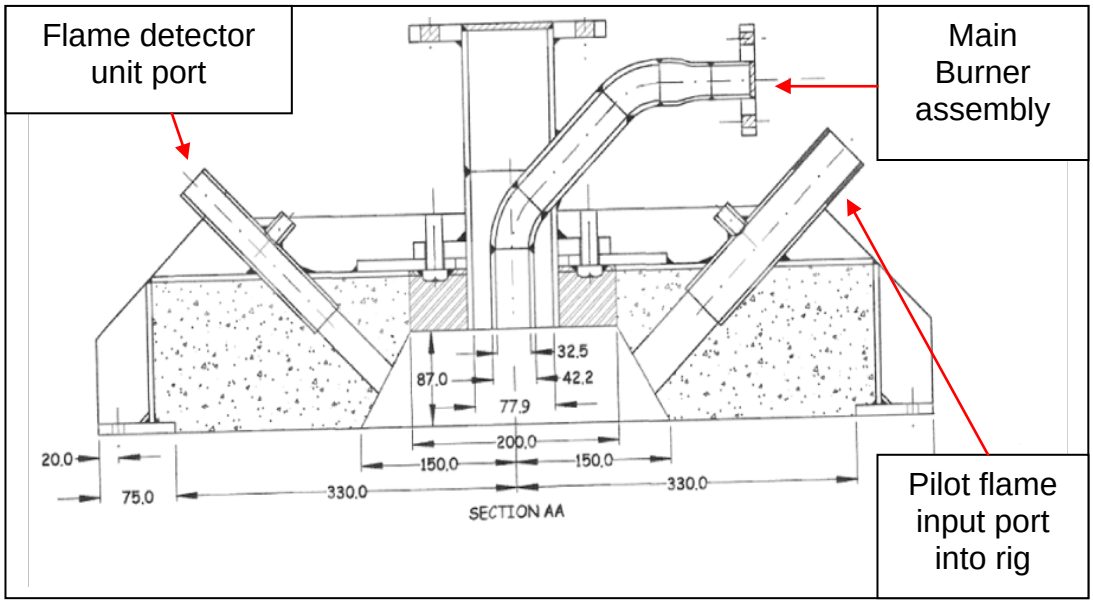

Fig 3.6 – Drawing illustrating the cross-section through the pilot flame input port and main burner assembly. The third port is for the flame detector unit. (not shown in figure 3.7)
(Energy Audit Services)

Figures 3.5 and 3.7 show the location of the pilot flame and the main burner assembly at the top of the PFC chamber. Both are started from the same control panel. and are controlled using separate rotameters on the
panel shown in Figure 3.4. Both units have safety interlocks in case of failure of any of the services to the rig. Figure 3.6 illustrates the location of the flame detector unit which serves as one of the interlocks. In this case, if the flame detector does not 'see' a flame within in PFC chamber, the gas supply is terminated immediately.

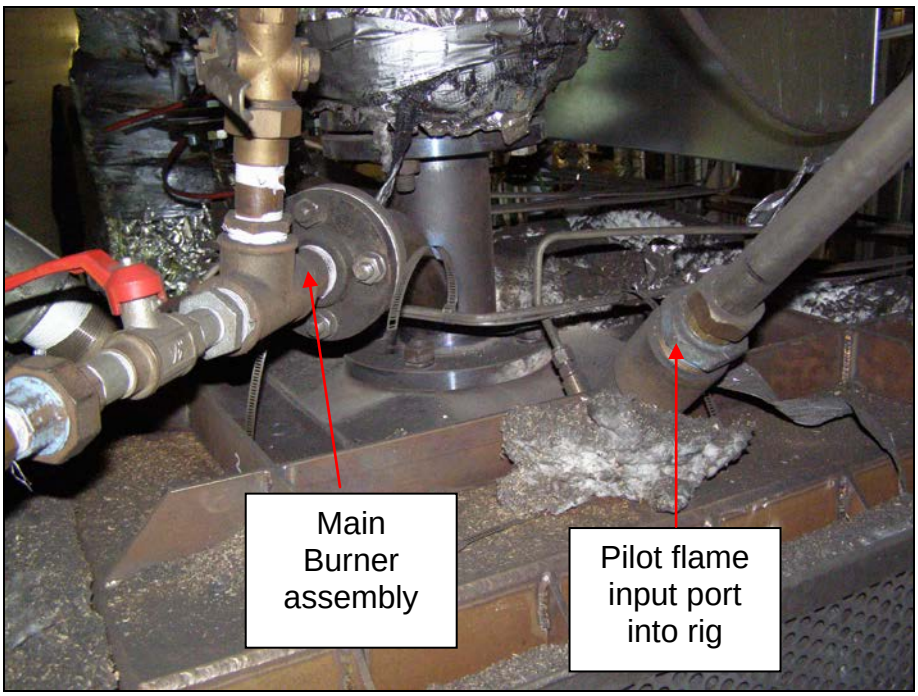

Fig 3.7 – Location of Main Burner & Pilot Flame ports on PFC chamber

The secondary chamber requires to be pre-heated to at least 800 °C before the combustion experiments can proceed. This is achieved with the following flow rates :

- Pilot Flame = 10 ltrs/min natural gas & 100-120 ltrs/min air
- Main Burner = 50 – 70 ltrs/min natural gas

The unit requires at least 20 hours to get to the required operating temperature.

3.4 Application of feedstock

Once the combustor rig has reached its operating temperature, different methods can be employed to inject various coal and biomass feedstocks into the unit. The main method of delivering the feedstock will now be discussed.

3.4.1. Pulverised fuel delivery application

This is one of the major improvements that has been has been developed during this research. The previous configuration utilised a twin hopper assembly that relied on a rotary valve and nitrogen flow to carry the fuel into the main combustion chamber. This was subject to blockages and a sporadic flow of feedstock. Figure 3.6 shows the current configuration of fuel delivery. The system is able to deliver the pulverised fuels, eg: coal species and the CCP mixes at a far more efficient rate. A vibrating bed with a cylinder assembly contains the fuel mixture. A baffle plate inside the cylinder allows the fuel to fall in a measured amount into the area where a venture assembly is fixed and has almost eliminated the problem of the blocking of the fuel feed hose.

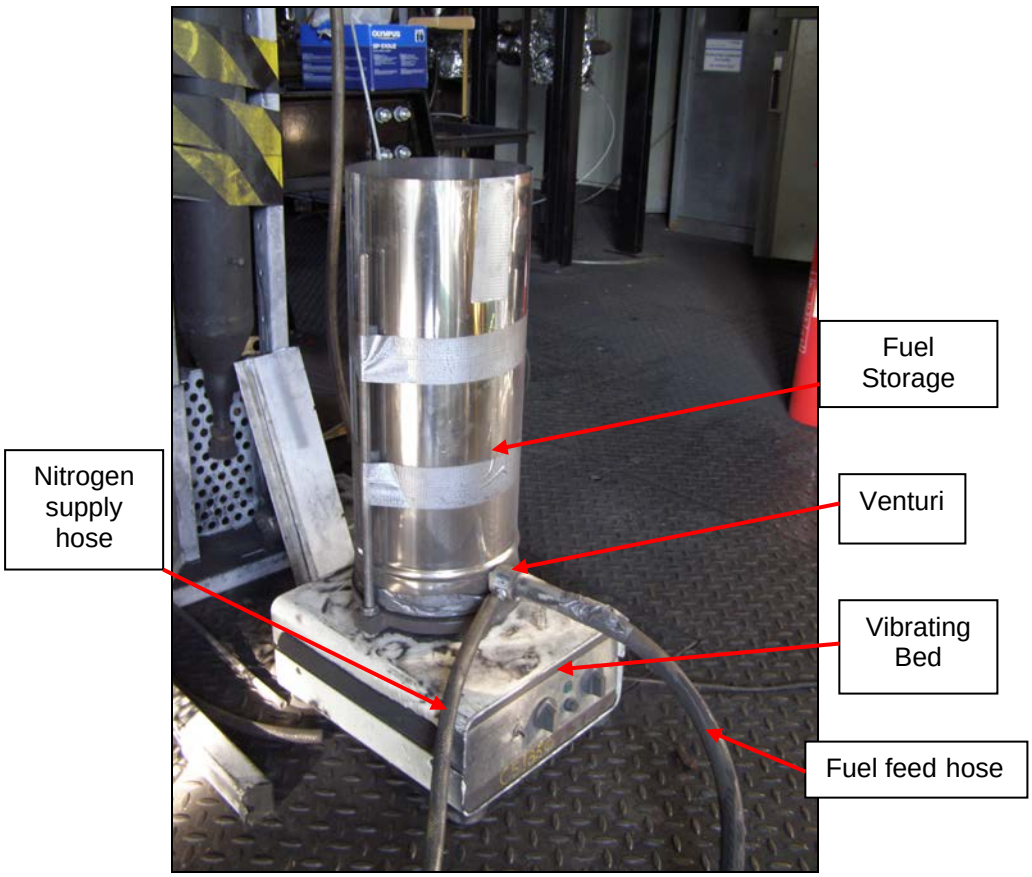

Figure 3.6 – Pulverised Fuel delivery system

The venturi is designed in such a way that the vacuum that is created from the nitrogen flow running through it allows the fuel to be drawn into the pipe leading from the assembly and then blown into the combustion environment. This can be controlled via a rotameter assembly and adjusting the amount of vibration on the fuel storage cylinder. The venturi is fixed to the bottom of the feed cylinder with the feed tube coming from the longer end of the unit. (see Figure 3.7).

Figure 3.7 – Venturi feed system (KV Products)

A comprehensive specification of the venturi used can be found in Appendix II. Once the assembly of the unit was complete, a calibration of the unit was carried out by feeding a known weight of fuel through the unit over a period of time. This gave an approximate feed rate for each experiment. The results of this part of the research are discussed in Chapter 4 .

3.5. Deposit capture probe

The design of the deposit capture probe is based on a common approach as outlined in Chapter 2, for cooled probes. However, in this application it has been modified to suit the requirements of the C.E.R.T's combustion unit. Previous tests utilising the same basic design have been carried out using 'Mulite' as the deposit capture area. Coleman (2008) utilised this material but with varying degrees of success. Mechanical failure of the deposit catch area was an increasing problem at higher gas temperatures; ie: + 850 ^{o}C. The result of such failures was the loss of the deposits. The probe now consists of an air cooled unit with removable centre section in order to change the deposit area as required - (see Figures 3.9 to 3.12). The interlocking sections are glued in place with 'Autostic' cement. (see specifications for this cement in the Appendix. Two 'K type' thermocouples are secured with

'Nichrome 5 ' wire onto the cylindrical metal surfaces, either side of the deposit area. (see Figure 3.14). and the third thermocouple is secured into the exhaust port of the each probe.

The deposit capture section is an alumina material – trade name 'Alsint 99.7' (see specifications the in Appendix) . Figures 3.9 through to 3.12 show the stages of assembly.

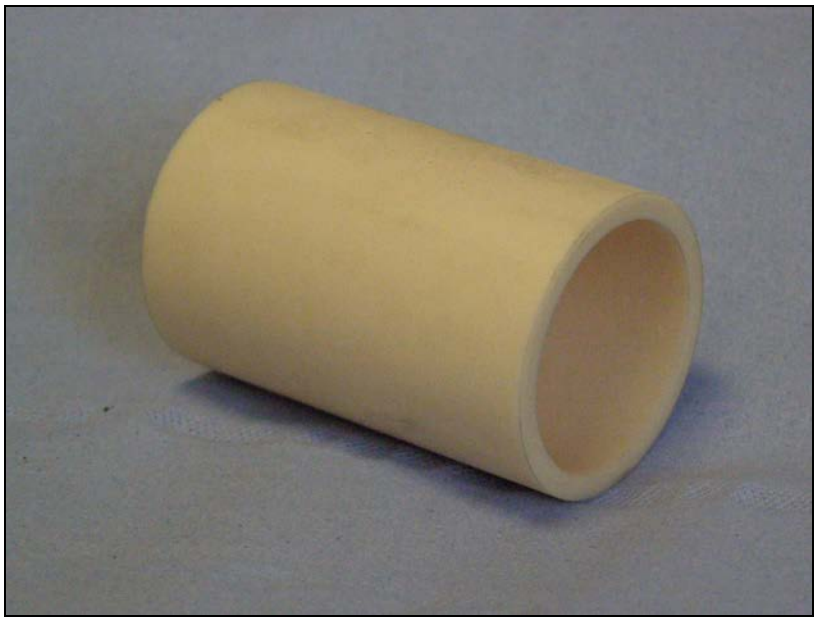

Fig 3.8 – Ceramic capture tube

Fig 3.9 – Ceramic capture tube with the interlocking 316 stainless steel pieces for the rest of the probe

Fig 3.10 – Close up of assembled deposit capture area

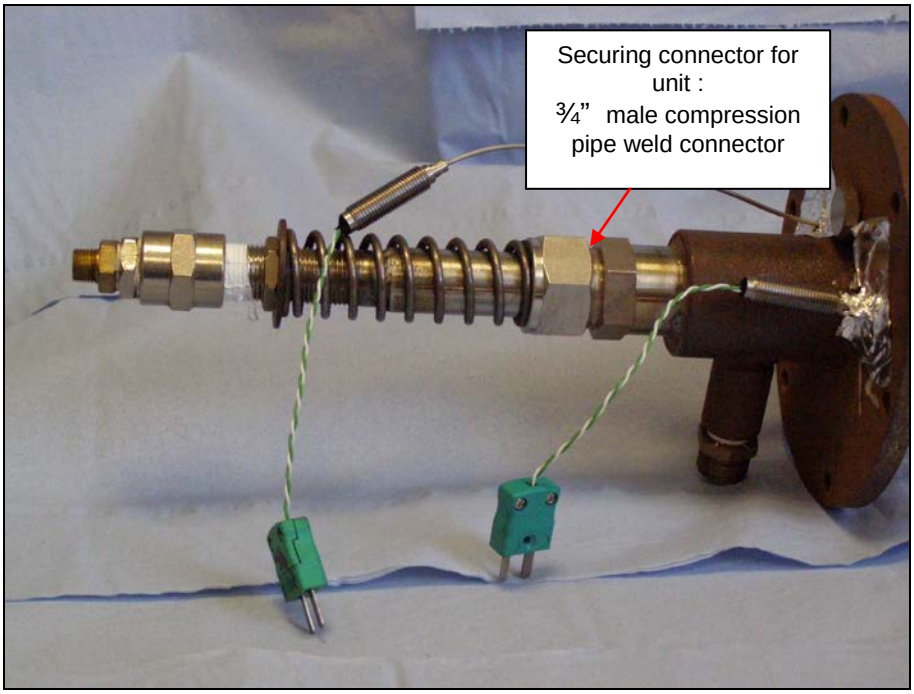

Fig 3.11– Securing connection for deposit probe with 'K' type thermocouple's connection plugs attached

Fig 3.12 – A fully assembled deposit capture probe

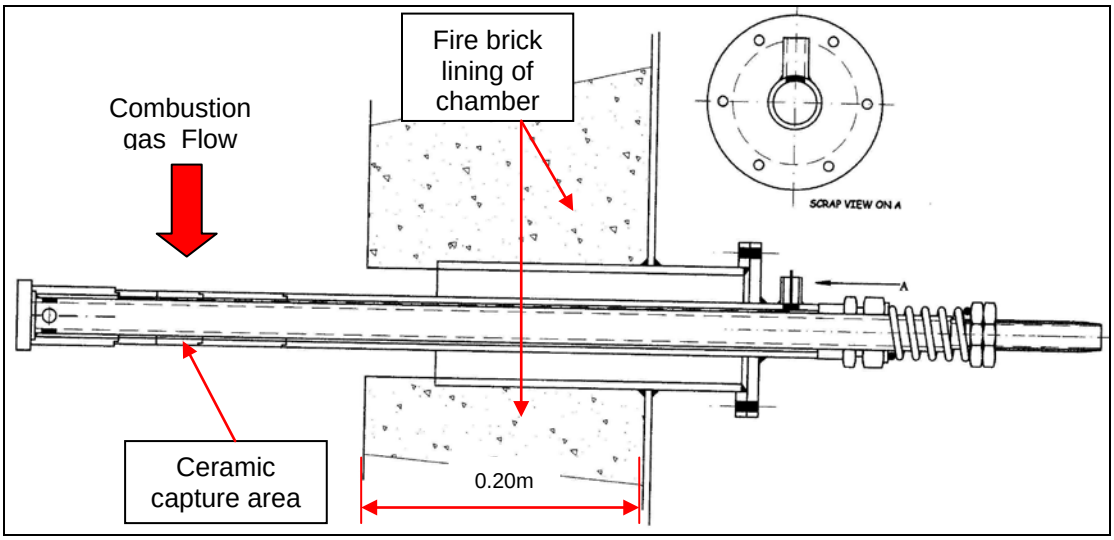

Fig 3.13 – Section through view of deposit capture probe in the pulverised fuel combustion chamber

The main part of the probe body is a welded construction and manufactured from 2.25 chromium steel. Figure 3.11 illustrates the male pipe weld connector with ¾" male compression fitting. Nylon ferrules have been used rather than the traditional stainless steel ferrule assembly (further details are illustrated in the Appendix). This is to allow ease of assembly and disassembly of the unit as stainless steel ferrules will 'bite' into the inner tube and prevent the centre section from coming apart. The spring assembly is to allow the probe to expand whilst still maintaining the integrity of the sealing surfaces of the deposit capture area with the interlocking parts. Figure 3.13 illustrates the probe in relationship with the internal geometry of the vertical chamber – the deposit capture part situated in the centre of combustion chamber.

Two other probes of the same design and materials were then placed into the vertical chamber of the pulverised fuel combustion chamber. During the course of the experiments, the surface temperatures of each of the probes were kept at approximately 700, 600 and 500 ºC. Each probe has its own individual air supply that is controlled via a rotameter. This allows each probe to have its cooling air rate set in order to obtain the desired surface temperature on the deposit capture area for the desired test conditions. The rotameters can be seen in the background of Figure 3.14.

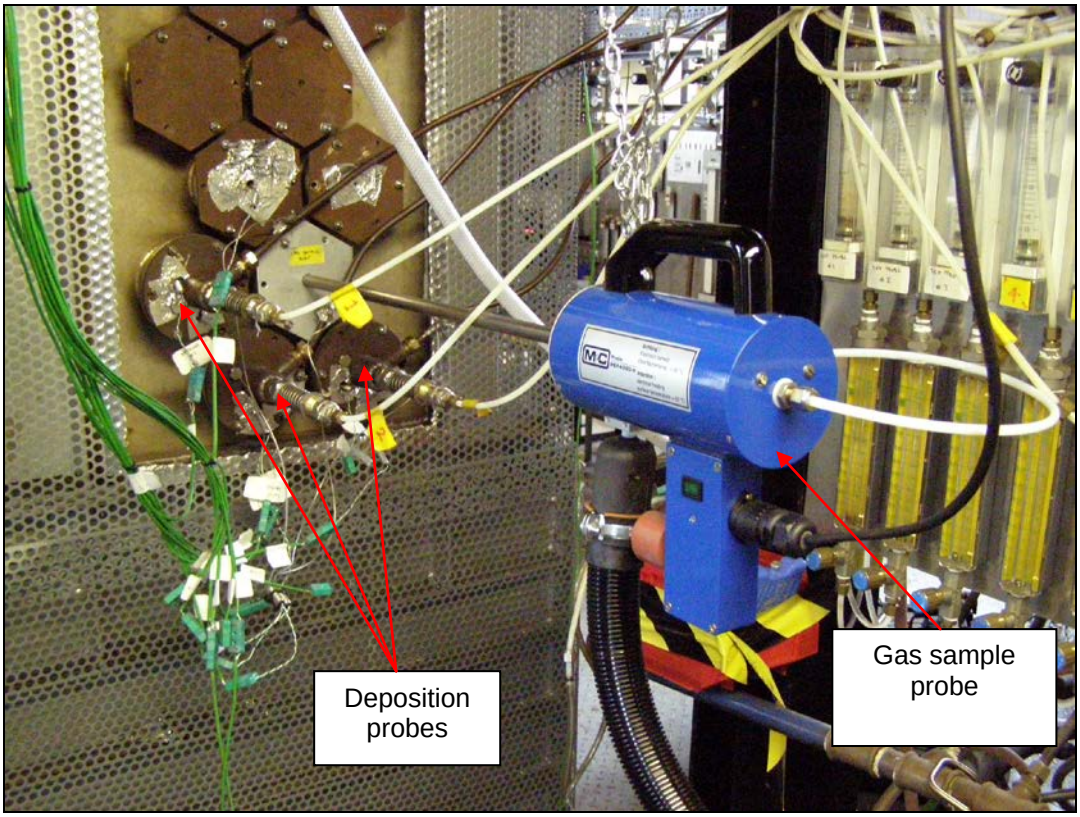

Fig 3.14– The vertical section of the pulverised fuel combustion chamber with the deposit capture probes in place.

Figure 3.14 illustrates the deposit capture probes in situ. (This figure also includes the gas sample probe. This will be discussed further in this chapter - section 3.7).

3.6 Temperature logging

The various temperatures were obtained by applying 'Pico Technology™' hardware. This comprised of two 'TC08' data logger units with associated software. As illustrated in Figure 3.15, the cables connect the 'K' type thermocouples to the data logger. Further specifications on the thermocouples and data logging hardware can be found in Appendix II.

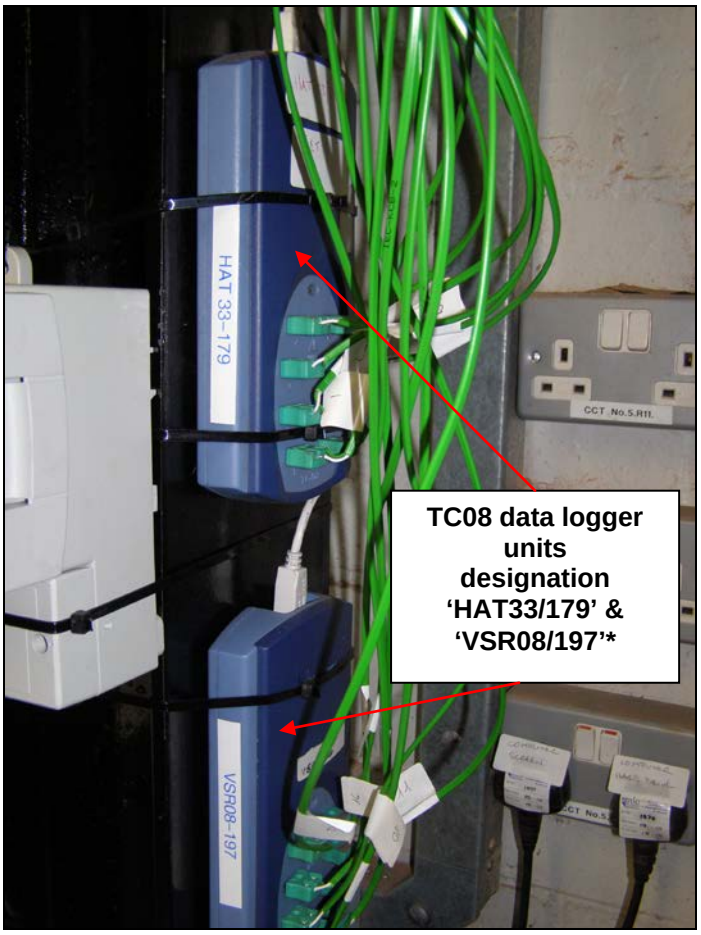

Fig 3.15 – TC08 data loggers

(* The designation of the TCO8 unit numbers are important so that the correct channel numbers for the various thermocouples are set up on the software. Table 3.2 will refer to these allocations)

A display screen provided a real-time insight into the various temperature readings via the Pico Technology software. The data logger units are connected to a standard desk top computer via a USB.

Following a particular test, the software file is saved and imported into a Microsoft Excel spreadsheet for further analysis. The designation of the TCO8 logger hardware were given the allocation of the various thermocouples. These are shown in Table 3.2. These allocations remained unchanged throughout the tests.

Pico logger designation HAT 33/179 (USB port)

Channel #	Wire label	Area
1	1	Probe 1- Inlet surface
2	2	Probe 1 – Outlet surface
3	3	Probe 1 – Exhaust air
4	4	Probe 2 – Inlet surface
5	5	Probe 2 - Outlet surface
6	6	Probe 2 – Exhaust air
7	7	Probe 3 – Inlet surface
8	8	Probe 3 – Outlet surface

Pico logger designation VSR08/197 (USB port)

Channel #	Wire label	Area
1	9	Probe 3 – Exhaust air
2	10	Combusted gas temperature
3	11	Gas analyser tube temperature
4	12	spare
5	13	spare
6	14	spare
7	15	spare
8	16	spare

Table 3.2 – Pico logger channel designation for the deposit capture probes

Figure 3.16 illustrates the locations of the thermocouples on the deposit capture probe.

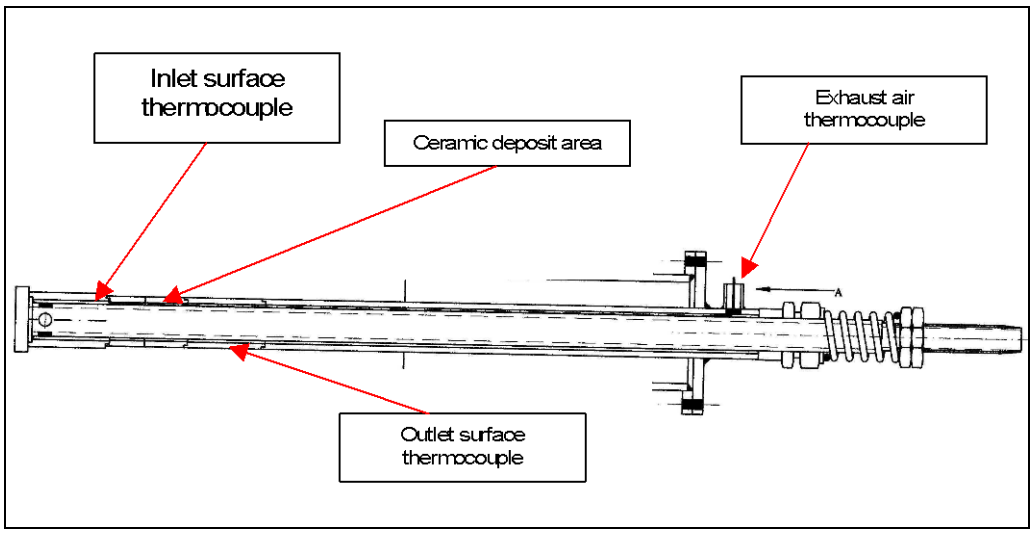

Fig 3.16 – Thermocouple locations on the deposit capture probe

3.7 Gas Analysis

The combustion gas analysis element of this research was another area where vast improvements have been made during this research.

Initially, the gas analysis utilised a quad-band, infrared analyser measuring carbon monoxide (CO), carbon dioxide (CO_2), sodium dioxide (SO_2) and oxygen (O_2) species. A separate analyser was used for nitrous oxide (NO_x) species. The outputs from these analysers were connected to the same type of 'Pico Technology' used for the temperature logging of the deposit capture probe. However, due to different compatibility of existing equipment in the centre, a small set of resistors were used to obtain the 4-20 mA signal required for collecting the data via the TC08. A second laptop was also used with a TC08 unit to assist in the data collection for the temperature logging. The analysis equipment required a number of in line filters, insulated gas lines, moisture traps and three separate pumps. This was found to be very labour intensive during testing and also produced sporadic data. Data from this method will not be presented in this thesis.

After May 2009, a FTIR analyser (Fourier Transform Infrared) spectroscopy was purchased that was far easier to control during the course of the experiments and to prepare for the next scheduled experiment. Figure 3.18 shows the unit in use and it relation to the overall setup of the workstation. Further details in Appendix I.

The FTIR assembly consists of the following apparatus:

- Main FTIR unit – this contains the gas cell, optics and purge / zero gas ports
- 5m heated line
- Dual pump system
- A heated gas sample probe
- Dedicated laptop with 'Protea' gas analyser control software

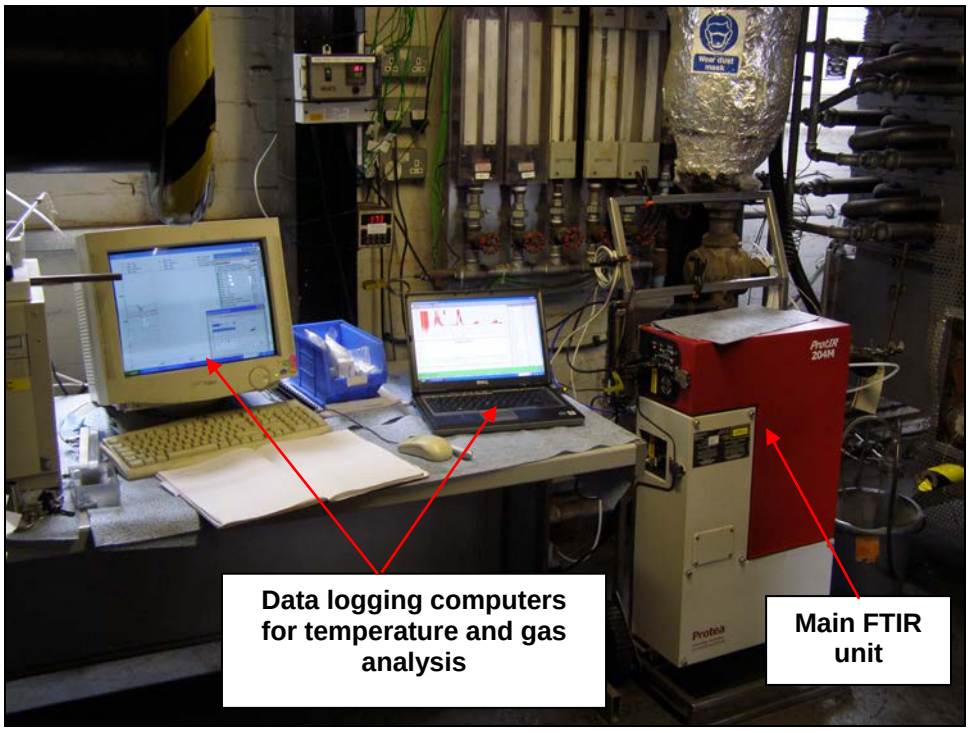

Fig 3.18 – The FTIR unit with associated data logging computers for temperature and gas analysis.

The gas sample probe is connected directly into the vertical chamber of the combustor (Figure 3.14 previously illustrated). This location was considered the best position for the gas analysis for accuracy at the point of deposition capture. Its position remained unchanged throughout the test series.

The gas sample probe is a independently heated unit that contains a 2μm ceramic filter (further details are in Appendix). The unit heated to 180 °C so that water condensation is eliminated. In addition, the unit has a 5m heated line that is attached to assist in keeping the sample gas at a constant temperature before analysis in the FTIR unit's gas cell. There is also the capability to purge the unit with nitrogen before and after sampling. Figure 3.19 illustrates the required set up of the FTIR unit before the gas samples are taken.

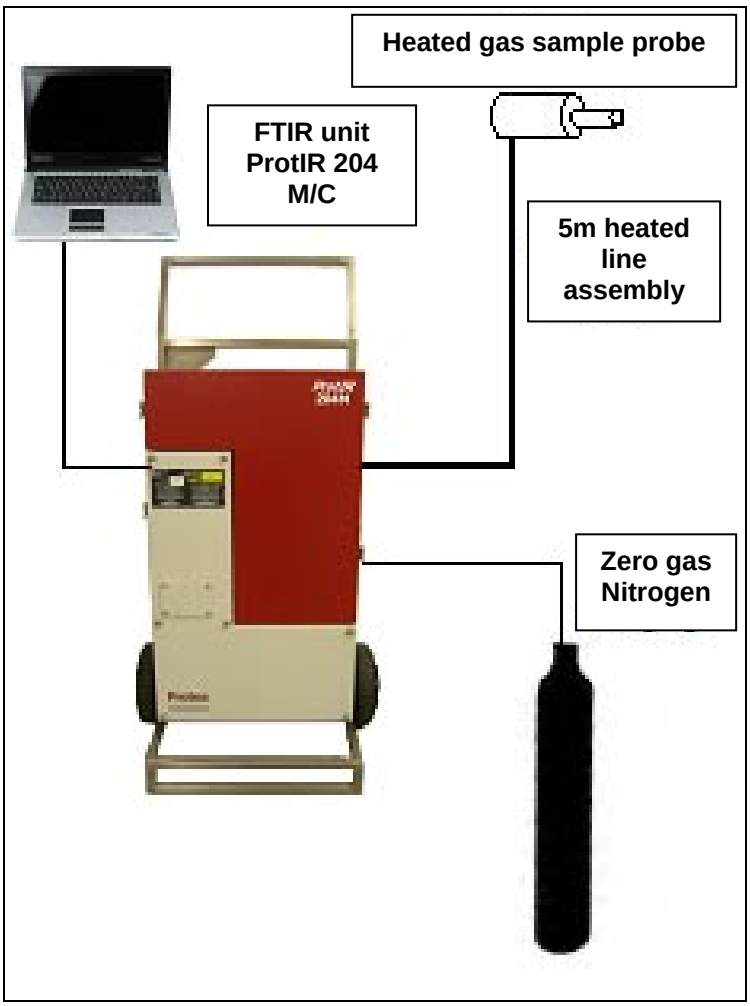

Fig 3.19 – Schematic of the FTIR unit (courtesy of Protea Ltd)

The gas species are drawn into the FTIR unit via the pump system that is positioned on the 'clean' side of the FTIR unit and the gas is exhausted to atmosphere.

FTIR system carries out its analysis by drawing combusted gas through the gas cell contain in the FTIR. Absorption takes place in the infrared cell and a comparison is carried out against stored absorption spectra standards.

The unit is able to identify a greater number of species than the previous units were unable to ; eg: hydrogen chloride (HCl), Ammonia (NH_3), and hydrogen cyanide (HCN). All species are shown in ppm valves. Water (H_2O), CO_2 and O_2 are expressed as vol%. A full list of detected species are presented in Chapter 4.

The combustion gas composition data is presented in real time in graphical and numerical form on the display screen. This shows the following information:

- A graphical 'spectrum' is produced from the absorption scan of the species. Six scans are produced for each spectra group and the result of this group is displayed in the 'data viewer' (see explanation below).
- A graphical 'trend' of the various gas species illustrates the levels of detection.
- A 'data viewer' gives a numerical value for the species detected .

Once a test has finished, the data is exported onto 'Excel' spreadsheets for further analysis.

3.8 Deposit collection method

Following an experiment, all probes were carefully removed from the vertical chamber for processing. This involves photographing, collection and weighing of the deposit, calculation of deposit flux and samples taken for scanning electron microscope (SEM) analysis.

Fig 3.20 – probes removed following a test ready for processing
(Daw Mill + 20% CCP)

By visually identifying the boundaries, the deposit was scraped off starting with the lower zone first then working around the circumference until the top deposit was reached. This will be discussed further in Chapter 4 , section 4.3.

The best method for obtaining the deposit was in the following way:

- A clean sheet of white paper was placed under the probe.
- Starting from the underside, a scalpel blade was utilised to scrape the deposit zone.
- The weight of the bags was noted before filling and then each of the zones were collected in separate bag.

- A clean sheet of paper was placed under the probe every time a new sample was taken.

3.9 Deposit Flux calculations

The calculations for the deposit flux are important as they represent the ratio of deposit that occurs. These results can are then be utilised by other researchers for further investigation into the rate of corrosion in such environments. The results of the deposit flux will be discussed further in Chapter 4.

3.9.1 The calculations

Each of the ceramic catch areas were measured. As they were found to not to be perfect cylinders, an average was calculated for each cylinder sample. The dimensions of each of the ceramic cylinders are shown in Appendix III.

A careful, circumferential indication was taken of the deposit affected areas with a piece string and then measured to obtain the width for the calculation of the total area.
The following example was taken from a #2 ceramic cylinder . This method was applied to all the deposit calculations in all tests.

The calculations take the curved surface area of the cylinder:

$$A = 2 \pi r h \qquad [15]$$

Where: A = area of the cylindrical surface

r = radius of cylinder

h = height of cylinder

The segmental surface area was calculated allowing for the curvature of the surface.

∴ Dimensions of #2 ceramic deposit area: (dimensions in mm's)

(average) Ø 39.005
r = 19.5025

Total surface area of cylinder = $2 \pi r h$

Where:

Radius (r) = 19.5025

Height (h) = 60

= 2 x 3.142 x 19.5025 x 60
= 9235.11 mm^2

Area of each segment:

Top 20 x 60 = 1200 mm^2
Side $(30 \times 60)^2$ = 4080 mm^2
Base 3973 mm^2 (remaining)

The deposit flux was then calculated in by the following equation:

$$\frac{\frac{\text{Ash weight (mg)}}{\text{Area (cm}^2\text{)}}}{\text{Time (hrs)}} = \text{mg/cm}^2\text{/hr}$$

An example of the layout of results for each test are shown in Table 3.1.

Cylinder part	Area (mm^2)	Sample weight (g)	Sample + Bag (g)	Difference (mg)	Deposit Flux ($mg/cm^2/hr$)
Top	1200.00	0.89236	1.22782	335.46000	**11.182**
Side	4080.00	0.90530	0.92509	19.79000	**0.194**
Underside	3973.00	0.89337	0.90618	12.81000	**0.129**
Totals	9253.00			368.06000	**11.505**

Table 3.3 – Example of results calculated

Comprehensive results of the calculations are discussed in Chapter 4.

3.10 Ceramic Deposit encapsulation

Once a test had been completed, a one off attempt was made to encapsulate the deposit by sealing it in resin for further examination. This was achieved by a certain amount of trial and error. The following method of capture was applied to the 100% CCP trial.

Once the probe was removed from the rig, the deposit was glued using a product called 'Photomount ™' – an aerosol application glue. This was sprayed onto the top of the area and allowed to fall. This was repeated several times – with drying times between each application. Securing the deposit to the cylinder would also limit the deposit moving freely around in the solution once the resin was poured. The ceramic tube was then removed from the main probe assembly. (Figures 3.21 and 3.22 illustrate)

Fig 3.21 – End view of the ceramic with glued ash deposit

Fig 3.22 – Side view of the ceramic with glued ash deposit

The moulding process was a variation on previous, standard moulding procedure but on a larger scale. A PTFE resin mould was utilised as the base and three stainless steel rings place atop of each other. A thin sheet of stainless steel sheet (16 swg) was wrapped around the assembly and secured in place with two 'jubilee' clips. (see Figure 3.23). The inside of the unit was covered in high vacuum grease to allow ease of disassembly. The cylinder was placed vertically into the mould with the mixture of resin / ballotini poured slowly, within the ceramic tube and then around the deposit area. See Figure 3.24.

One concern that was apparent was when the unit was placed in the vacuum chamber to remove residual air pockets that the deposit would be dislodged. Figure 3.32 clearly shows an amount of air rising to the surface

.

Figure 3.23 – Mould assembly with ceramic shown inside the mould

Figure 3.24 – Resin / Ballotini applied to mould

Once the resin had been left to dry, the mould was removed (Figure 3.25) and was prepared for cutting and polishing for further examination.

Fig 3.25 – Mould removed from resin cast ceramic tube

Fig 3.26 – Cross-section of deposit

4. Results

4.1 Introduction

The results of the experimental work contains the following :

- PF feed calibration
- Visual observation of deposit behaviour
- Photographic details of 100% 'pure' fuels test series
  - Daw Mill coal
  - El Cerrejon coal
  - Miscanthus biomass
  - CCP biomass
- Extensive analysis of the Daw Mill CCP test series
  - SEM / EDX
  - Deposit comparison
  - Gas analysis
  - Temperature profile of deposit probes

4.2 PF Feed Delivery calibration

As previously stated in Chapter 3, section 3.4.1, the PF delivery system was tested and several fuel feed rates were produced. These are average results as there are a number of other factors that influenced the final figures.

Table 4.1 illustrates the calibration results of the PF feed assembly.

Shaker Setting	Time run (mins)	Start Weight (kgs)	End Weight (kgs)	Weight Diff (kgs)	Kg/hr
10	5	0.9	1	0.1	1.2
20	5	1	1.2	0.2	2.4
30	5	1.2	1.9	0.7	8.4
40	5	1.9	2.8	0.9	10.8
50	5	1	2.1	1.1	13.2
60	5	2.1	3.4	1.3	15.6
70	5	2.9	4.5	1.6	19.2

Table 4.1 - Calibration results of PF feeder assembly

4.3 Visual observations

It was noted throughout the experimental work that distinct deposit divisions were formed on the ceramic capture surface. These varied greatly in size, area and consistency. These sectors are illustrated in Figure 4.1. The identifying areas of 'Top', 'Side' and 'Base' will be used throughout this chapter.

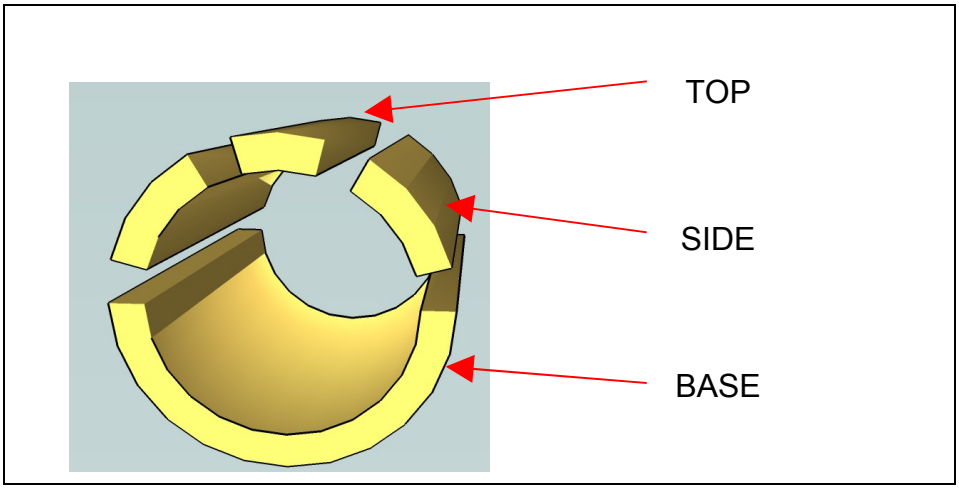

Fig 4.1 – An exploded view of the graphical illustration of the division on the ceramic capture surface

4.3.1 Photographic illustrations of 'Pure Fuels' test series and Daw Mill / CCP blends

Figures 4.2 - 4.13 illustrate the variance of deposit in relation to the pure fuels - ie: Daw Mill, El Cerrejon, CCP and Miscanthus. The resultant deposits have come from an average 3 hour test run. Three out of the four deposits have used an average of 9 kg/hr - (PF fuel feed setting of ~ 35 –Table 4.1, section 4.2). The Miscanthus used 40kg in total – 13kg/hr (PF fuel feed setting of ~ 45 – Table 4.1, section 4.2).

The two pure fossil fuels, i.e.: Daw Mill and El Cerrejon show a far greater difference in deposit structure compared to the two biomass fuels (CCP and Miscanthus). The Daw Mill fuel illustrates a greater circumferential deposit compared to the El Cerrejon fuel despite having similar test conditions, run time and quantity of fuel used. The CCP deposit displays a much more fibrous, concentrated deposit structure on the top with little circumferential deposit on the side or base or the probe. Miscanthus shows little deposit despite the test utilising more fuel (40kg – 13kg/hr). The colour of the deposits varies greatly. A light brown/yellow colour is observed in the Daw Mill and Miscanthus deposit compared to a much darker deposit on the El Cerrejon. The CCP shows a mid grey to dark grey deposit colour.

Figures 4.14 – 4.25 illustrate the variance in deposit of the Daw Mill and CCP blends, i.e.: 20, 40, 60 and 80 % (wt%). In all cases, a circumferential deposit was observed. Daw Mill 20, 60 and 80% blends show a reasonably consistent colour – getting slightly darker at the Daw Mill and 80% blend. The Daw Mill and 40% CCP illustrates a much darker deposit.

Daw Mill coal (100%)- 3.5 hour run – 28kg used

(Probe temperatures expressed as a Mean surface temperature during test run)

Fig 4.2 Probe # 1 – (670 °C)

Fig 4.3 Probe # 2 – (580 °C)

Fig 4.4 Probe # 3 – (505 °C)

El Cerrejon coal (100%) - 3 hour run – 27.5 kg used

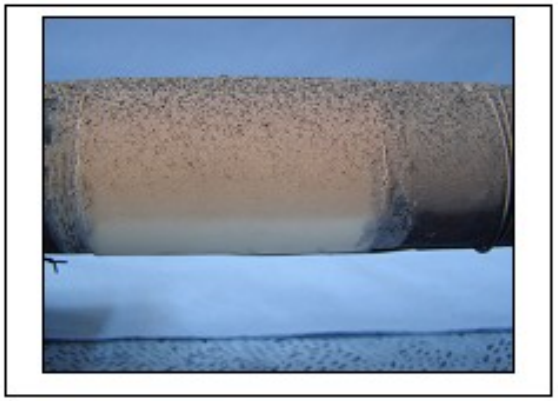

Fig 4.5 – Probe #1 – (655 °C)

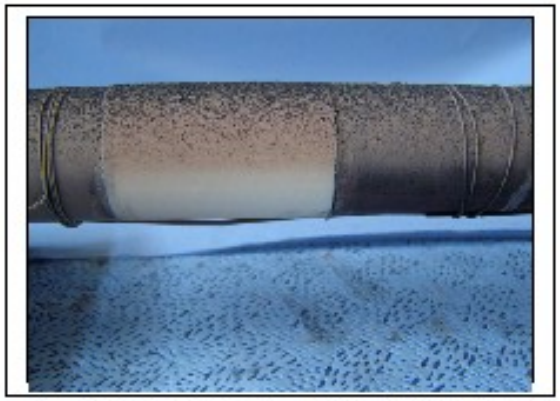

Fig 4.6 – Probe #2 – (600 °C)

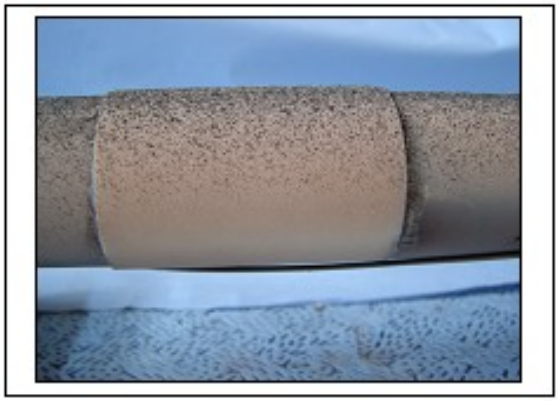

Fig 4.7 – Probe #3 – (540 °C)

CCP (Cereal Co-product) - 2.75 hour run – 27.5 kg used

(Probe temperatures expressed as a Mean surface temperature during test run)

Fig 4.8 – Probe #1 – (640 °C)

Fig 4.9 – Probe #2 – (570 °C)

Fig 4.10 – Probe #3 – (510 °C)

Miscanthus (*Giganteus* variety) - 3 hour run – 40 kg used

Fig 4.11 – Probe #1 – (675 °C)

Fig 4.12 – Probe #2 – (605 °C)

Fig 4.13 – Probe #3 – (540 °C)

Daw Mill coal + 20% CCP (wt%) coal - 3.25 hour run – 30kg used

(Probe temperatures expressed as a Mean surface temperature during test run)

Fig 4.14 Probe # 1 – (690 °C)

Fig 4.15 Probe # 2 – (590 °C)

Fig 4.16 Probe # 3 – (505 °C)

Daw Mill coal + 40% CCP (wt%)- 3.45 hour run – 28.5kg used

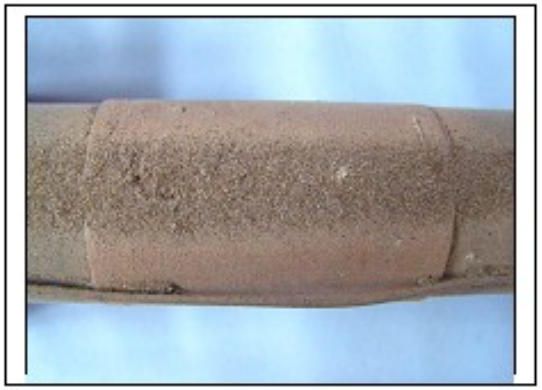

Fig 4.17 Probe # 1 – (670 °C)

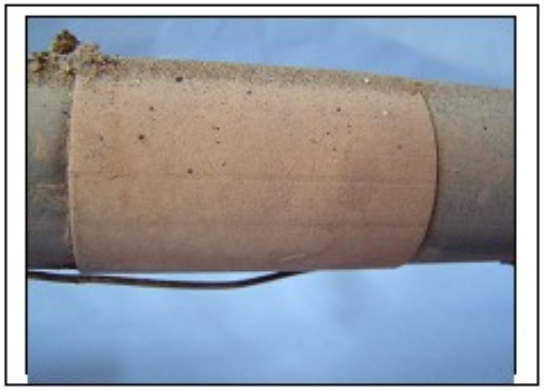

Fig 4.18 Probe # 2 – (580 °C)

Fig 4.19 Probe # 3 – (510 °C)

4.4 SEM analysis

The following SEM images (Figures 4.27 – 4.44c) are deposit samples following combustion tests - Daw Mill and CCP (pure fuel) and the Daw Mill + CCP test series (20, 40, 60 and 80%) . All images are at 1mm scale and taken utilising a Siemens ESEM X200 and 'Inca' software.

Ash samples were successfully taken from all the probes. The only exceptions to this was Daw Mill (pure fuel) -,probe #1, base section and Daw Mill + 40% CCP – probe #1, base section. CCP (pure fuel) had a few more areas where no viable sample could be taken – probe #1, side and base sections, probe #2, base section and probe #3, base section.

Figures 4.27a – 4.38c illustrate the sequence from Daw Mill + 20% CCP through to Daw Mill + 80% CCP. They show distinct but subtle changes have occurred in particle size on all probes. The top, side and base sections of all probes shows a gradual change in particle size within the blends. The lower blends of Daw Mill to CCP; e.g.: Daw Mill + 20% CCP, a porous structure has formed on the side section (Fig 4.29b) compared to a far greater particle size on the side of Daw Mill + 80% CCP (Fig 4.37b).

Figures 4.39a – 4.44c); the pure fuels – Daw Mill and CCP, have show a similar trend compared to the Daw Mill + CCP blends. The Daw Mill - top section illustrate a large, granular sample as does the CCP. However the latter appears longer and less uniform in shape

SEM / EDX analysis – 'Daw Mill' + CCP test series

Probe 1 – Daw Mill + 20% CCP (wt %

Fig 4.27 – Probe 1

Fig 4.27a - top

Fig 4.27b – side

Fig 4.27c – base

Probe 2 – Daw Mill + 20% CCP (wt %) (1mm magnification)

Fig 4.28- Probe 2

Fig 4.28a - top

Fig 4.28b – side

Fig 4.28c – base

SEM / EDX analysis – 'Daw Mill' + CCP test series

Probe 3 – Daw Mill + 20% CCP (wt %)

Fig 4.29 – Probe 3 top

Fig 4.29a - top

Fig 4.29b – side

Fig 4.29c – base

SEM / EDX analysis – 'Daw Mill' + CCP test series

Probe 1 – Daw Mill + 40% CCP (wt %) (1mm magnification)

Fig 4.30 – Probe 1

Fig 4.30a - top

Fig 4.30b – side

No viable sample

Fig 4.30c – base

Probe 2 – Daw Mill + 40% CCP (wt %) (1mm magnification)

Fig 4.31 – Probe 2

Fig 4.31a - top

Fig 4.31b – side

Fig 4.31c – base

SEM / EDX analysis – 'Daw Mill' + CCP test series

Probe 3 – Daw Mill + 40% CCP (wt %) (1mm magnification)

Fig 4.32 – Probe 3

Fig 4.32a - top

Fig 4.32b – side

Fig 4.32c – base

SEM / EDX analysis – 'Daw Mill' + CCP test series

Probe 1 – Daw Mill + 60% CCP (wt %) (1mm magnification)

Fig 4.33 – Probe 1

Fig 4.33a- top

Fig 4.33b side

Fig 4.33c – base

Probe 2 – Daw Mill + 60% CCP (wt %) (1mm magnification)

Fig 4.34 – Probe 2

Fig 4.34a - top

Fig 4.34b – side

Fig 4.34c – base

SEM / EDX analysis – 'Daw Mill' + CCP test series

Probe 3 – Daw Mill + 60% CCP (wt %) (1mm magnification)

Fig 4.35 – Probe 2

Fig 4.35a - top

Fig 4.35b – side

Fig 4.35c – base

SEM / EDX analysis – 'Daw Mill' + CCP test series

Probe 1 – Daw Mill + 80% CCP (wt %) (1mm magnification)

Fig 4.36 – Probe 1

Fig 4.36a - top

Fig 4.36b – side

Fig 4.36c – base

Probe 2 – Daw Mill + 80% CCP (wt %) (1mm magnification)

Fig 4.37 – Probe 2

Fig 4.37a - top

Fig 4.37b – side

Fig 4.37c – base

SEM / EDX analysis – 'Daw Mill' + CCP test series

Probe 3 – Daw Mill + 80% CCP (wt %) (1mm magnification)

Fig 4.38 – Probe 3

Fig 4.38a - top

Fig 4.38b – side

Fig 4.38c – base

SEM / EDX analysis – 'Daw Mill' (pure fuel)

Probe 1 – Daw Mill 100% (wt %) (1mm magnification)

Fig 4.39 – Probe 1

Fig 4.39a - top

Fig 4.39b – side

No viable sample

Fig 4.39c – base

Probe 2 – Daw Mill 100% (wt %) (1mm magnification)

Fig 4.40 – Probe 2

Fig 4.40a - top

Fig 4.40b – side

Fig 4.40c – base

SEM / EDX analysis – 'Daw Mill' (pure fuel)

Probe 3– Daw Mill 100% (wt %) (1mm magnification)

Fig 4.41 – Probe 3

Fig 4.41a - top

Fig 4.41b – side

Fig 4.41c – base

SEM / EDX analysis – Cereal co-product (CCP) (pure fuel)

Probe 1– CCP 100% (wt %) (1mm magnification)

Fig 4.42 – Probe 1

Fig 4.42a - top

No viable sample

Fig 4.42b – side

No viable sample

Fig 4.42c – base

Probe 2– CCP 100% (wt %) (1mm magnification)

Fig 4.43 – Probe 2

Fig 4.43a - top

Fig 4.43b – side

No viable sample

Fig 4.43c – base

SEM / EDX analysis – Cereal co-product (CCP) (pure fuel)

Probe 3– CCP 100% (wt %) (1mm magnification)

Fig 4.44 – Probe 3

Fig 4.44a - top

Fig 4.44b – side

No viable deposit

Fig 4.44c – base

4.5 Temperature profile

Temperature profiles were produced for all combustion tests. The temperature was recorded in °C and over an average test time of 3 hours.

The following illustrations (Figures 4.45, 4.46 and 4.47) show examples of the temperature profiles obtained in real-time taken from three tests; Daw Mill + 40% CCP; Daw Mill and CCP as pure fuels. They illustrate the average temperatures for each of the probes as well as the vertical chamber's gas temperature. They also give an indication on how successful the fuel feed was with keeping the temperature stable. This aspect will be discussed in further detail in the next chapter

Figures 4.48 and 4.49 illustrate the average temperature for the deposition probes and vertical chamber gas temperature for all pure fuel tests and Daw Mill + CCP series respectively. These bar charts also have an error bar factored in. This again is an indication to how successful a particular experiment was in keeping a constant feed rate and temperature and will be discussed in the next chapter.

The remaining real-time temperature data for Daw Mill + 20%, 60% and 80% CCP blends are illustrated in the Appendix.

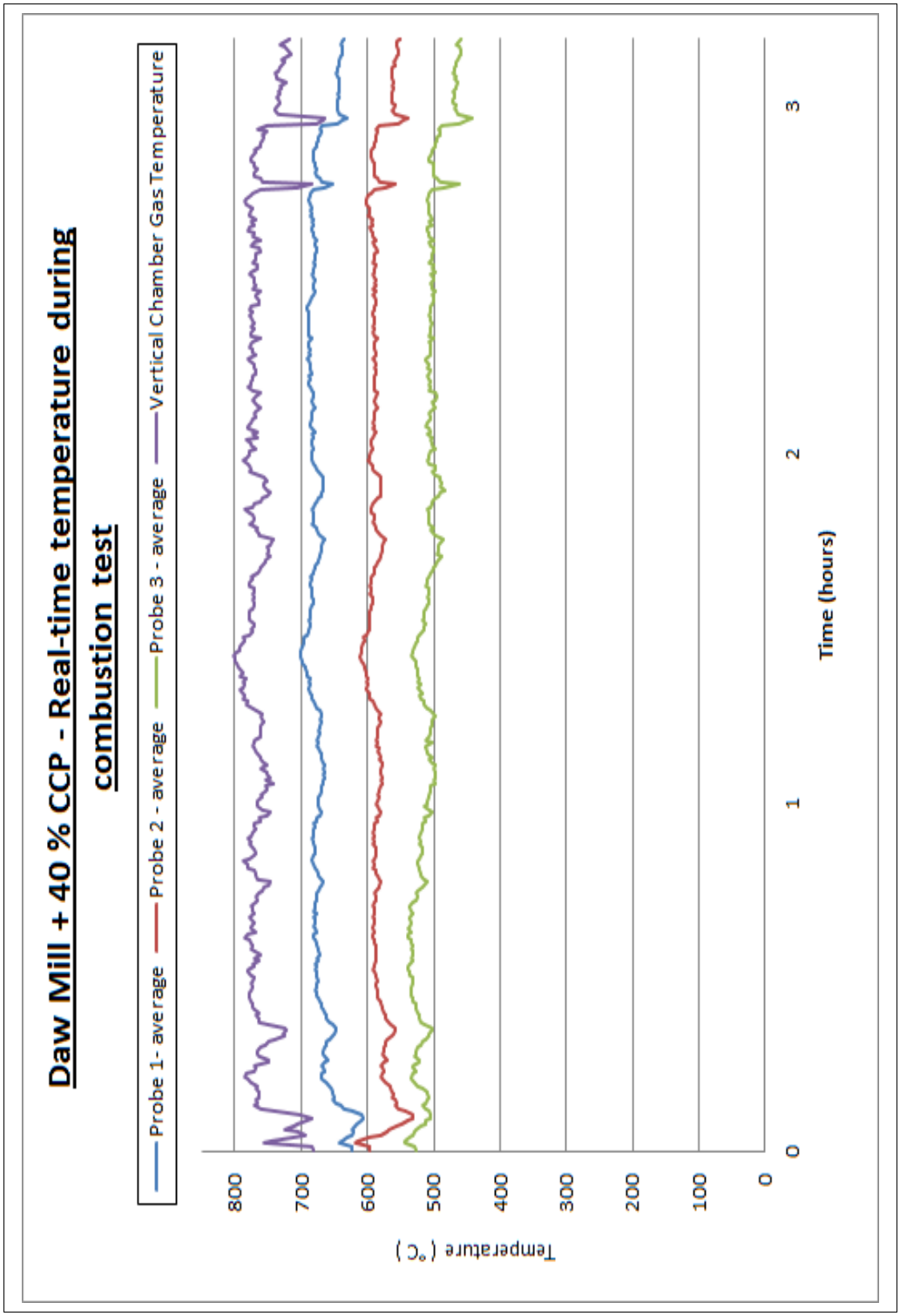

Fig 4.45 – Example 1 of 'real-time' temperature profile of the three deposition probes (Daw Mill + 40% CCP [wt %]

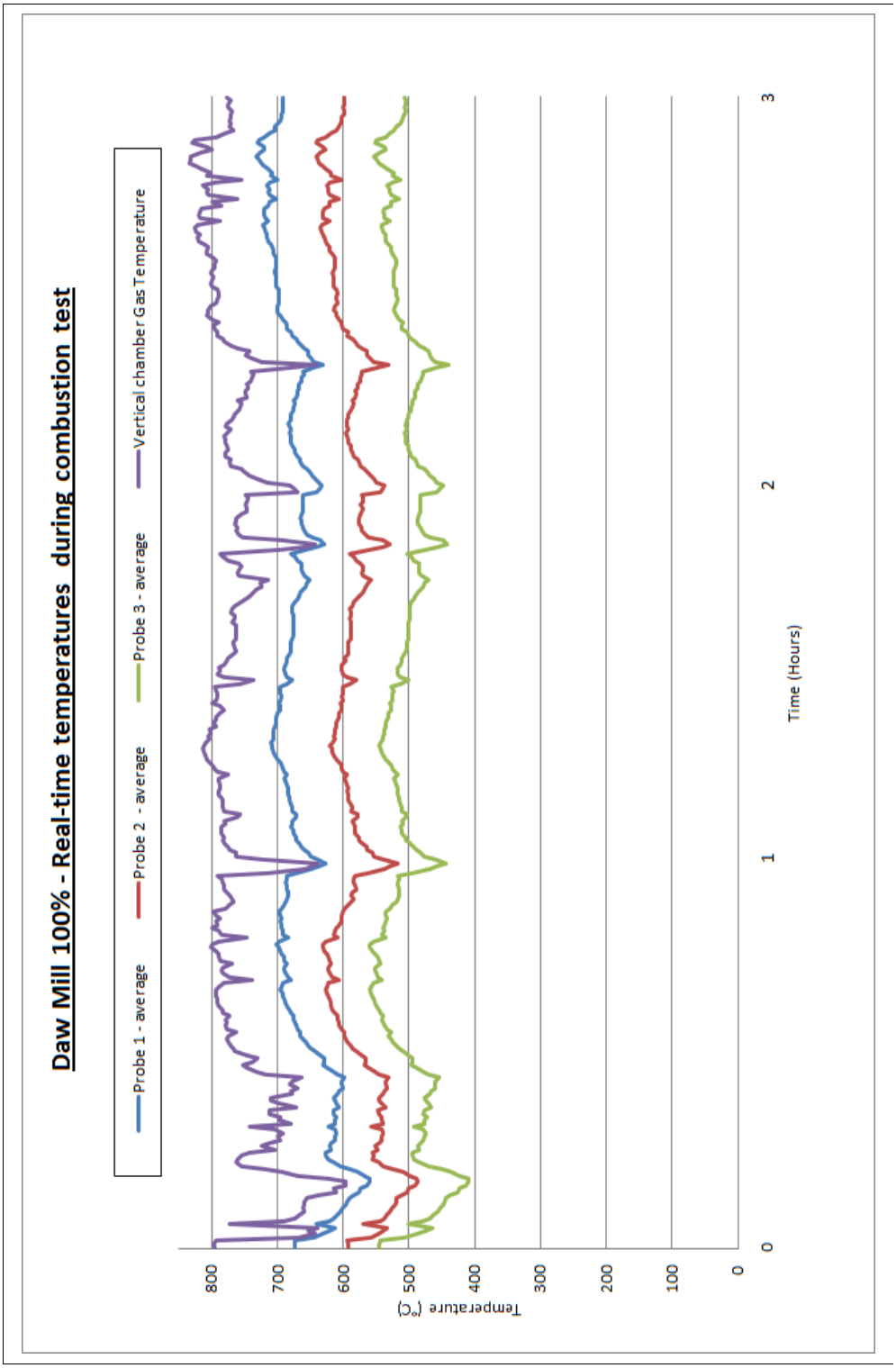

Fig 4.46 – Example of 'real-time' temperature profile of the three deposition probes (Daw Mill (pure fuel)

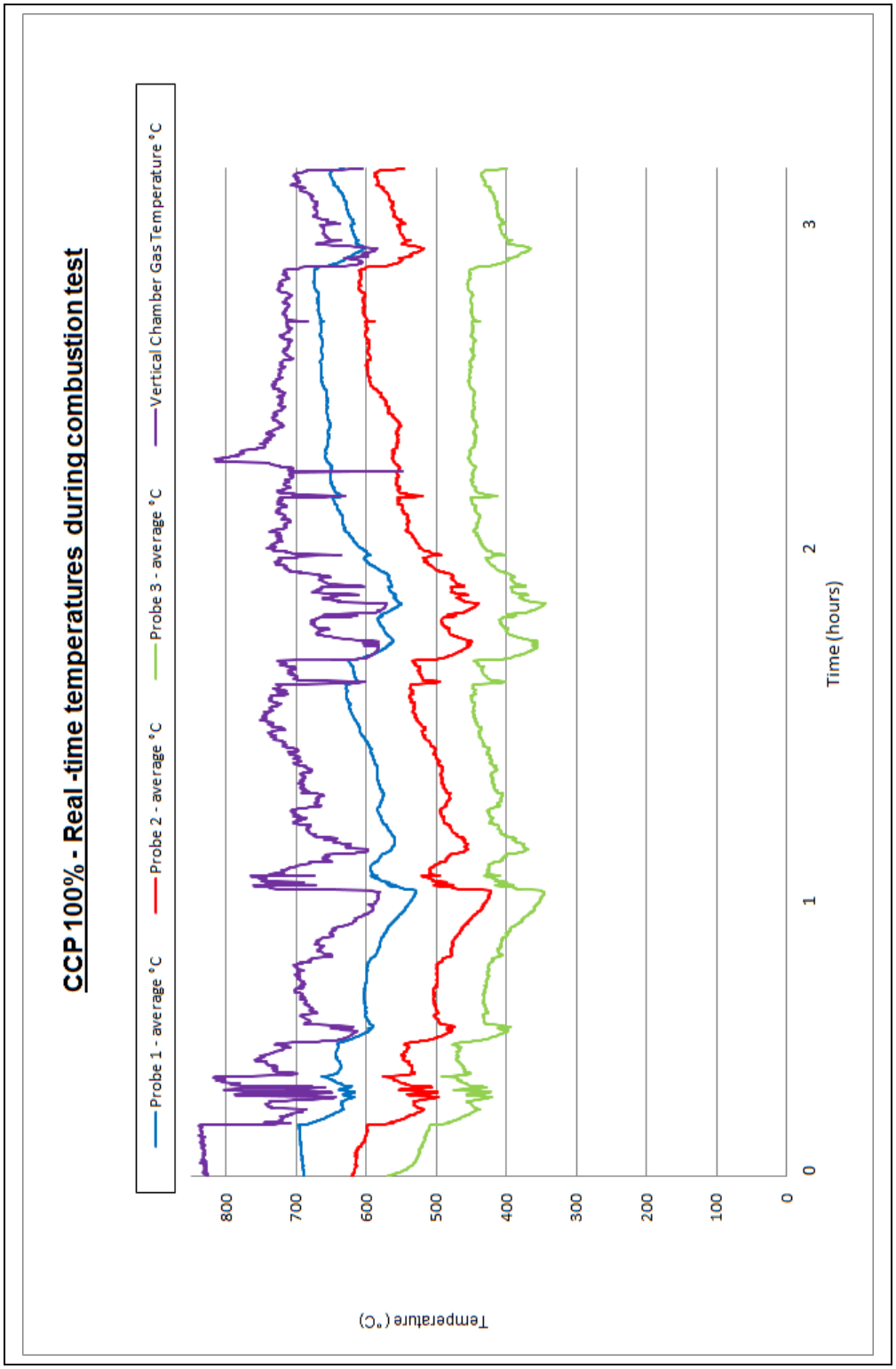

Fig 4.47 – Real-time temperature data during 100% CCP test

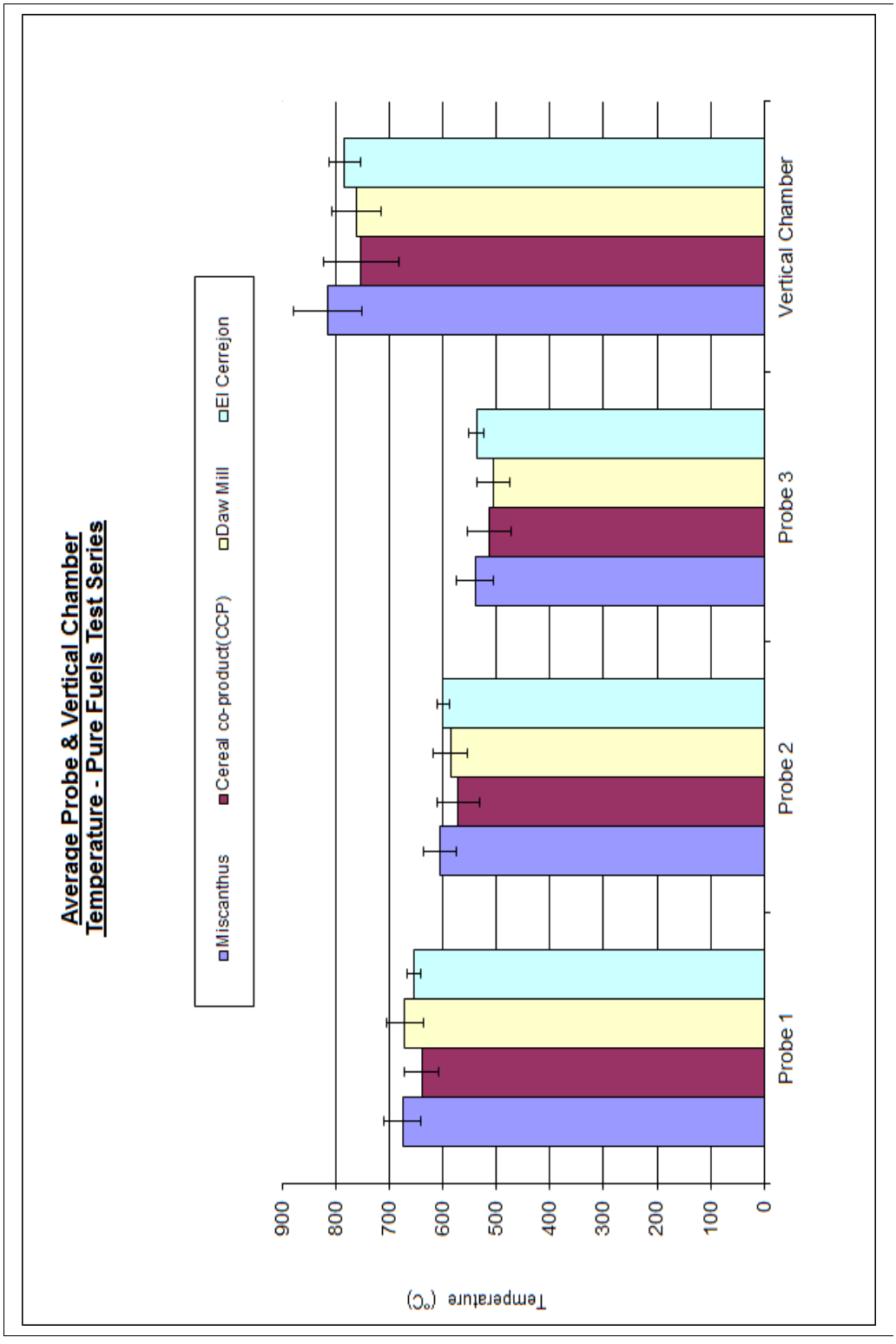

Fig 4.48 – Average temperature of the deposition probes and vertical chamber gas temperature for all pure fuel tests

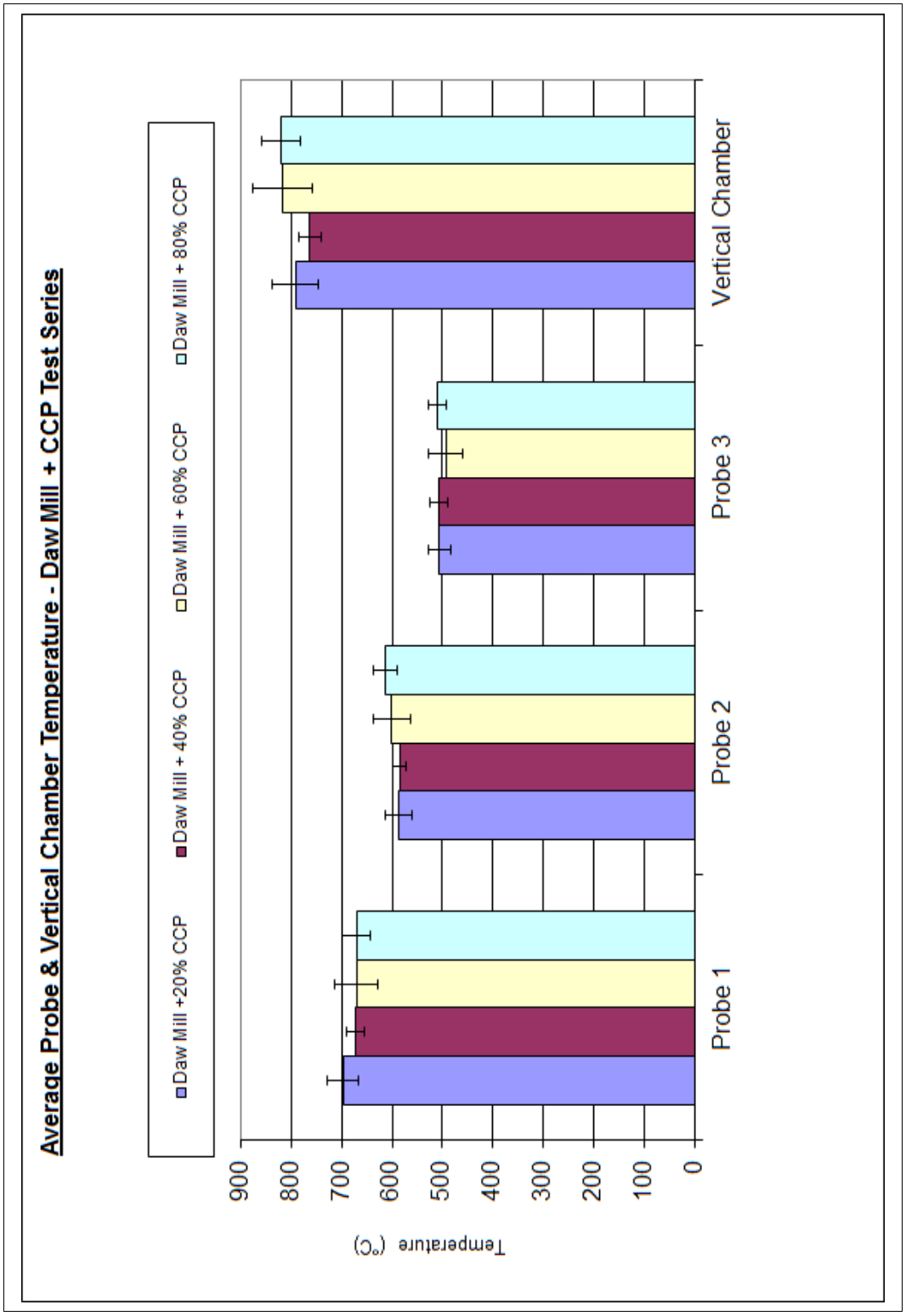

Fig 4.49 – Average temperature of the deposition probes and vertical chamber gas for Daw Mill +CCP test series all pure fuel tests

4.6 EDX analysis for deposits

Figure 4.50 illustrates a summary plot of major elemental EDX analysis for the Daw Mill and CCP test series – both as pure fuels and as blends. The elements are expressed in (wt%) and cover the following elements: Na, Mg, Al, P, S, K, Ca, Ti, Fe, and Si. The trace depicts the trend of the elements present dependant of the content of the fuel blend. For example, Al drops from approximately 13(wt%) to < 1 (wt%) from 100% Daw Mill to 100% CCP respectively . Also, K increases as the blend of CCP to Daw Mill (from ~2(wt% to 17(wt%) . This will be discussed further in the next chapter.

Figure 4.51 illustrates an example of EDX data that illustrates a greater detailed plot of analysis on a different format. This depicts the samples collected from probe #2 (top) for , Daw Mill and CCP as pure fuels and Daw Mill + CCP test series. This data includes other elements that have not been included in Figure 4.50, ie: Mn, Cu, Pb, Pt and Cl.

All numerical values for ESEM analysis can be found in the Appendix.

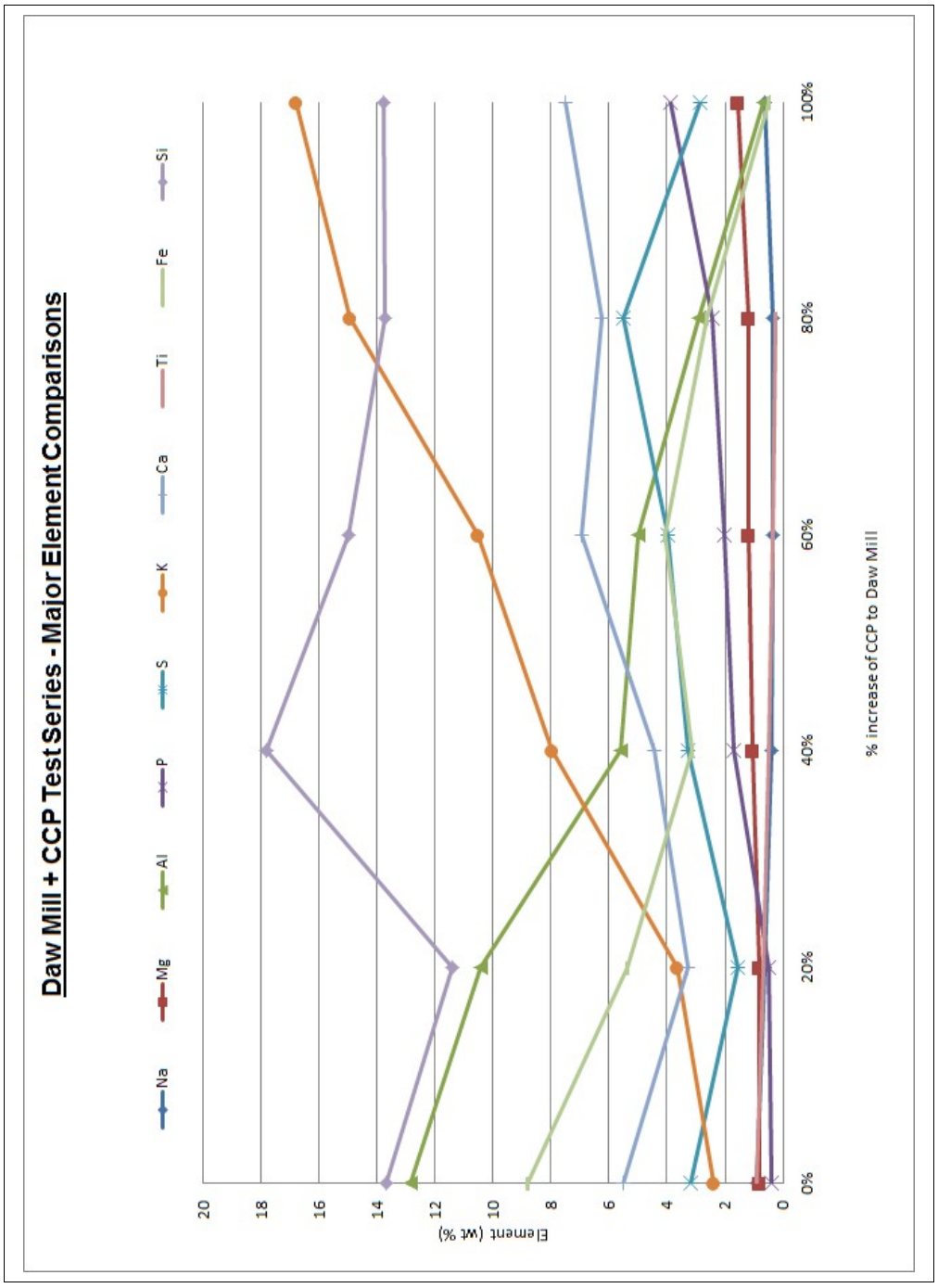

Fig 4.50 – Illustration of major elemental trend comparison from SEM analysis of Daw Mill CCP fuels in addition to their blends

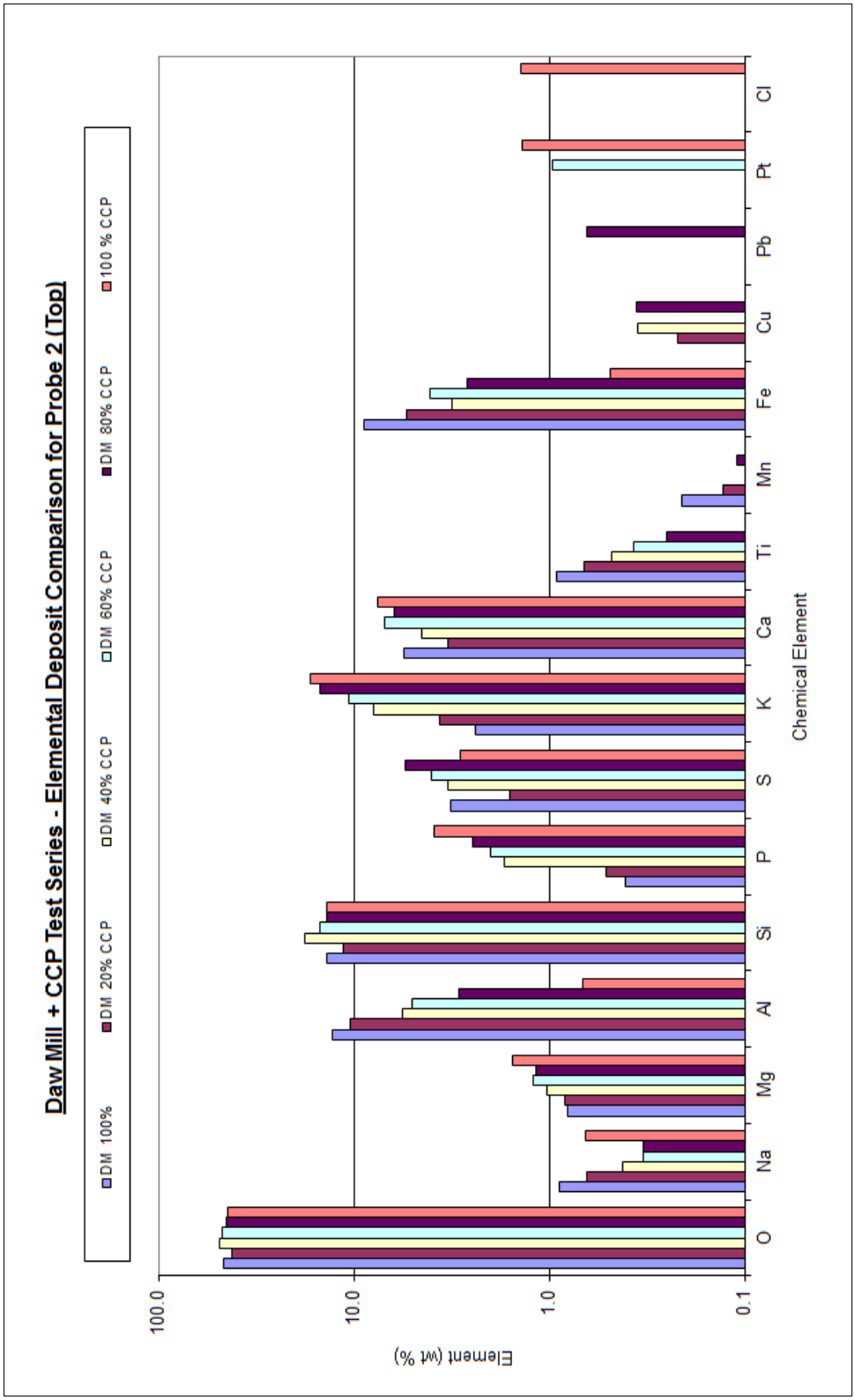

Fig 4.51– An example of EDX data from the deposit for Probe #2 (top)

4.7 Gas analysis

The gas analysis was carried out during the experimental runs by the FTIR unit (Chapter 3, section 3.7. Full specifications are in the Appendix). Major species H_20, CO_2 and O_2 are expressed as volume %. Minor species , eg: HCl, CO and NO_x are expressed in ppm.

Figures 4.52 and 4.53 shows an example of 'real-time' gas analysis data for the Daw Mill + 40% CCP (wt%) test.

The data illustrated in Figure 4.52 shows that H_2O was recorded at ~ 8-10 (vol%) during this time period. O_2 and CO_2 illustrate the data plot as an almost 'mirror image' of each other and show that combustion process was running efficiently. Fig 4.53 illustrates the minor species data collected during the same test run.

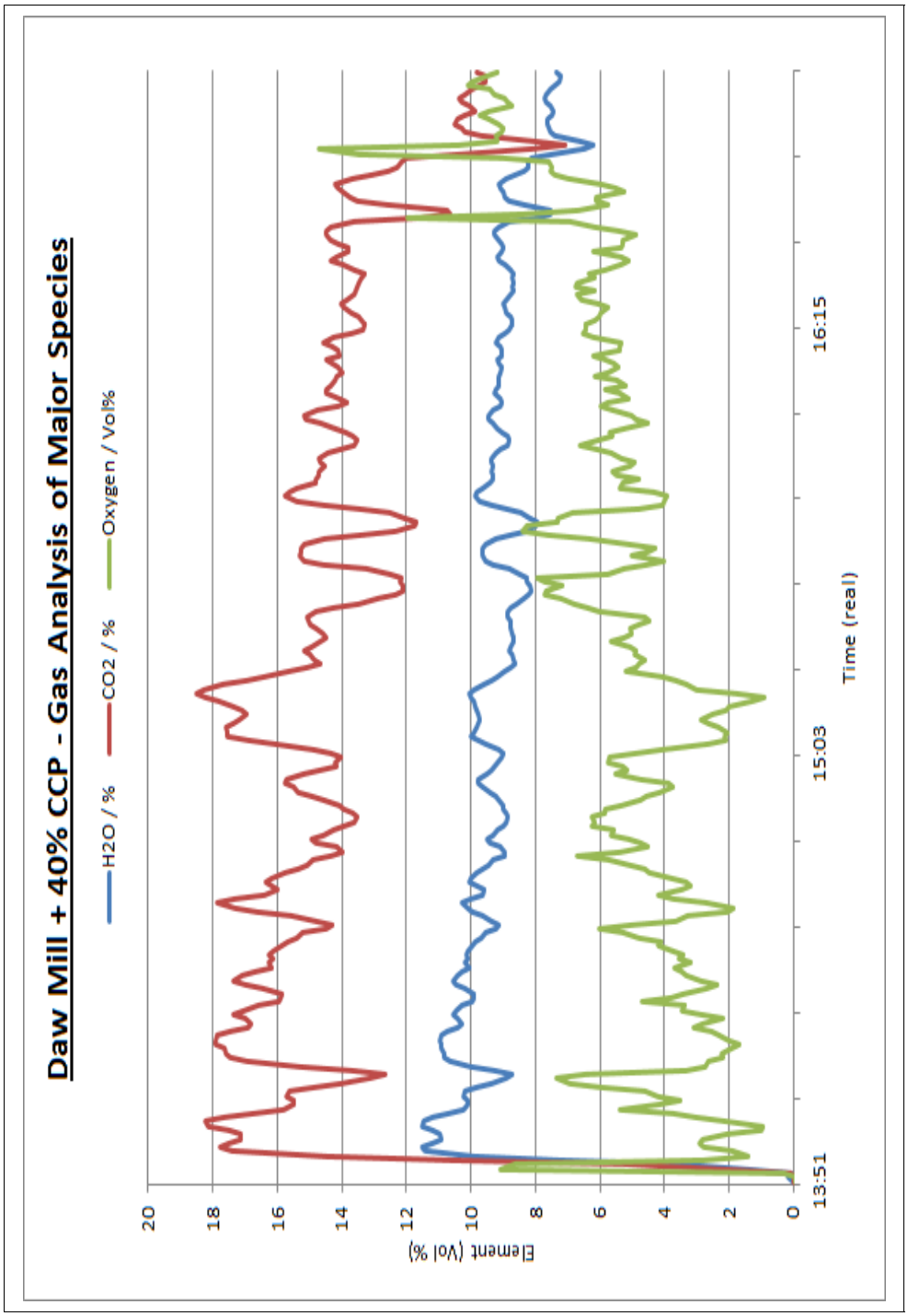

Fig 4.52 – An example of real-time gas analysis (major species for CO_2, O_2 & H_2O

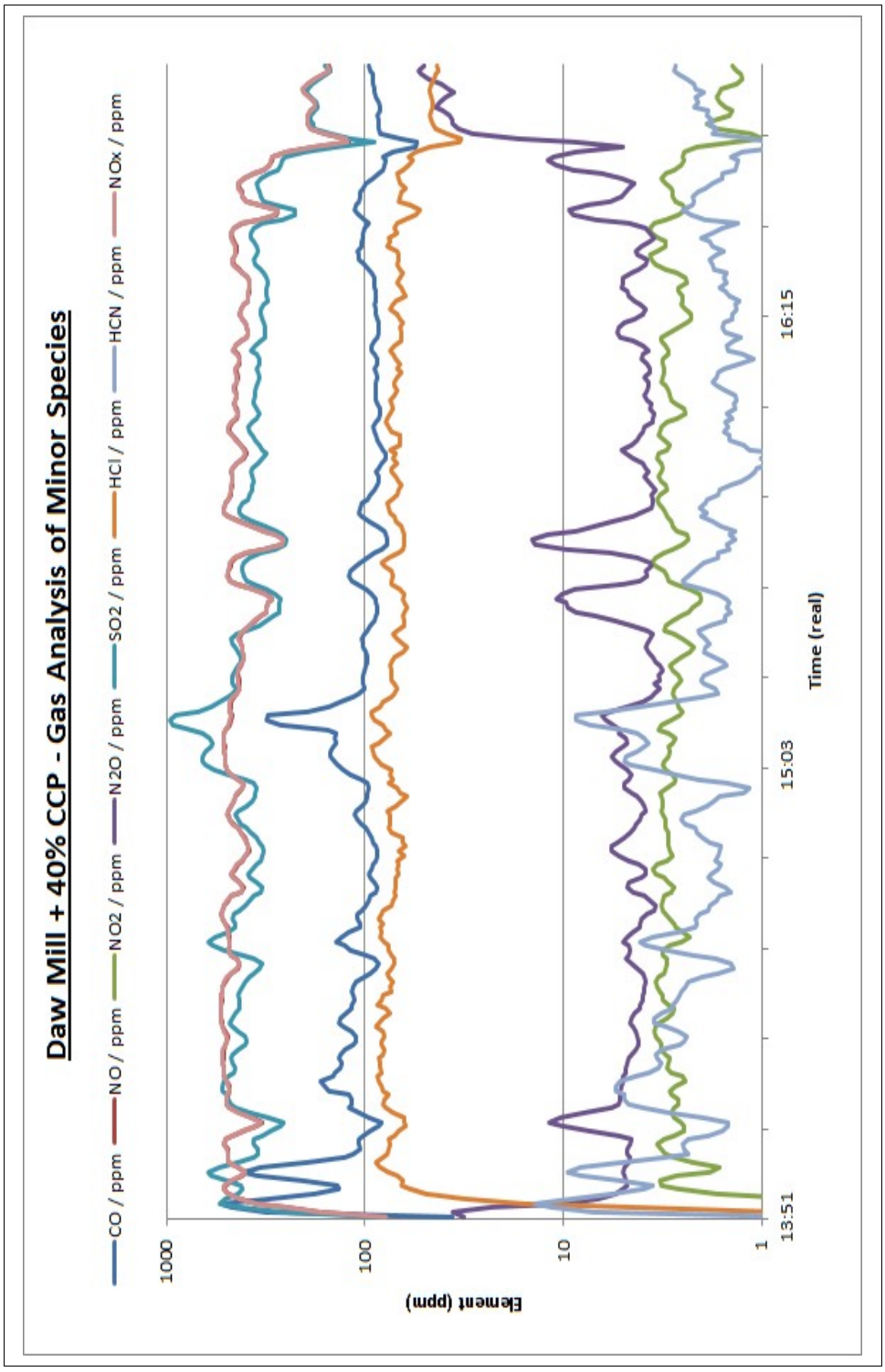

Fig 4.53 – An example of real-time gas analysis (minor species)

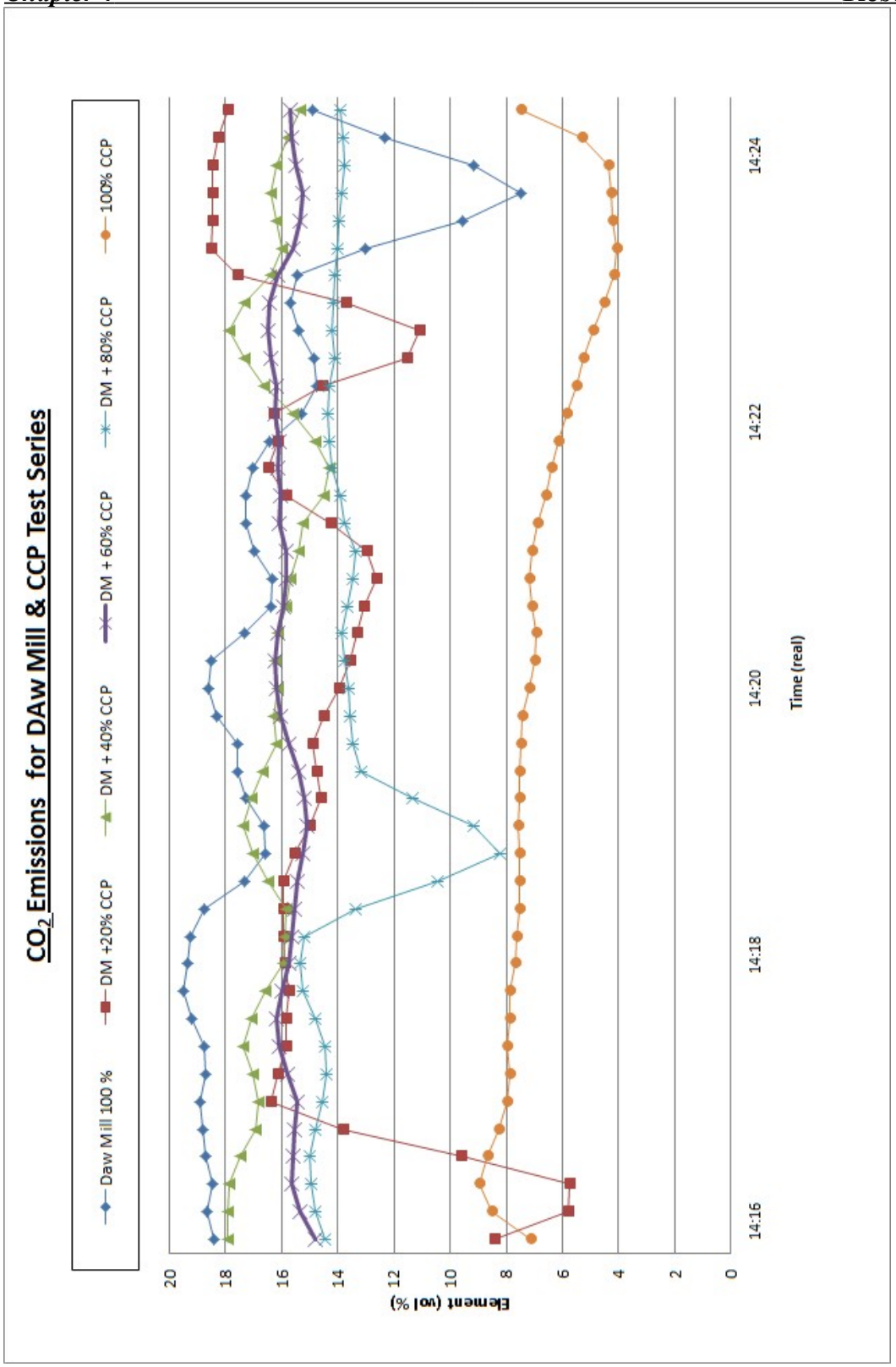

Fig 4.54 – Illustration for CO_2 emissions for Daw Mill & CCP test series

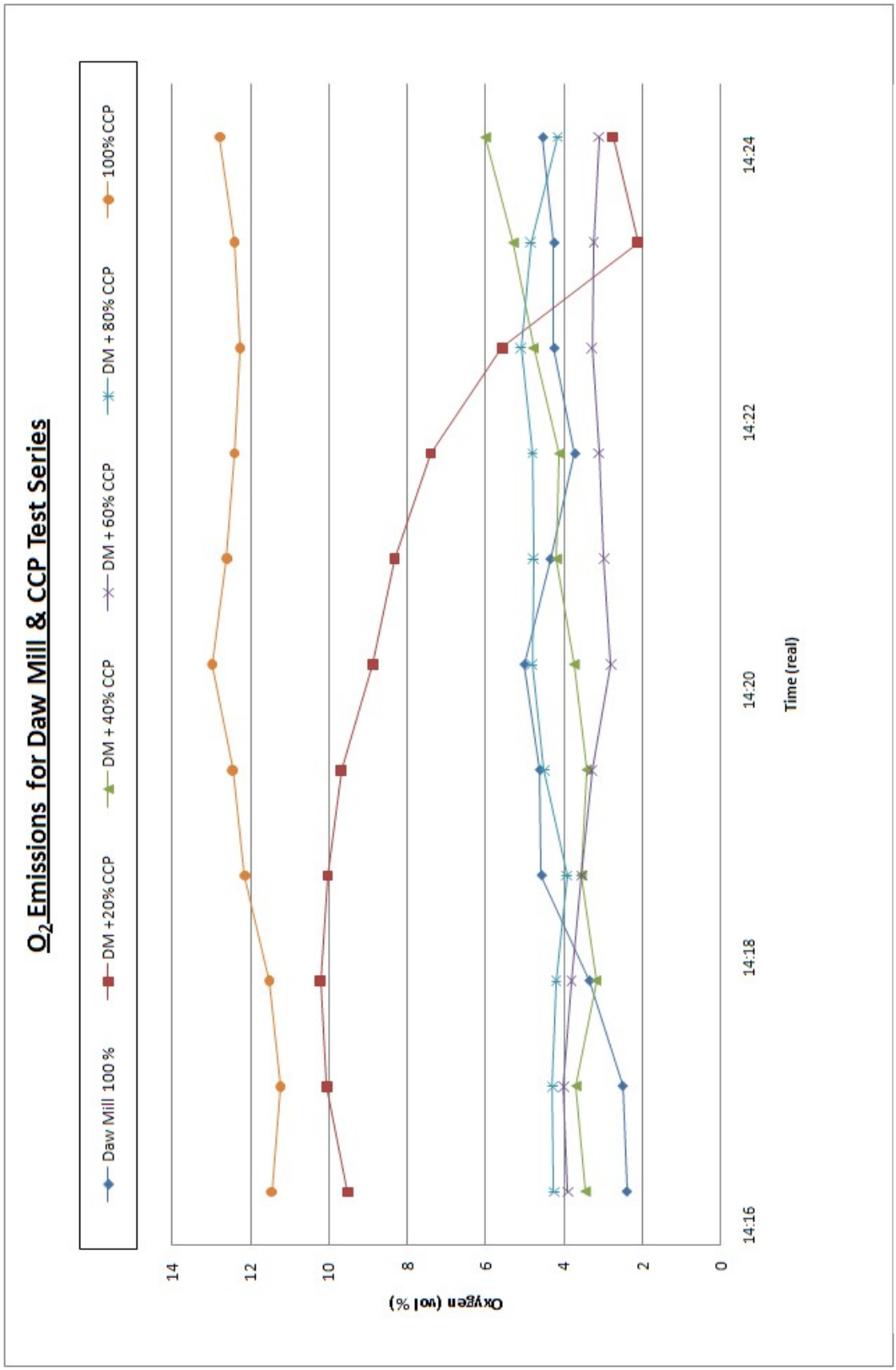

Fig 4.55 – Illustration for O_2 emissions Daw Mill & CCP test series

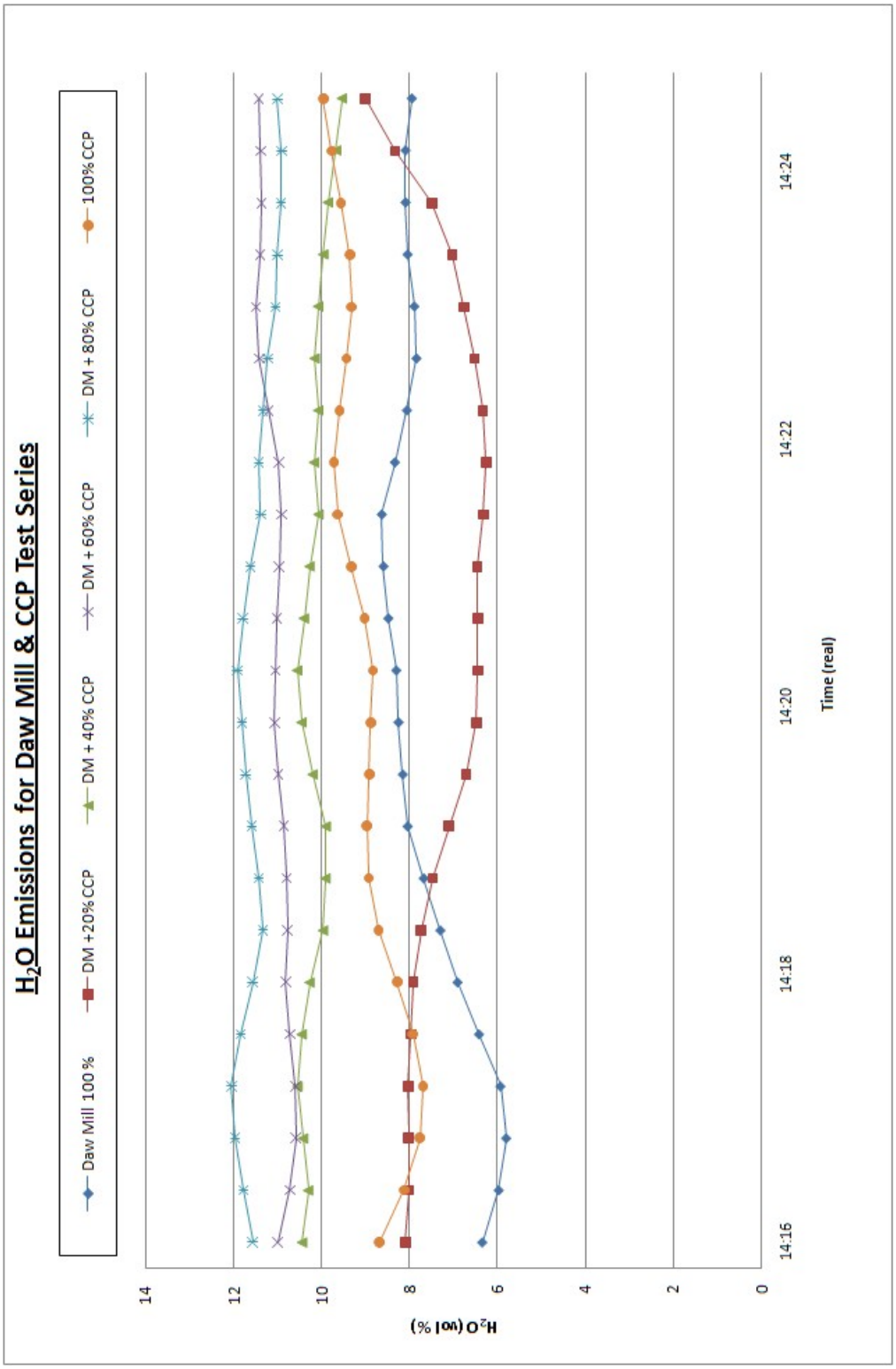

Fig 4.56 – Illustration for H_2O emissions for Daw Mill & CCP test series

4.8 Deposition flux

Figure 4.57 illustrates the deposition flux data obtained during the Daw Mill & CCP test series. It shows that the highest deposition flux was obtained on probe #1 at ~ 500 °C. The one exception to this is CCP as a pure fuel. Earlier data illustrated in this chapter (Figures 4.8 – 4.10), suggests that deposit flux would be higher as there appears to be more deposit.

In general, the deposit shows a decrease as the CCP wt% increases to the Daw Mill + CCP blend.

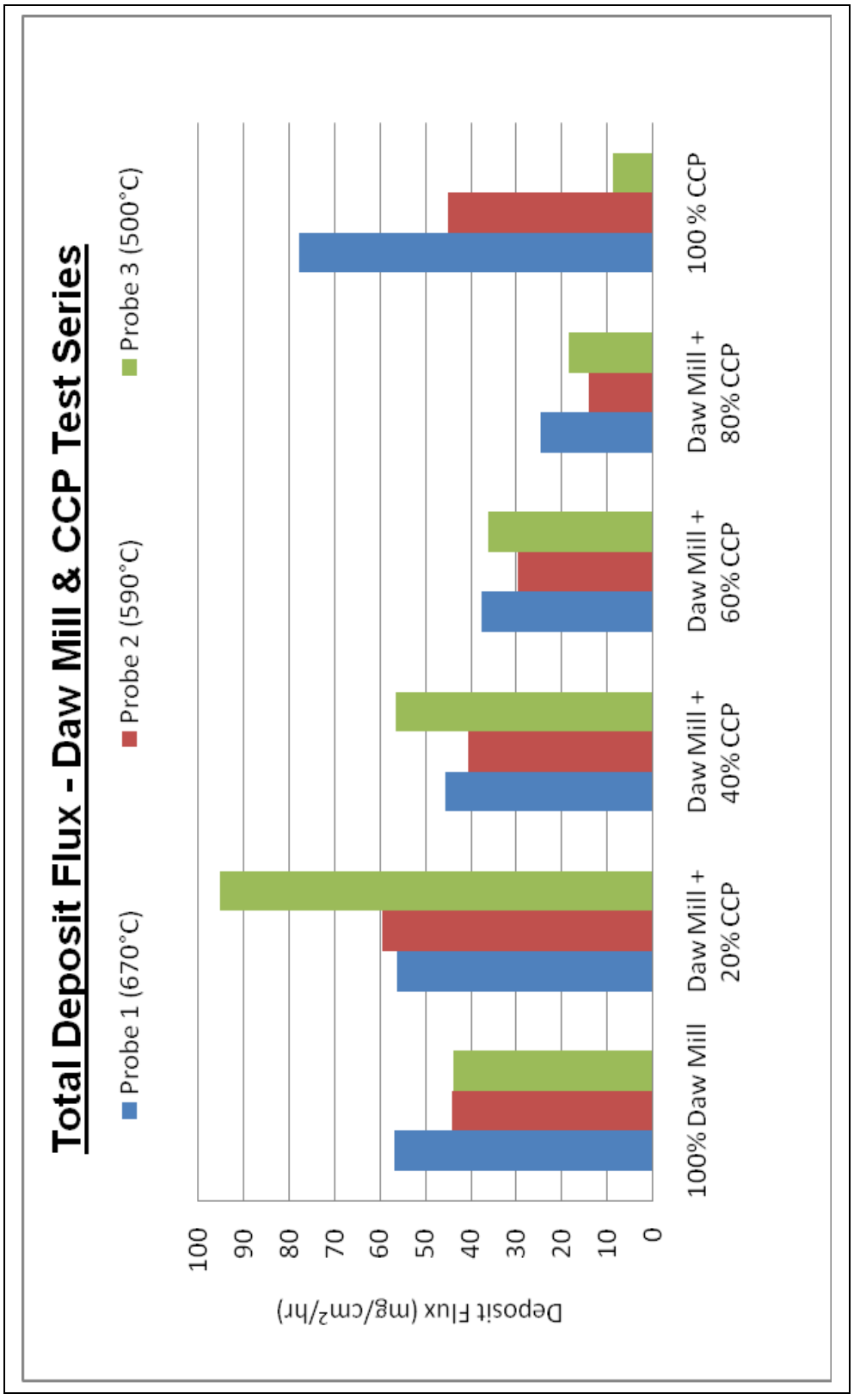

Fig 4.57 – Illustration for Deposition Flux for Daw Mill & CCP fuels in addition to their blends

5. Discussion

5.1 Introduction

This study has investigated the deposition and gas chemistry from the gas streams produced by the combustion of coal / biomass blends. In particular, it has concentrated on Daw Mill and CCP (as separate pure fuels and as blends) and explored some of the issues that affect the utilisation of such fuel mixtures. The issues that will be discussed are as follows:

- Deposition characteristics of the pure fuels and their blends
-
- Elemental analysis of the deposits generated
- Gas analysis trends with varying coal and biomass mixes.
- Variation of fuel feed rates and temperature with coal and biomass blends

5.2 Deposition characteristics of the fuel blends

For the purposes of this research, Daw Mill, CCP and Daw Mill and CCP blends are feedstocks of primary concern. Khodier (2011) investigated El Cerrejon and Miscanthus aspure fuels and as blends in separate experiments.

From a visual perspective, the results displayed differences between each of the tests. In all experiments, three probes with different surface temperatures (~700, 600 and 500 °C respectively) were utilised to capture the deposits. Figures 4.2 to 4.13 illustrate distinct differences with the pure fuels. As stated in the previous chapter, (section 4.3.1) Daw Mill had a far greater circumferential deposit than the CCP. The CCP displays a far greater, fibrous

deposit volume that is concentrated on the top sector of the probe. This will be discussed in section 5.2.1.

5.2.1 100% CCP

The 100% CCP (Chapter 4, section 4.3.1, figures 4.8 – 4.10) presented a fibrous ash deposit localised on the top section of each of the probes. This is following a 2.75-hour run time with 27.5 kgs of fuel used. It is suggested that the deposition mechanism of inertial impaction has influenced the structure of this deposit. Tomeczek & Waclawiak (2009) confirm this as the particles are required to be >10 μm (Chapter 2, section 2.9.2). Also, due to the fibrous nature of the deposit, the particles have been able to interlock with one another. This would assist in the deposit growth. The SEM illustrations for CCP (Figures 4.43a and 4.43b) illustrate a larger fibrous deposit on the top section of all the probes. A much finer covering was identified on the side section but nearer the top section on probes #2 and #3. These appear to be >1 μm but < 10 μm. No viable sample were successfully be obtained from the side section of probe #1 nor the base section from all probes in this particular experiment. One other observation that may have affected the deposit could be the averages of both probe surfaces and gas temperature within the vertical chamber. Data obtained (Chapter 4, figure 4.48) illustrate the target temperatures (as stated in section 5.2 of this chapter) were achieved. However, the real-time temperature data taken (Chapter 4, figure 4.47) illustrates greater fluctuations in the temperature gradients. The vertical gas chamber temperature plotted suggest an average of ~ 800 °C. The real-time temperature plot shows this same average but with a ± 150°C difference throughout the test. This in turn would affect the surface temperatures and would require constant adjustment for the cooling air into the probes. Further observations on these temperature variations will be discussed further in this chapter.

5.2.2 100% Daw Mill

The 100% Daw Mill (Chapter 4, section 4.3.1, figures 4.2-4.4) illustrates a greater circumferential deposit . This is following a 3.5-hour run time and 28 kg of fuel being used. A more even coating of fly ash is distributed over the side and base sections and displaying pronounced deposit sections for the top, side and base. SEM illustrations (Figures 4.39a to 4.41c) confirm the particle size is larger on the top section, compared to the sides and base section of the probes. The ash particles on the top section appear to be more granular in appearance and <10µm in size. This would suggest that eddy diffusion / impaction would be the deposit mechanism that has occurred. This appears to fit the characteristics suggested by Kaufmann *et al* (2002) and Tomaczek & Waclawiak (2009) (Chapter 2, section 2.9.4). The sides and base sections (except base section of probe #1 where no viable sample was able to be obtained), appear to be finer, more porous and more evenly distributed. These appear to be < 1µm on the base section. This appears to fit the description of thermophoresis (Baxter & Desollare (1993) (Chapter 2, section 2.9.3). Eddy impaction also contributes to this mechanism as suggested by Kaufmann *et al* (2002).

The colour of the ash deposits were very different when 100% Daw Mill and 100% CCP when compared. The Daw Mill being a light brown / yellow colour. The 100% CCP appears to be a mid grey to dark grey appearance.

5.2.3 Deposit weights & fluxes for 100% Daw mill & 100% CCP

The deposit weights collected for both pure fuels are similar. The tests ran for ~3 hours and consumed ~28kgs of fuel on each test. Each test and combining the three probes), 100% Daw Mill = 4.5mg and 100% CCP = 4.8mg.

The largest proportion was collected on probe #1 obtained by 100% CCP (2.16mg). The ash weights for all tests are shown in the Appendix. As stated in the earlier section of this chapter (5.2.2), the ash covering was circumferential for the 100% Daw Mill test. However, there were temperature fluctuations during the course of both tests (Figures 4.46 and 4.47) may of affected the deposition rates onto the probes' surfaces. This may be particularly significant for 100% CCP test.

5.2.4 Daw Mill + CCP Test series (20,40,60 & 80% wt)

The Daw Mill + CCP test series used blends at 20,40,60 and 80% (wt%). The tests ran ~3.5 hours and consumed ~33 kg of fuel. Visually, most of the probes developed a circumferential covering of ash, (Chapter 4, figures 4.14 – 4.25). The only exceptions were the base sections of Probe #1 – Daw Mill + 20% CCP and Daw Mill + 40% CCP. The colour change in the deposits are subtle but apparent. The lighter brown / yellow colour to a slightly darker appearance as the CCP to Daw Mill share increases.

The ash weights (totals) show a significant decrease as the share of CCP to Daw Mill increases. For example, Daw Mill + 20% CCP shows a total weight obtained of 6.75 mg compared to Daw Mill + 80% CCP of 1.77 mg. The ash weights for these tests are listed in the Appendix.

5.2.5 Deposition flux of Daw Mill + CCP test series

Deposition flux is calculated from the weight of the deposit collected on a given cylindrical area during a given period of time. Deposition fluxes calculated from the pure fuels (ie: Daw Mill and CCP) and Daw Mill and CCP blends.

When considering the deposition flux for 100% Daw Mill and 100% CCP, (Chapter 4, figure 4.57), 100% CCP, probe #1 has accumulated a higher deposition flux at 670°C (~80 mg/cm^2/hr) compared to 100% Daw Mill (~55 mg/cm^2/hr) at the same temperature. Probe #2 appears to have ~42–45 mg/cm^2/hr for both 100% Daw Mill and 100% CCP respectively. Probe #3 shows another big difference between the two fuels. At ~500°C , 100% Daw Mill is ~ 42 mg/cm^2/hr but 100% CCP is < 10 mg/cm^2/hr.

The Daw Mill + CCP blends (20, 40, 60 and 80 %) presented a uniform drop in the deposition flux over the four separate tests. Probe #3 (~500 °C) expresses the largest drop - from ~95 mg/cm^2/hr (Daw Mill + 20% CCP) to ~28 mg/cm^2/hr. (Daw Mill + 80% CCP).

Livingstone (2006) suggests that with higher calcium (Ca) and iron (Fe) coals (eg: Daw Mill) have a higher slagging and fouling tendency. Data shown in Chapter 2, section 2.8.2, table 2.8 would suggest that the Daw Mill coal utilised in the test is shown to have a high iron content (Fe_2O_3 : 14.1 % wt) . When comparing this to the CCP, table 2.9, the iron content (Fe_2O_3) is expressed as 2.2 %(wt)

5.3 EDX analysis of the fuel blends

Chapter 4, figure 4.50 illustrates a summary of the major elemental comparison of the pure fuels (Daw Mill and CCP) and the Daw Mill + CCP blends. This illustrates distinct differences from Daw Mill (pure fuel), through

the Daw Mill and CCP blends, to CCP (pure fuel). Particular attention is observed with potassium (K), Fe, silicon (Si), Ca and aluminium (Al)

Therefore, studying the data from the test range stated above, it can be demonstrated that the trends plotted in Figure 4.50 , show that:

- Fe and Al drop according to the blend of the combusted feedstock – 100% Daw Mill to 100% CCP wt%; Fe ~9% (wt) to <1% (wt); Al from ~13%(wt) to ~1%(wt).
- K raises significantly (<3% wt) to ~17% wt). CCP contains a greater amount of that element
- Ca is seen to rise only slightly (peaks at ~8% wt).
- Si appears to be stable but have peaked at Daw Mill + 40% CCP.

In all the points above, the data appears to correspond with data taken from tables 2.8 and 2.9 of Chapter 2, section 2.8.2.

It could be worth noting that Livingstone (2006) further suggests that the combination of CaO and Fe_2O_3 within the mineral matter increases the assimilation of aluminosilicate glass. This may suggest why with Si peaks with Daw Mill + 40% CCP when both CaO and Fe_2O_3 are of equal amounts than anywhere else on the plotted data.

Other data plotted in a different format and is a little more comprehensive, is shown in figure 4.51 for probe #2 – top section. This includes all the test range; i.e.: Daw Mill 100% - Daw Mill + CCP blends and CCP 100%. A similar trend for other elements was observed with linear increases of CCP to Daw Mill share , e.g.: magnesium (Mg) and phosphorus (P) and a linear decrease in the same fuel blend of tin (Ti). Chlorine (Cl) levels were not observed until 100% CCP was combusted. Further data for Cl levels in

biomass at higher CCP to Daw Mill was identified by Khodier (2011) and were not predicted. This is subject to further research elsewhere in the future.
Full elemental analysis for all tests are in the Appendix

5.4 Variation of feed rates and temperature with coal and biomass blends

The higher ratio of CCP to Daw Mill (i.e.: 80% CCP)caused a 'bridging effect' within the fuel feed hopper. Figure 5.1 illustrates this phenomenon. The main cause of this effect could have been the fibrous nature of the CCP and the ability of the small CCP stalks to interlock with each other. One of these many stalks can clearly be seen within the red circle. This may have acted as a support to prevent the smaller granules of coal from falling in a far more fluid fashion. Sami *et al* (2001) identified a similar problem when co-firing other coal and biomass blends. One of the ideas discussed was to make the particle size of the biomass smaller by pulverising the fuel far more efficiently. Zulfiqar (2006) tried to overcome the feeder issue from another angle. This involved placing a mesh basket directly below a belt driven feeder. This fed the fuel into the mesh basket that had a shaker attached. This again caused a 'bridging effect' and the basket became clogged.

Fig 5.1– Bridging effect with 80(wt)% CCP + Daw Mill mix within the hopper assembly

It also possible that the feed system for the fuel mixes (as described in Chapter 3, section 3.4.1) could have contributed to some of the sporadic feed patterns in certain blends. Some of the following problems that came to light were:

- The variation in the feed pipe diameter going into the combustion chamber. Even though this was improved, further modifications were required at later stages of testing as fuel blends were blocking up the assembly (e.g.: Daw Mill + 80% CCP).

- When large amount of fuel fell from the 'bridged' area of the hopper, it was found that the venturi (Chapter 3, figure 3.8 and 3.9) was overcome by the increase of extra fuel. To try and stabilise these variations in the fuel flow, the flow rate of the carrier gas (N_2) was increased or

decreased very slightly as well as adjusting the vibrating plate on the feed hopper during the same period.

- An immediate problem of static came to light in earlier tests. This occurred in the fuel feed hose (section 3.4.1, Figure 3.6). It was observed that fuel was sticking to the inside of the transparent feed hose which over a period of time assisted in the slowing down of the fuel. Therefore, an earthing wire was looped around the length of the fuel feed hose and connected to a suitable part of the combustor's platform structure.

Overall, there was partial success from the improved fuel feed system. However, these issues with the fuel feeding caused a number of temperature fluctuations in some parts of a test. This is especially apparent in the 100% CCP test. The trend plotted (Chapter 4, figure 4.7) illustrate a very sporadic feed pattern. Troughs in the plotted data for other tests (Daw Mill + 20, 60 and 80% CCP blends are shown in the Appendix) illustrate reasonable feed pattern with fewer disturbances. On occasion, these troughs in the plotted data are also attributed to the refilling of the fuel feed system so that the test could continue.

5.5 Gas analysis trends for Daw Mill and CCP Test Series

During the course of all of the tests, it was observed that if the fuel feed rate was constant and did not fluctuate then a reasonable data pattern was produced with gas analysis data. The key features stated in Chapter 4, section 4.7 are illustrating the Daw Mill +40% CCP (figures 4.52 and 4.53). In addition minor gas species do not show significant increase or decrease as the tests progressed. The only time a reasonable trace was not seen was when the feed unit was refilled or there was blockages occurring in the fuel feed unit. Figures 4.54, 4.55 and 4.56 illustrate collective data for CO_2, O_2 and H_2O over all of the

Daw Mill & CCP test series. This data illustrates a much shorter timeframe where all tests were stable and gave a reasonable data plot. Figure 4.54

suggests that the combustion of CCP as a pure fuel gave a much lower CO_2 level (~ 6 vol %) than Daw Mill as a pure fuel at ~ 18 Vol %. The data plot for the Daw Mill + CCP blends appear to sit between these two pure fuels in a reasonable pattern. Figures 4.55 and 4.56 illustrate much clearer data plots over the same given timeframe. O_2 showing a higher content on CCP as a pure fuel (~ 13 vol %) with the Daw Mill + CCP blends around the ~ 2-4 vol % . It may be considered that the Daw Mill + CCP (20%) may be a spurious data trend and further analysis of the emissions data is required. The H_2O data plots show a reasonable trend but appears to show Daw Mill + CCP (60 and 80% blends) with the highest H_2O emissions content (~ 11 vol%) with CCP as a pure fuel at ~ 9 vol%. Daw Mill + CCP (20%) shows another fluctuating result that appears in the preceding graphs around the same timeframe.

6. Conclusions & further work

6.1 Conclusions

A series of experiments have been carried out on co-firing activities in a controlled combustion environment. These experiments have utilised a selection of pure fuels, i.e.: fossil fuels and biomass, as well fossil fuel and biomass blends. The fuels that have been utilised are currently being used in the UK's power station facilities (e.g.: Daw Mill) or are being researched further and promoted as low CO_2 emitting fuel (e.g.: CCP). This is further encouraged as part of the UK's governmental and international commitment to lower CO_2 production (e.g.: in the power generation industry) that contribute to greenhouse gases and to so-called global warming.

The tests have collated data that can utilised in further deposition studies elsewhere in the future. It has also improved the operational parameters of the combustion rig at CERT and further knowledge has been obtained in creating tests that are reliable, have repeatability and can be run with efficiency.

A summary of experimental work carried out is as follows:

- Studies of previous deposit probes and applying improvements as required
- The fuel feed delivery system; resolving issues and improving where possible
- Carry out reliable combustion rig experiments ensuring repeatability and consistency with controlled, safe manner.
- Co-firing fossil fuels and biomass (in their pure form)
    - Daw Mill and El Cerrejon
    - CCP and Miscanthus(*Giganteus*) biomass

- Co-firing fossil fuel and biomass (in blended form)
    - Daw Mill and CCP blends were co-fired at varying weight % (ie: Daw Mill and 20, 40, 60 and 80% CCP blends).

    - The collection of ash deposits on three probes that have surface temperatures of ~ 700, 600 and 500 °C
    - Observe, collect and analyse the ash deposits utilising SEM / EDX methods and hardware (primarily concentrating on Daw Mill, CCP and Daw Mill + CCP blends)
    - Monitor and collect gas emissions data for CO_2 , O_2 , CO, NO_X , HCl, SO_2 etc utilising a FTIR unit.

The experimental program produced some excellent data and has given some major insight and reinforced current knowledge on the behaviour of deposition onto simulated heat exchanger surfaces.

The following results following this experimental program can be summarised as follows:

- Deposits were formed on most of the probes from ~500 °C upwards with larger particle size concentrations on the top section of the probes and smaller particle sizes being collected on the side and base sections.
- Behavioural characteristics of the deposit mechanisms (e.g.: thermophoresis and eddy impaction) have been created on the probe surfaces and support the theories as reported by previous authors in relation to particle size.
- Deposit flux is reduced as the CCP to Daw Mill blend is increased with the Daw Mill and CCP blends.
- CO_2 emissions are reduced as the CCP to Daw Mill in increased. This is also dependant on the combustion efficiency during the test.

6.2 Further work

Following the experimental work, the following could be investigated to ensure that further progress is made in this area:

- Improvement to the fuel feed system is required to ensure that a continuous, uninterrupted flow of fuel is delivered into the combustion rig. This would smooth out further the fluctuations in the temperature plot and gas analysis.
- It would also be useful to ensure a larger capacity of fuel storage for delivery. This would ensure that the replenishment of fuel does not interrupt the fuel delivery cycle.
- Modify the surface thermocouples on the probes by investigating if a flat thermocouple is on the market rather than the traditional, round type. This is to ensure that the eddy currents that act upon the probe surface are not interrupted.
- Being able to observe the deposit creation whilst the probe(s) are in the rig. This could be done via an extra view port and the addition of time-lapsed photography.
- Further improvements to the deposit collection. It was observed that some particles were sticking to the paper and considerable effort was required to ensure that deposits were not lost.
- Investigate other biomass feedstocks that are in abundance in the UK eg: barley corn stalks and oil seed rape stalks that can be subjected to a similar study.

1. Alberts B, Johnson A, Lewis J, *et al* (2002) ***Molecular Biology of the Cell***; 4th edn, Garland Science, New York

2. Aryes, C. (Jun 14, 2008) ***"Garbage in, petrol out: how tiny bugs may fuel the world"***. *The Times* World; Fuel Technology edn, 52-53. Times Newpaper Group. World; Fuel Technology.

3. Bassam, N. (1998) ***Energy Plant Species***, 1st edn. London, UK: James & James (Science Publishers) Ltd.

4. Baxter, L. & DeSollar, R. (1992) ***A mechanistic description of ash deposition during pulverised coal combustion: predictions compared with observations***. *Fuel* 72, 1411-1418.

5. Baxter, L (2005) ***Biomass-coal co-combustion: opportunity for affordable renewable***; Fuel 84 1295-1302

6. Berkovitch, I. (1978) ***Coal - Energy & Chemical Storehouse***, 1st edn. Norwich, UK: Portcullis Press.

7. Bolton, W. (2000) ***Engineering Materials***, 3rd edn. Jorden Hill, Oxford, UK: Butterworth Heinemann (Newes).

8. Bourne, J.K. (Oct, 2007) ***"Green Dreams"***. *National Geographic* 38-59. Tampa, Florida, USA

9. Boyle, G *et al* (2004) ***Energy Systems & Sustainability*** 2nd edn, , Oxford, UK, Oxford University Press (in assoc. with the Open University)

10. Brink, A., Lauren, T., Yrjas, P., Hupa, M. and Friesenbichler, J. (2007) ***Development & Evaluation of a long-term deposit probe for on-line monitoring of deposit growth***. *Fuel Processing Technology* 88, 1129-1135.

11. Cassedy, E.S. (2005) ***Prospects for Sustainable Energy - A Critical Assessment***, 3rd edn. Cambridge, UK: Cambridge University Press.

12. Coleman, K. (2008) ***Fireside Corrosion in Biomass Combustion Plants***. Cranfield University, Bedfordshire, UK

13. Davies, C. (1970) ***Calculations in Furnace Technology***, 1st edn. Headington Hill Hall, Oxford, UK: Pergamon Press.

14. DeRenzo, D.J. (1977) ***Energy from Bioconversion of Waste Materials***, 1st edn. Park Ridge, New Jersey, USA: Noyes Data Corporation.

15. Doshi V, Vuthaluru H B, Korbee R & Kiel J H A (2009) ***Development of a modelling approach to predict ash formation during co-firing coal and biomass***, Fuel 90, 1148-1156.

16. Gifford J, Hooper G, Nicholas I, Hall P, Li J, Senelwa K, Sims R & Clements T (2000) , ***Woody Biomass as a sustainable energy source***, Proceedings of the Renewable Energy Research Showcase Seminar from Renewable Technologies in New Zealand – Paper 3, Massey University, Palmerston North.

17. Greer, A. & Hancock, D.J. (1991) ***Tables, Data & Formulea for Engineers***, 2nd edn. Leckhampton, Cheltenham, UK: Stanley Thornes.

18. Hall, D.O. & Overend, R.P. (1987) ***Biomass - Renewable Energy***, 1st edn. Chichester, West Sussex, UK: John Wiley & Sons.

19. Hall, J. (1998) ***Kemps Engineers Yearbook 1998***, 103rd edn. Tonbridge, Kent, UK: Miller Freeman PLC.

20. Higgins, R.A. (2002) ***Materials for the Engineering Technician***, 3rd edn. Jorden Hill, Oxford, UK: Butterworth Heinemann.

21. Holman, J.P. (1997) ***Heat Transfer***, 8th edn. London, UK: McGraw-Hill.

22. Huang, L.Y, Norman, J.S, Pourkashanian, M & Williams, A (1996) ***Prediction of ash deposition on superheater tubes from pulverized coal combustion***, Fuel 75, 271-279

23. Keyse, R.J., Garratt-Reed, A.J., Goodhew, P.J. and Lorimer, G.W. (1998) ***Introduction to Scanning Transmission Electron Microscopy***, 1st edn. Oxford, UK: BIOS Scientific Publishers.

24. Kitani, O and Hall, C. (1989) ***Biomass Handbook***, 1st edn, South Africa, Gordon & Breach Science Publishers.Notes: Contains multiple authors

25. Khodier A, Legrave, N.A, Simms N.J, & Kilgallon, P J (2010) ***Investigation of gaseous emissions and ash deposition in a pilot scale PF combustor co-firing cereal co-product biomass with coal***, Cranfield University, Bedfordshire, UK

26. Khodier , A.H.M (2011) ***Co-firing Fossil Fuels & Biomass: Combustion, Deposition & Modelling***, Cranfield University, Bedfordshire, UK

27. Klass, D.L. (1998) ***Biomass for Renewable Energy, Fuels & Chemicals***, 1st edn. London, UK: Academic Press Ltd.

28. Kunii, D. & Levenspiel, O. (1991) ***Fluidization Engineering***, 2nd edn. Stoneha, MA, USA: Butterworth-Heinemann.

29. H. Lachas, R. Richaud, A. A. Herod, D. R. Dugwell, R. Kandiyoti, K. E. Jarvis (1999) ***Determination of 17 trace elements in coal and ash reference materials*** ; Analyst Vol. 124, no. 2, pp. 177-184,

30. Law, S. (1921-2008) "***Brewing Biomass***". *Engineering & Technology - IET Journal* 3, 56-57.

31. Livingston, W R (2006) ***Advanced biomass co-firing technologies for coal-fired boilers*** ,Exco 55 Workshop (2006)

32. Lokare, S.S (2008) ***A Mechanistic Investigation of Ash Deposition in Pulverized Coal & Biomass combustion,*** Brigham Young University

33. Nathan, S. (Jul, 2007-Aug 31, 2007) ***"Field of Dreams"***. ***The Engineer*** 20-25. London, UK: Centur Publications.

34. Pagnamenta, R. (Jun 14, 2008) ***"Oil traders fear London may lose out to new markets"***. *The Times* Business edn, 63 The Times Newspaper Group. Business.

35. Pearce, F. (2008) ***"Time to bring in Plan B for Biofuel"***. *New Scientist* 30-31.

36. Raask, E. (1985) ***Mineral Impurities in Coal Combustion***, 1st edn. USA: Hemisphere Publishing Corporation.

37. Rao, T.R & Sharma (1998) ***Pyrolysis Rates of Biomass Materials***, Energy Vol 23, No 11, 973-978

38. Robinson A L, Junker H & Baxter L L (2001) ***Pilot-Scale Investigation of the Influence of Coal-Biomass Co-firing on Ash Deposition***, Energy & Fuels 16, 343 – 355

39. Sami M, Annamalai K & Wooldridge M (2001) ***Co-firing of Coal and Biomass Fuel Blends***,. Progress in Energy & Combustion Science, No 27, 171-214 (Dept of Mechanical Engineering, Texas A & M University)

40. Sheng, C & Azevedo, J.L.T (2005) ***Estimating the higher heating value of biomass fuels from basic analysis data***, Biomass & Bioenergy 28, 499-507

41. Sims, R.E.H. (2002) ***The Brilliance of Bioenergy***, 1st edn, James & James Ltd, London, UK : The Cromwell Press.

42. Simeons, C. (1978) ***Coal - Its Role in Tomorrow's Technology***, 1st edn. Heading Hall, Oxford, UK: Pergamon Press.

43. Shao Y, Xu C, Zhu J & Preto F (2010) ***Ash Deposition during Co-firing Biomass and Coal in a Fluidized-Bed Combustor*** Energy & Fuels,

44. Timings, R. & May, T. (1990) ***Mechanical Engineer's Pocket Book***, 1st edn. Tiptree, Essex, U.K.: Heinemann Newes.
Notes: Used for general reference only

45. Tomeczek, J. (1994) ***Coal Combustion***, unknown edition edn. Malabar, Florida, USA: Krieger Publishing Company.

46. Tomeczek, J. & Palugniok, H. (2002) ***Kinetic of mineral matter transformation durling coal combustion***. *Fuel* 81, 1251-1258.

47. Tomeczek, J, Palugniok, H & Ochman, J (2004) ***Modelling of deposits formation on heatingtubes in pulverized coal boilers***; Fuel 83, 213-221

48. Tomeczek,J & Waclawiak,K (2009) ***Two-dimensional modelling of deposits formation on platen superheaters in pulverised coal boilers***. *Fuel* 88, 1466-1471

49. Venables, M. (2008) ***"The Power of Plants"***. Engineering & Technology - *IET Journal* , Vol 3, Issue 15

50. Venables, M (2008) ***"Back to Black"***. Engineering & Technology – IET Journal Vol 3, Issue 19

51. Webster, B. (Nov 10, 2007) ***"Green tax puts £1,000 on family cars"***. *The Times* 2 www.timesonline.co.uk.
Notes: Article on reduction of CO2 emissions; interview of Professor Julia King, Aston University regarding the use of bio fuels in motor vehicles

52. Wigley F, Williamson J, Malmgren A & Riley G (2007) ***Ash deposition at higher levels of coal replacement by biomasss***, Fuel 88, 1148-1154

53. Wigley, F, Williamson J & Riley, G (2007) ***The effect of mineral additions on coal ash deposition***, Fuel Processing Technology 88, 1010-1016

54. Williiams A , Jones J M , Skorupska N & Pourkashanian M (1964) ***Combustion & Gasification of Coal***, 1st edn. New York, USA: Taylor & Francsis.

55. Zulfiqar M H, Moghtaderi B, Wall T F, Spero C & Holcombe D (2006) ***Co-firing of Coal & Biomass in 150KW Pilot Scale Boiler Simulation*** Furnace; Technology Assessment Report No 54, QCAT Technology Transfer Centre, Pulenvale, Austrialia – collaboration with the University of Newcastle, Australia

Internet References

1. http://www.ucsusa.org/clean_energy/technology_and_impacts/energy_technologies/how-coal-works.html - Union of Concerned scientists - USA

2. http://www.caer.uky.edu/kyasheducation/glossary.shtml (LIGNITE & Bituminous coal) Uni of Kentucky – centre for applied energy research

3. http://kaltimprimacoal.wordpress.com/2007/11/08/coal-main-source-of-energy-for-power-plants/ (Sub bit coal – Coal for Indonesia)

4. http://www1.newark.ohio-state.edu/ (Anthracite coal)

5. http://en.citizendium.org/wiki/Coal#Coal_classification

6. http://www.astm.org/Standards/D388.htm (Coal ranking)

7. http://www.bcura.org/coalbank.html Coal Bank

8. http://www.chemistryexplained.com/Ce-Co/Coal.html (Coal history classification)

9. http://www.woodgas.com/proximat.htm Biomass energy foundation

10. http://www.iea.org/ International Energy Agency

11. http://www.et.byu.edu/~larryb/index.htm Energy Laboratory,

12. http://www.ecn.nl Biomass, Coal and Environmental Research, P.O. Box 1, 1755 ZG Petten, Westerduinweg 3, Petten, The Netherlands

13. http://www.bios-bioenergy.at/en/working-field/analyses

14. http://princeton.edu/basics/01_chemistry/ (Lignin and Cellulose structures)

Conference Proceedings, Reports, etc.

1. Abbott, M. F., Douglas, R. E., Fink, C. E., Deluliis, N. J. and Baxter, L. L. (1994) In ***The Impact of Ash Deposition on Coal-Fired Plants***(Eds, Williamson, J. and Wigley, F.) Taylor & Francis, Washington D.C., pp. 165-176.
2. Bakker, R. R., Jenkins, B. M., Williams, R. B., Carlson, W., Duffy, J., Baxter, L. L. and Tiangco, V. M. (1997) "***Boiler Performance and Furnace Deposition During a Full Scale Test with Leached Biomass****,"* In *3rd Biomass Conference of the Americas*, Vol. 1 (Eds, Overend, R. P. and Chornet, E.) Elsevier Science Limited, Montréal, Ontario, Canada, pp. 497-510.
3. Baxter, L. (1991) "Preliminary Hazard Assessment: Multifuel Combustor Laboratory*,"* Sandia National Laboratories, .
4. Baxter, L., Davis, K., Sinquefield, S., Huey, S., Lipkin, J., Shah, D., Ross, J. and Sclippa, G. (1995) "Combustion Aspects of The Reapplication of Energetic Materials as Fuels As a Viable Demil Technology*,"* In *1995 Global Demilitarization Symposium and Exhibition*, Vol. 1 St. Louis, MO, pp. 17-27.
5. Baxter, L., Davis, K., Sinquefield, S., Huey, S., Lipkin, J., Shah, D., Ross, J. and Sclippa, G. (1995) "Reapplication of Energetic Materials as Fuels*,"* In *Joint Conference of the American Flame Research Committee and the Combined Central States/Western States/Mexican National Sections of the Combustion Institute*, Vol. 1 San Antonio, TX, pp. 382-387.
6. Baxter, L. L. (1990) "Ash Composition Prediction as a Function of Coal Type, Operating Conditions, and Boiler Location*,"* In *EPRI conference on the Effects of Coal Quality on Power Plants*(Eds, Mehta, A. K. and Harding, N. S.) Electric Power Research Institute, St. Louis, Missouri, pp. 5/59-5/74.

7. Baxter, L. L. (1992) "Boiler Performance with Blends of Eastern and Western Coals," In *EPRI Conference on The Effects of Coal Quality on Power* Plants San Diego, CA.
8. Baxter, L. L. (1994) "The effect of Low-NOx Firing on Fireside Performance," In *International Joint Power Generation* Conference Scottsdale, AZ, pp. 211-220.
9. Baxter, L. L. (1994) In *Coal-Blending and Switching of Low-Sulfur Western Coals*(Eds, Bryers, R. W. and Harding, N. S.) ASME, New York, pp. 255-264.
10. Baxter, L. L. (1995) "The effect of Low-NOx Firing on Fireside Performance," In *The Economic and Environmental Aspects of Coal Utilization* VI Santa Barbara, CA.
11. Baxter, L. L. (1995) In *The Impact of Ash Deposition on Coal-Fired Plants*(Eds, Williamson, J. and Wigley, F.) Taylor & Francis, Washington D.C., pp. 313-323.
12. Baxter, L. L. (1996) "Influence of Ash Deposit Chemistry and Structure on Physical and Transport Properties," In *American Chemical Society Annual Meeting - Fuel* Section New Orleans, LA.
13. Baxter, L. L. (1999) "Application of Combustion Modeling to Boiler Problem Solving: Strengths and Weaknesses," In *CODE Kickoff Seminar*, Vol. 1 Tekes, Helsinki, Finland.
14. Baxter, L. L., Blander, M., Dayton, D. and Milne, T. A. (1996) "Thermochemical Equilibrium as an Indicator of Ash Deposition Problems in Biomass Boilers," In *Developments in Thermochemical Biomass* Conversion Banff, Canada.
15. Baxter, L. L., Blander, M., Dayton, D. and Milne, T. A. (1997) In *Developments in Thermochemical Biomass Conversion*, Vol. 2 (Eds, Bridgwater, A. V. and Boocock, D. G. B.) Blackie Academic & Professional, London, pp. 1278-1292.

16. Baxter, L. L., Chaney, J. and Mehta, A. (2000) "Fireside Coal Quality Impacts Predicted by Boiler Simulator," In *Effects of Coal Quality on Power Plant Management: Ash Problems, Management and* Solutions Park City, Utah, pp. accepted.
17. Baxter, L. L. and DeSollar, R. W. (1991) "Ash Deposition as a Function of Coal Type, Location in a Boiler, and Boiler Operating Conditions: Predictions Compared to Observations," In *International Conference on Environmental Control of Combustion* Processes Honolulu, HA.
18. Baxter, L. L. and Dora, L. (1992) "The Combustion Behavior of a Blend of Eastern and Western Coals: Comparisons Between a Blend and Its Individual Components," *ASME Paper No. 92-JPGC-FACT-14,* .
19. Baxter, L. L., Gale, T., Sinquefield, S. and Sclippa, G. (1997) In *Developments in Thermochemical Biomass Conversion*, Vol. 2 (Eds, Bridgwater, A. V. and Boocock, D. G. B.) Blackie Academic and Professional, London, pp. 1247-1262.
20. Baxter, L. L., Grebenkov, A., Kofman, P., Allen, D., Roed, J. and Junker, H. (1998) "Chernobyl Bioenergy Project: Final Report, Phase 1," Elsamprojekt, Fredericia.
21. Baxter, L. L., Huey, S., Lipkin, J., Shah, D., Ross, J. and Sclippa, G. (1996) "Boiler Fuel as a Recycling Option for Energetic Materials," In *Fourth International Symposium on Special Topics in Chemical* Propulsion Stockholm, Sweden.

Appendix

Hardware specifications & suppliers

Deposit Probe – deposit area – Alsint 99.7 ™

Supplied by Multi-Lab Ltd, Tynevale Works, Newbun, Newcastle-upon-Tyne, Tyne & Wear, NE15 8LN

Specifics	Units	Measurements
Al_2O_3	%	99.7
Alkali content	%	0.05
Type acc to DIN VDE 0335*	-	799
Water absorption	%	≤ 0.2
Leakage rate at 20˚C (Helium)	mbar	10^{-10}
Density	$g.cm^{-3}$	3.80-3.93
Flexural strength	MPa	300
Hardness (Mohs scale)	-	9
Thermal expansion	20-700 ˚C 20-1000 ˚C	7.8 8.6
Thermal Conductivity	20-100 ˚C ($W.m^{-1}.K^{-1}$	26.0
Maximum working temperature	˚C	1700
Permissible permanent temperature for temperature measurement	˚C	1600+/1800++
Dielectric strength related to 1.5mm wall thickness	$kV.mm^{-1}$	17
Volume resissitivity D.C @ 20 ˚C	Ω.cm	10 14
Thermal shock resistance	-	Good
Pore size	µm	-

(Table 1 – Specifications from Multi-lab Ltd)

8 DIN standard

Deposit Probe – ceramic capture area measurements

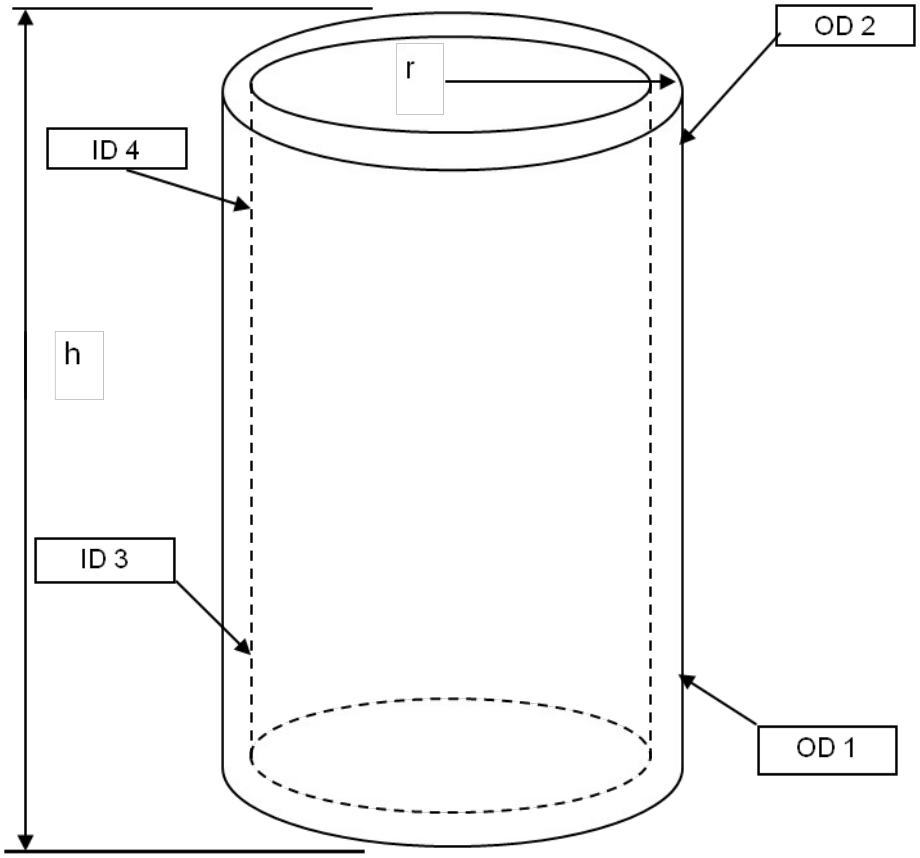

NB:The deposit ceramics were found to not be perfectly cylindrical. All dimensions were checked with a digital vernier calipier, vee block and DTI

Dimensions of ceramic catch areas

Cylinder no	OD 1 (mm's)	OD 2 (mm's)	Average	ID 3 (mm)	ID 4 (mm)	Average
1	39.08	39.16	39.12	32.28	31.99	32.14
2	38.86	39.15	39.01	32.14	32.07	32.11
3	39.22	39.15	39.19	32.39	32.42	32.41
4	39.29	39.03	39.16	32.08	32.13	32.11
5	39.24	39.23	39.24	32.32	32.24	32.28
6	39.21	39.13	39.17	32.11	32.04	32.08
7	39.17	39.14	39.16	32.11	32.05	32.08
8	38.96	39.15	39.06	32.35	32.31	32.33
9	39.09	39.10	39.10	32.42	32.29	32.36
10	39.33	39.20	39.27	32.31	32.45	32.38
11	39.03	39.12	39.08	32.02	31.91	31.97
12	39.65	39.38	39.52	32.24	32.44	32.34
13	39.20	39.05	39.13	32.31	32.09	32.20
14	38.95	39.10	39.03	32.15	32.22	32.19
15	38.99	39.30	39.15	32.51	32.46	32.49
16	39.10	39.29	39.20	32.92	32.35	32.64
17	38.99	39.20	39.10	32.51	32.21	32.36
18	39.27	39.33	39.30	32.47	32.50	32.49

Cylinder no	OD 1 (mm's)	OD 2 (mm's)	Average	Radius (r)	r * height)	Total surface area (mm^2)
1	39.08	39.16	39.12	19.56	1173.60	7374.90
2	38.86	39.15	39.01	19.50	1170.15	7353.22
3	39.22	39.15	39.19	19.59	1175.55	7387.16
4	39.29	39.03	39.16	19.58	1174.80	7382.44
5	39.24	39.23	39.24	19.62	1177.05	7396.58
6	39.21	39.13	39.17	19.59	1175.10	7384.33
7	39.17	39.14	39.16	19.58	1174.65	7381.50
8	38.96	39.15	39.06	19.53	1171.65	7362.65
9	39.09	39.10	39.10	19.55	1172.85	7370.19
10	39.33	39.20	39.27	19.63	1177.95	7402.24
11	39.03	39.12	39.08	19.54	1172.25	7366.42
12	39.65	39.38	39.52	19.76	1185.45	7449.37
13	39.20	39.05	39.13	19.56	1173.75	7375.85
14	38.95	39.10	39.03	19.51	1170.75	7356.99
15	38.99	39.30	39.15	19.57	1174.35	7379.62
16	39.10	39.29	39.20	19.60	1175.85	7389.04
17	38.99	39.20	39.10	19.55	1172.85	7370.19
18	39.27	39.33	39.30	19.65	1179.00	7408.84

Appendix

Thermocouples

Farnell

Farnell Components, Canal Road, Leeds, LS12 2TU

- Type 'K' thermocouple – (L) 500 mm; ∅ 1.5 mm
  Order code – 707-8160
- Type 'K' connector – Plug
  Order code – 381-0392
- Type 'K' connector – Socket
  Order code – 381-0446

Main Probe Body (drawing no A1) - 2.25 Cr
Round Plate ∅125 mm
¼" socket

Inner Tube (drawing no A2) - 316 stainless steel
Comprising of : 1" OD Tube @ 200 mm (L)
¾" OD tube @ 460 mm (L)
3/8" NB @ 60 mm (L)

End Cap (drawing no A3) - 310 stainless steel

Compression fitting on main body: (A4)

Swagelok

Supplied by – Swagelok London, Kingley Park, Station Road, Kings Langley, Hertfordshire, WD4 8GW

- ¾" OD Male Compression Fitting – part no: SS – 1210-1-12W
- ¾" Nylon Ferrules – front: part no: NY-1213-1
  back: part no: NY-1214-1

Appendix

Sealer between main probe, metallic cylinders and ceramic deposit area:

'AutoStic' ceramic cement – FortaFix Ltd, First Drove, Fengate, Peterborough, PE1 5BJ

Data Logging :

TC08 data logging details:

Pico Technology, James House, Marlborough Road, Colmworth Business Park, Eaton Socon, St Neots, Cambridgeshire, PE19 8YP

USB TC-08 Specifications	
Number of channels	8
Conversion time	100 ms (thermocouple and cold junction compensation)
Temperature accuracy	Sum of ±0.2 % of reading and ±0.5 °C
Voltage accuracy	Sum of ±0.2 % of reading and ±10 µV
Overload protection	±30 V
Maximum common mode voltage	±7.5 V
Input impedance	2 MΩ
Input range (voltage)	±70 mV
Resolution	20 bits
Noise free resolution	16.25 bits
Thermocouple types supported	B, E, J, K, N, R, S, T
Input connectors	Miniature thermocouple
Output connector	USB — cable supplied
PC connection	USB 1.1
Power supply	From USB port
Dimensions	201 x 104 x 34 mm (7.91 x 4.09 x 1.34 in)
Supplied software	PicoLog Software Development Kit Linux drivers
PC requirements	**Processor**: Pentium class processor or equivalent **Memory**: 32 MB minimum **Disk space**: 10 MB minimum **OS**: 32-bit edition of Microsoft Windows XP (SP2) or Visa **Ports**: USB 1.1 or USB 2.0 compliant port. Must be connected direct to the port or a powered USB h

Table 2 : Specifications of data logging unit

Gas Analysis

FTIR unit supplied by:

Protea Ltd
First Avenue
Crewe
Cheshire
CW1 6BG

Assistance given by:
Dr Stephen Hall
Mr George Dennett
Mr Andy Toy

Specifications:

Dimensions and Weight:	117 x 66.5 x 43cm. 71.3kg
Main Power:	115V, 10A or 230V, 5A, 50/60 Hz (1200 VA startup, 150 VA typical operation)
Sample Temperature:	Gas Cell @ 180°C. Warm-up time 1 hour. Heated sample line and sample probe required
Ambient operating temperature:	+5°C to +40°C
Outputs:	Analogue, 16 channels. Digital, 5 channels
Inputs:	Analogue and digital, depending on analyser specification
Resolution:	Variable resolution FTIR. Maximum resolution 1cm-1
Gas Cell:	Aluminum gas cell of volume 2.7 litres. Ambient pressure during normal operation. Recommended pressure range, -0.8 to 1.2 bar
Optics:	Zinc Selenide beam splitter. Does not require interferometer purge. 6.4m Path length gas cell with pre-aligned coated mirror carriage Barium Fluoride optical gas cell windows (changeable dependant on application –calibration required)
Zero Gas:	99.999% Nitrogen

Gas Sample Probe

M&C TechGroup

UK Sales Office
Glenholme
Main Road
Stanton-in-Peak
Derbyshire
DE4 2LX

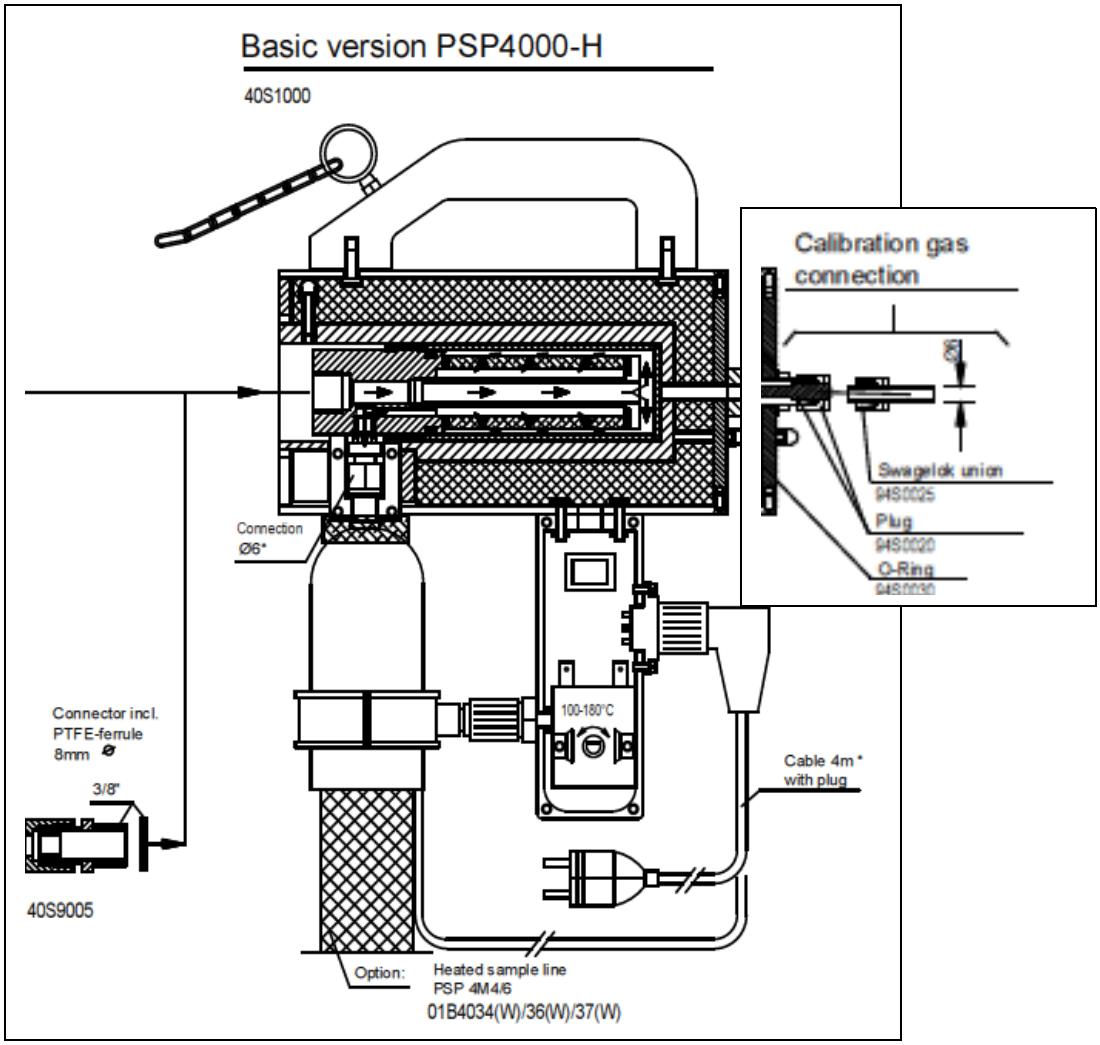

Cut through diagram of PSP 4000-H gas sample probe with purge / calibration attachment

(Courtesy of M & C Tech Group)

Probe Series SP® Portable Version PSP4000	PSP4000-H	PSP4000-H /C	PSP4000-H /C /T
Part No. 230V Part No. 115V	40S1000 40S1000a	40S1005 40S1005a	40S1015 40S1015a
Sample temperature	max. 600 °C *standard		
Sample pressure	max. 1 bar		
Ambient temperature	-20°C to +60°C		
Filtration chamber volume	40 cm^3		
Filter element	S-2K ceramic, 2 µm		
Probe temperature	adjustable between 100 to 180°C, pre-set at works to 180°C		
Ready for operation	After approximately 30 minutes		
Gas inlet	Basic connection G 3/8"i, probe tube or adapters optional		
Gas outlet	1/8" NPT + tube connector 6 mm (8 mm optional) and pipe clamp for attachment of heated sample line		
Electrical power supply	220-240V 50/60Hz, 200 W or 115V 60Hz		
Electrical connection	Plug and socket connector 7 pin with 4 meter connection cable		
Electrical equipment standard	EN 61010, EN 60335-1		
System of protection	IP40 EN 60529		
Material	Stainless steel 316Ti, ceramic, FPM		
Weight	3 kg		
Calibration gas connection for SS-tube/Plastic hose ø 6 mm	no	yes	yes
Temperature measurement with Thermocouple sensor FeCuNi, length 600 mm with 4 m connection cable and standard plug.	no	no	yes

Product specifications of PSP 4000-H gas sample probe The variant used in combustion trials is the PSP4000 H/C. (Courtesy of M & C Tech Group)

Pulverised Fuel feed system – Venturi assembly

UK Headquarters
Parker Hannifin Ltd.
Automation Group
Parker KV Division
Presley Way, Crownhill
Milton Keynes
Buckinghamshire
MK8 0HB, UK

Materials

Vacuum Pump body:	Anodised aluminium (standard) Stainless steel and

Dimensions and Performance Data

units mm

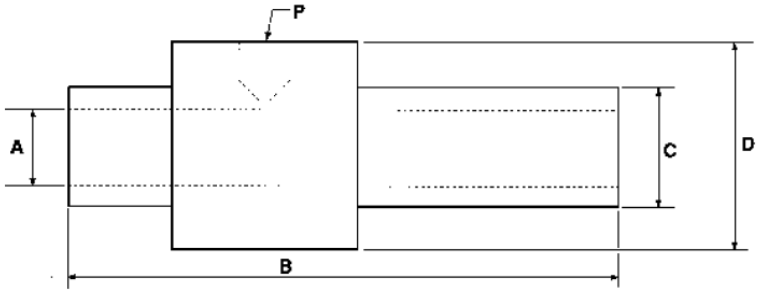

Part number	ØA	B	ØC	ØD	P
KVPDF1-3	3.7	88.9	18.8	31.5	G1/8
KVPDF2-3	6.4	88.9	18.8	31.5	G1/8
KVPDF3-3	9.5	88.9	18.8	31.5	G1/8
KVPDF3-6	9.5	88.9	18.8	31.5	G1/8
KVPDF5-3	12.7	139.7	25.2	37.6	G1/4
KVPDF5-6	12.7	139.7	25.2	37.6	G1/4
KVPDF7-3	19.1	190.5	31.5	50.3	G3/8
KVPDF7-6	19.1	190.5	31.5	50.3	G3/8
KVPDF10-3	25.4	190.5	37.6	56.7	G3/8
KVPDF10-6	25.4	190.5	37.6	56.7	G3/8
KVPDF15-3	38.1	190.5	50.3	69.4	G3/8
KVPDF15-6	38.1	190.5	50.3	69.4	G3/8
KVPDF20-3	50.8	190.5	63.0	82.0	G3/8
KVPDF20-6	50.8	190.5	63.0	82.0	G3/8

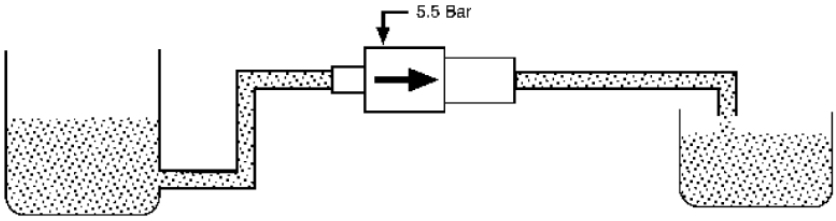

Part Number	Vacuum level (-mbar)	Vacuum flow nl/min	Compressed air consumption (nl/min) @ input pressure of 5.5 bar
KVPDF1-3	271	85	57
KVPDF2-3	271	283	170
KVPDF3-3	152	425	170
KVPDF3-6	203	510	283
KVPDF5-3	102	708	255
KVPDF5-6	339	850	680
KVPDF7-3	146	1416	680
KVPDF7-6	271	1699	1360
KVPDF10-3	102	2124	680
KVPDF10-6	196	2690	1350
KVPDF15-3	44	4672	680
KVPDF15-6	85	5663	1350
KVPDF20-3	27	6796	680
KVPDF20-6	51	8495	1350
Units with -6 suffix create higher vacuum levels than -3, but use the same internal diameters			

Deposition Probe – Main body – Drawing A1

Dims in mm's – Material: 2.25Cr (Energy Audit Services)

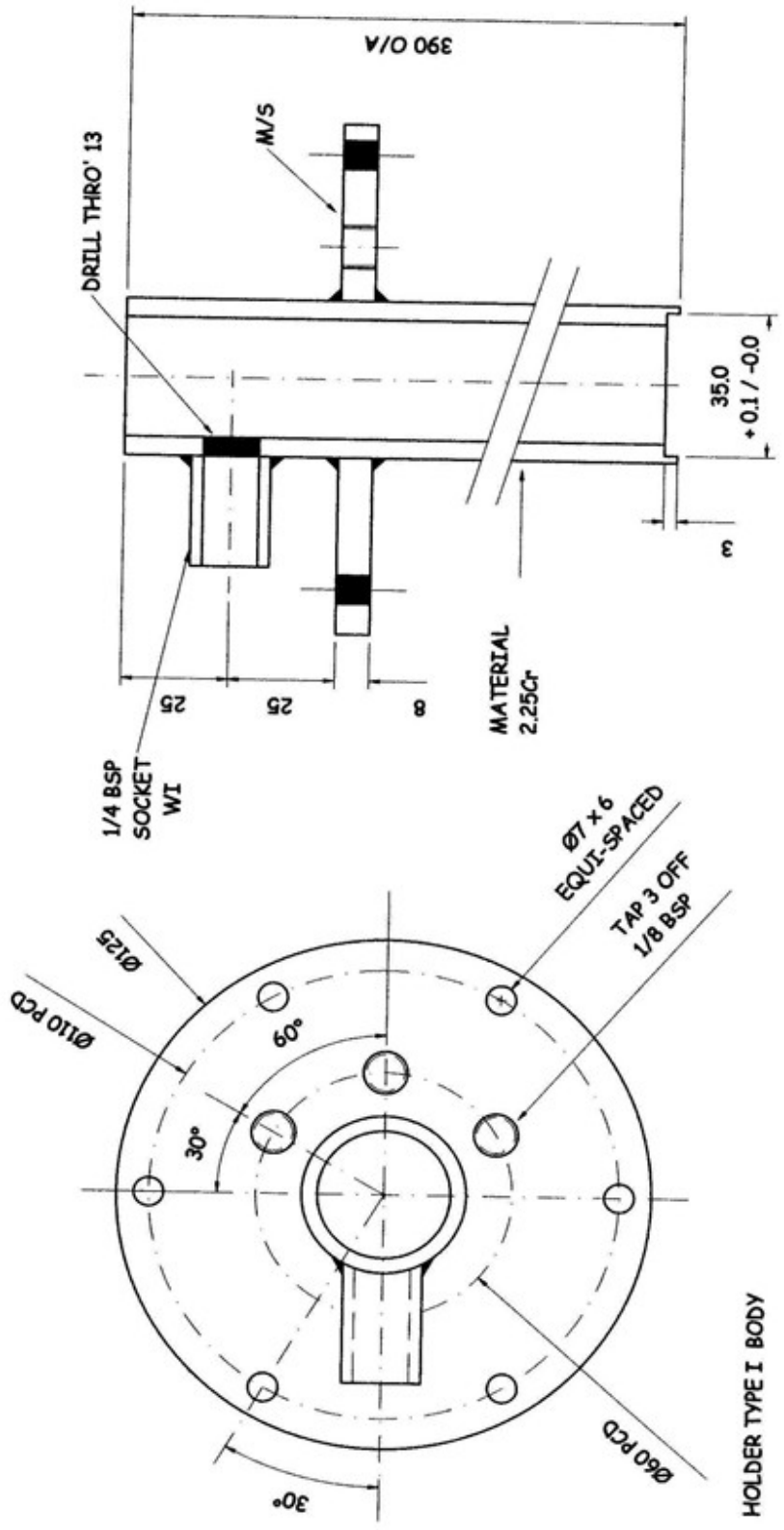

Deposition Probe – Inner tube – Drawing A2

Dims in mm's – Material: 316 s/s (Energy Audit Services)

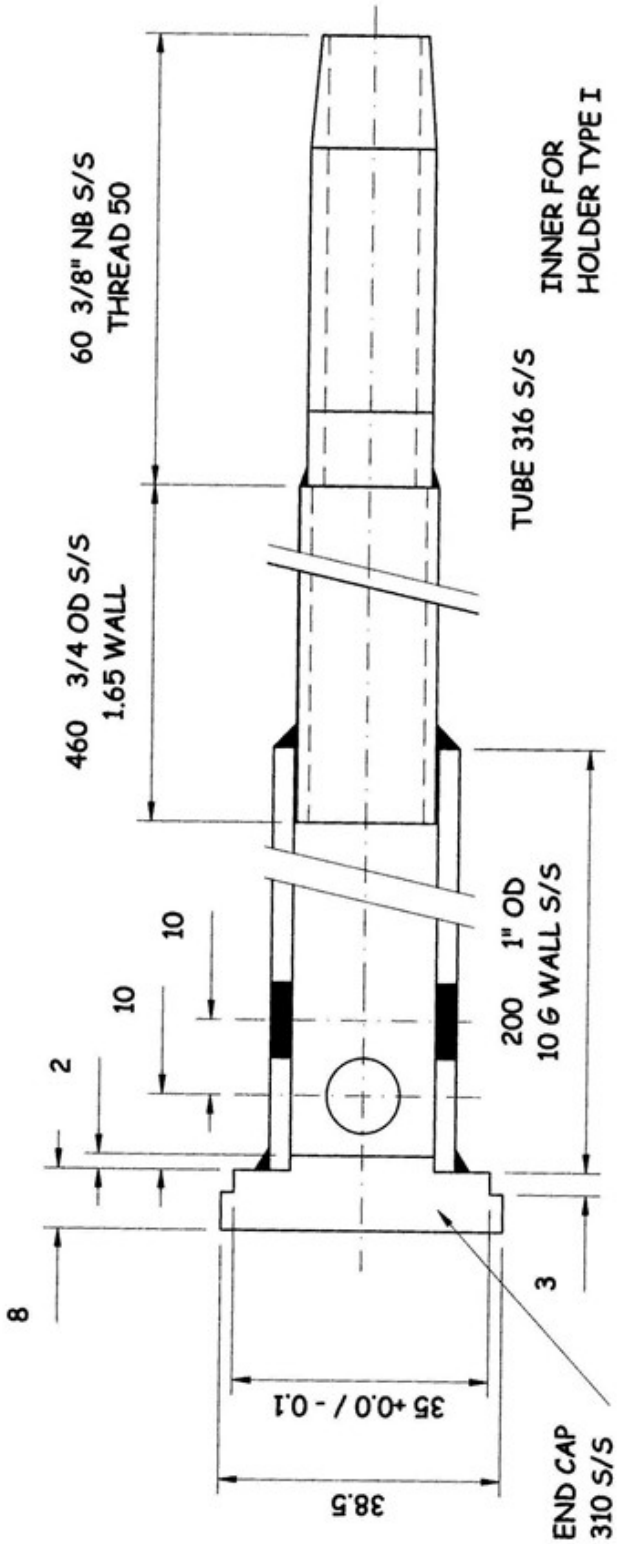

Deposition Probe – End Cap – Drawing A3

Dims in mm's – Material: 310 s/s (Energy Audit Services)

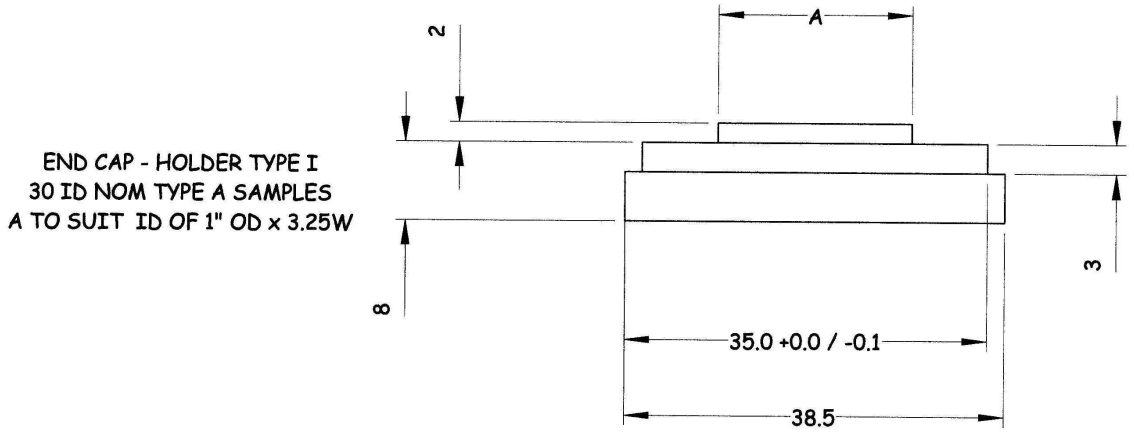

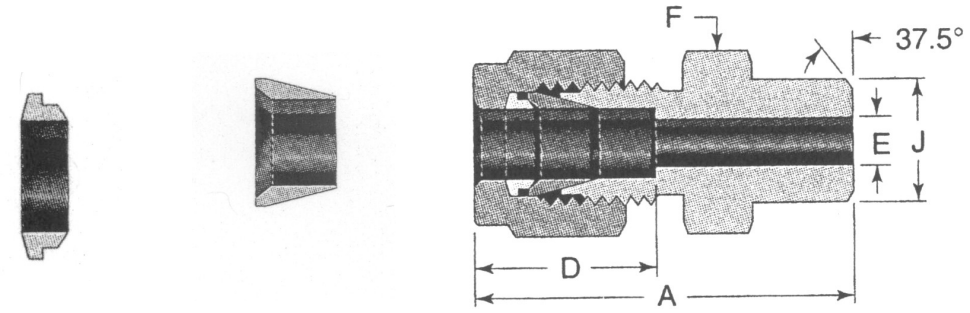

Fuel compositions & analysis

(Details extracted from 'Phyllis' database)

'El Cerrejon' species – South America

Phyllis ID-number 1273

Reference: E. Kurkela: Formation and removal of biomass-derived contaminants in fluidized-bed gasification processes, VTT Publications 287, Espoo, Finland, VTT, 47 p. (1996).

Proximate analysis (wt. %)

	dry	daf	Ar
Ash	12.1		11.3
Water			7
Volatiles	34.7	39.5	32.3

Calorific value (kJ/kg)

	dry	daf	ar
HHV	29469	33526	27406
LHV	28400	32309	26241
HHV_{Milne}	29691	33778	27612

Ultimate analysis (wt. %)

	dry	daf	ar
C	71.9	81.8	66.9
H	4.9	5.6	4.6
O	8.6	9.8	8
N	1.5	1.71	1.4
S	1	1.14	0.93
Cl	0.013	0.015	0.012
F	-	-	-
Br	-	-	-
Total:	100	100	100

Elemental analysis (mg/kg sample (dry))

Al	ND	**Fe**	ND	Msr	**Pb**	-	ND
As	ND	**Hg**	-	ND	**Sb**	-	ND
B	ND	**K**	2600	Msr	**Se**	-	ND
Ba	ND	**Mg**	8	Cal	**Si**	-	ND
Ca	ND	**Mn**	1.4	Msr	**Sn**	-	ND
Cd	ND	**Mo**	-	ND	**Sr**	-	ND
Co	ND	**Na**	446	Msr	**Te**	-	ND
Cr	ND	**Ni**	-	ND	**Ti**	-	ND
Cu	ND	**P**	-	ND	**V**	-	ND
					Zn	-	ND

'Daw Mill' species – United Kingdom of Great Britain

(Details extracted from 'Phyllis' database)

Phyllis ID-number 1374
Reference: ECN laboratories.
Remarks:

Proximate analysis (wt. %)

dry	daf	ar

Ash	12.8		12.4
Water			3.2
Volatiles	28.5	32.7	27.6

Calorific value (kJ/kg)

	dry	**daf**	**ar**
HHV	27156	31142	26287
LHV	26218	30066	25301
HHV_{Milne}	27823	31908	26933

Ultimate analysis (wt. %)

	dry	**daf**	**ar**	
C	69.3	79.5	67.1	Msr
H	4.3	4.9	4.2	Msr
O	10.7	12.2	10.3	Msr
N	1.2	1.38	1.16	Msr
S	1.48	1.7	1.43	Msr
Cl	0.241	0.276	0.233	Msr
F	0.016	0.018	0.015	Msr
Br	-	-	-	ND
Total:	100	100	100	

Elemental analysis (mg/kg sample (dry))

Al	15800	Msr	**Fe**	6900	Msr	**Pb**	7.4	Msr
As	11	Msr	**Hg**	-	ND	**Sb**	3	Lim
B	47	Msr	**K**	2260	Msr	**Se**	2	Lim
Ba	290	Msr	**Mg**	1500	Msr	**Si**	17900	Msr
Ca	5700	Msr	**Mn**	210	Msr	**Sn**	1.2	Msr
Cd	0.6	Lim	**Mo**	1.5	Msr	**Sr**	95	Msr
Co	4.5	Msr	**Na**	810	Msr	**Te**	-	ND
Cr	18	Msr	**Ni**	17	Msr	**Ti**	450	Msr
Cu	17	Msr	**P**	330	Msr	**V**	27	Msr
						Zn	14	Msr

-

Cereal Co-Product

(Details supplied by EoN)

Moisture, % Total	8.1
Ash: % AR	4.2
Volatile matter; % AR	70.8
CV, kJ/kg; AR Gross	17610
AR Net	16340
Sulphur; % AR	0.16
Chlorine; % AR	0.17
Volatile matter; % DAF	80.7
CV, kJ/kg DAF Gross	20080
Ash: SiO_2	44.32
Al_2O_3	2.79
Fe_2O_3	2.47
CaO	7.78
MgO	3.96
K_2O	24.72
Na_2O	0.36
TiO_2	0.12
BaO	0.05
Mn_3O_4	0.10
P_2O_5	12.04

Miscanthus

(Details supplied by EoN)

Moisture, % Total	10.8
Ash: % AR	4.6
Volatile matter; % AR	71.2
CV, kJ/kg; AR Gross	17270
AR Net	15914
Sulphur; % AR	0.11
Chlorine; % AR	0.09
Volatile matter; % DAF	84.2
CV, kJ/kg DAF Gross	20414
Ash: SiO_2	55.85
Al_2O_3	3.14
Fe_2O_3	2.12
CaO	8.77
MgO	3.76
K_2O	12.69
Na_2O	0.50
TiO_2	0.19
BaO	0.03
Mn_3O_4	0.15
P_2O_5	12.30

Elemental ash analysis (Probe 2)

Elemental ash analysis (ESEM) for Pure Fuels and Daw Mill + CCP Test Series (wt %)

Element → / Test ↓	O	Na	Mg	Al	Si	P	S	K	Ca	Ti	Mn	Fe	Cu	Pb	Pt	Cl
DM 100%	46.6	0.9	0.8	12.9	13.7	0.4	3.2	2.4	5.5	0.9	0.2	8.8				
DM 20% CCP	42.0	0.6	0.8	10.4	11.4	0.5	1.6	3.7	3.3	0.7	0.1	5.4	0.2			
DM 40% CCP	48.9	0.4	1.0	5.6	17.8	1.7	3.3	8.0	4.5	0.5		3.2	0.4			
DM 60% CCP	47.3	0.3	1.2	5.0	15.0	2.0	4.0	10.5	7.0	0.4		4.1			1.0	
DM 80% CCP	44.7	0.3	1.2	2.9	13.7	2.5	5.5	15.0	6.2	0.3	0.1	2.7	0.4	0.6		
100 % CCP	44.4	0.7	1.5	0.7	13.8	3.9	2.9	16.8	7.5			0.5			1.4	1.4

Ash weights taken from Deposition probes - all experiments

Experiment - Pure fuels (weight %)	Top	Probe 1 Side	(mg) Base		Probe 2 T	Probe 2 S	(mg) Base		Probe 3 T	Probe 3 S	(mg) Base	Total(mg)
El Cerrejon 100%	0.2822	0.0613			0.1966	0.0617			0.1975	0.2413		**1.0406**
Daw Mill 100%	1.5297	0.1172			1.2816	0.1412	0.0089		1.2776	0.1827	0.0598	**4.5987**
CCP 100%	2.1340	0.0293			1.3407	0.0237			1.3278	0.0061		**4.8616**
Miscanthus 100%	0.3309				0.4025				0.3255			**1.0589**
Fuel blends												
Daw Mill + 20% CCP	1.4908	0.2014			1.7309	0.1109	0.0433		2.8232	0.2156	0.1416	**6.7577**
Daw Mill + 40% CCP	1.2175	0.1366			1.1771	0.0682	0.0288		1.7228	0.0886	0.0315	**4.4711**
Daw Mill + 60% CCP	0.9866	0.0551	0.0627		0.8276	0.1218	0.0513		1.0468	0.0952	0.0873	**3.3345**
Daw Mill + 80% CCP	0.6648	0.0040	0.0269		0.4088	0.0106	0.0168		0.5263	0.0632	0.0523	**1.7737**

No visual deposit taken

Ash samples taken from : Top, side and base of deposition area

Weighing equipment : 'Sartorius' CP225D
Serial no: 14908304
(Calibrated to ISO 9001 standard)

Total elemental analysis for Pure fuel - CCP

Test		C	O	Na	Mg	Al	Si	P	S	Cl	K	Ca	Ti	Mn	Fe	Ni	W	Pb	Pt
Cereal	Probe 3 - side	14.8	26.9	1.03	0.32	0.67	1.71	1.26	7.53	13.1	29.8	1.65			0.33				
Co-Product -100%	Probe 3 - underside																		
	Probe 3 - top	1.84	44.8	0.8	1.54	0.82	15.3	3.58	2.3	1.56	15.3	8.88	0.11	0.14	1.05	0.24	1.36	0.52	
	Probe 2 - side	19.3	31.2	0.59	0.63	0.54	3.35	1.48	6.85	6.42	23.2	2.73			0.4			0.91	2.36
	Probe 2 - top	4.64	44.4	0.65	1.54	0.67	13.8	3.87	2.87	1.39	16.8	7.51			0.49				1.38
	Probe 2 - underside																		
	Probe 1 - side																		
	Probe 1 - top	4.24	47.3	0.61	1.16	0.4	17.6	2.77	1.92	0.55	16.6	5.99			0.84				

Total elemental analysis for Daw Mill + CCP test series

Test	Element (%)	C	O	Na	Mg	Al	Si	P	S	K	Ca	Ti	Mn	Fe	Cu	Pb	Cr	Pt	Zn	Cl
Daw Mill	Probe 3 - side	20.64	45.79	0.81	0.73	10.58	10.91	0.28	1.31	2.42	1.89	0.59		3.69	0.36					
100%	Probe 3 - underside	9.55	45.87	0.77	0.92	13.38	13.52	0.26	1.43	2.97	3.37	0.92		6.39	0.64					
	Probe 3 - top	3.68	47.19	0.58	0.81	13.25	15.19	0.40	2.08	1.99	4.66	0.95	0.19	8.60	0.42					
	Probe 2 - side	7.06	46.48	0.93	0.93	12.75	13.29	0.29	2.56	5.41	2.97	0.86		5.61		0.86				
	Probe 2 - top	3.76	46.56	0.89	0.80	12.86	13.67	0.41	3.18	2.40	5.52	0.92	0.21	8.83						
	Probe 2 - underside	14.29	45.41	0.68	0.77	10.78	11.18	0.26	2.94	6.31	2.20	0.70		4.48						
	Probe 1 - side	2.06	46.49	1.06	0.72	11.71	12.63	0.34	4.65	10.97	2.81	0.83		5.73						
	Probe 1 - top	3.47	47.12	0.69	0.82	13.77	13.99	0.51	2.40	2.62	4.95	0.99		8.65						
Daw Mill	Probe 3 - side		46.65	1.10	1.47	4.09	12.15	3.69	1.79	4.38	18.25	0.49		5.56			0.38			
20% CCP	Probe 3 - top	10.98	46.84	0.37	0.89	6.77	15.60	1.03	2.33	4.22	4.76	0.46		4.79	0.43			0.53		
(wt %)	Probe 3 - underside	6.19	44.91	0.91	0.95	11.50	12.83	0.66	3.39	7.38	3.33	0.79		5.87	0.55	0.73				
	Probe 2 - side	3.47	45.69	1.13	0.84	10.46	11.46	0.64	5.05	9.71	3.90	0.76		5.64	0.47	0.78				
	Probe 2 - top	19.26	42.04	0.64	0.83	10.42	11.39	0.51	1.58	3.66	3.29	0.66	0.13	5.37	0.22					
	Probe 2- underside	3.15	46.28	0.75	0.95	12.44	13.54	0.70	3.77	8.44	3.19	0.77	0.22	5.40					0.40	
	Probe 1 - side	4.91	45.57	1.58	0.73	10.08	12.00	0.68	4.53	8.61	3.80	0.76	0.22	6.54						
Daw Mill	Probe 3 - side	10.48	43.68	0.89	0.80	9.21	10.17	0.61	4.27	10.85	2.59	0.65		4.48	0.52	0.81				
40% CCP	Probe 3 - top	3.31	47.04	0.47	1.10	7.37	16.97	1.96	2.73	8.01	4.82	0.55	0.12	5.30	0.25					
(wt%)	Probe 3 - underside	15.39	43.04	0.63	0.91	9.41	11.60	0.83	2.67	7.12	3.15	0.68		4.58						
	Probe 2 - side	3.49	45.68	0.98	0.91	9.55	11.40	0.85	5.71	12.44	3.10	0.62		5.26						
	Probe 2 - top	4.79	48.93	0.42	1.03	5.61	17.84	1.71	3.28	7.95	4.46	0.48		3.15	0.35					
	Probe 2- underside	30.65	41.34	0.66	0.43	6.28	6.34	0.60	2.59	6.40	1.28	0.37		2.40	0.66					
	Probe 1 - side	5.31	45.40	1.77	0.79	8.84	10.44	0.87	5.53	12.14	2.65	0.63		4.74		0.87				
	Probe 1 - top	3.44	47.25	0.47	1.13	5.89	17.30	1.93	3.04	8.22	5.99	0.47	0.13	4.38	0.30		0.08			
Daw Mill	Probe 3 - side	5.98	39.41	1.52	0.48	4.91	5.78	1.14	9.80	25.14	2.04	0.34		2.44		1.03				
60% CCP	Probe 3 - top	3.38	46.98	0.35	1.03	5.43	16.52	1.75	3.55	10.02	5.42	0.40	0.14	3.48	0.25	0.44		0.86		
(wt%)	Probe 3 - underside	10.73	42.75	0.69	0.83	7.38	10.23	1.18	4.64	13.79	3.33	0.57		3.90						
	Probe 2 - side	4.82	41.09	1.93	0.51	5.31	6.77	1.16	9.03	21.68	3.44	0.38		3.02		0.86				
	Probe 2 - top	2.35	47.27	0.33	1.20	5.00	14.97	2.01	3.98	10.52	6.97	0.37		4.07				0.97		
	Probe 2- underside	22.6	38.1	1.43	0.49	3.93	5.3	0.94	6.74	14.9	2.72	0.3	0.18	2.35						
	Probe 1 - side	3.89	41.6	1.19	0.53	4.87	6.19	1.01	9.23	23.3	2.94	0.32		3.38		1.57				
	Probe 1 - top	3.02	47.7	0.33	1.1	4.95	18.9	1.96	2.54	9.68	5.29	0.37	0.13	2.86	0.42			0.81		
	Probe 1 - underside	19.2	39.7	1.06	0.49	4.54	5.92	0.88	6.74	15.4	2.21	0.28		2.29	0.39	0.97				
Daw Mill	Probe 3 - side	6.04	31.9	0.95	0.31	2.4	3.34	1.14	9.4	32.1				1.33		3.23				7.92
80% CCP	Probe 3 - top	6.08	44.6	0.33	0.99	2.97	14.4	2.03	4.83	14.5	4.93	0.22		2.4	0.32	0.42		1.04		
(wt%)	Probe 3 - underside	13.1	38.4	0.59	0.68	4.61	8.29	1.53	5.27	18.1	2.86	0.35		2.37		1		0.82		2.11
	Probe 2 - side	5.19	37.5	1.33	0.41	2.28	3.76	1.18	11.9	30.1	3.15	0.22		1.67		1.35				
	Probe 2 - top	4.05	44.7	0.33	1.17	2.9	13.7	2.46	5.49	15	6.24	0.25	0.11	2.65	0.36	0.64				
	Probe 2- underside	12.3	35.5	1.27	0.28	2.03	2.85	0.87	12.2	29.3				0.88	0.44	1.51				0.6
	Probe 1 - side	8.68	35.9	1.09	0.33	2.97	3.42	1.22	11.7	28.6	3.4			1.55		1.15				
	Probe 1 - top	2.7	45.9	0.42	1.29	3.01	15.3	2.76	4.34	14.1	5.83	0.24	0.17	2.33		0.36		1.24		
	Probe 1 - underside	25.4	34.4	2.11	0.3	1.83	2.32	0.83	9.53	18.9	2.42	0.14		0.87		1.02				

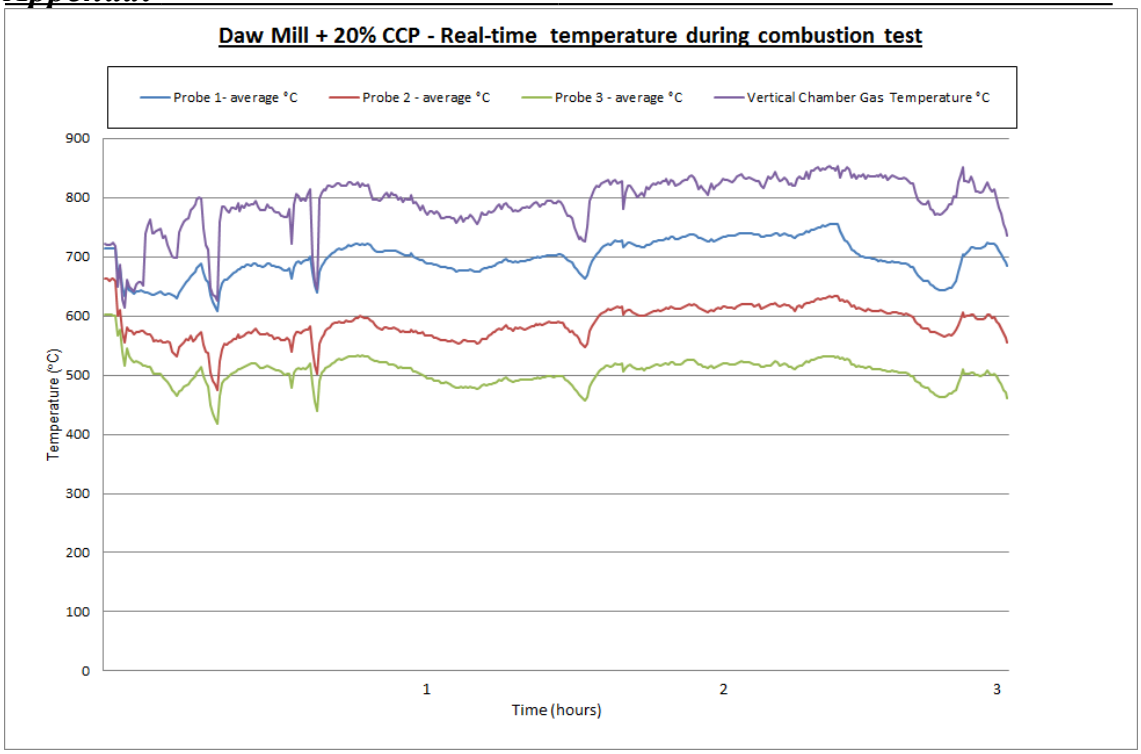
Daw Mill + 20% CCP - Real-time temperature during combustion test
Probe 1- average °C
Probe 2 - average °C
Probe 3 - average °C
Vertical Chamber Gas Temperature °C
Temperature (°C)
900
800
700
600
500
400
300
200
100
0
1
2
3
Time (hours)

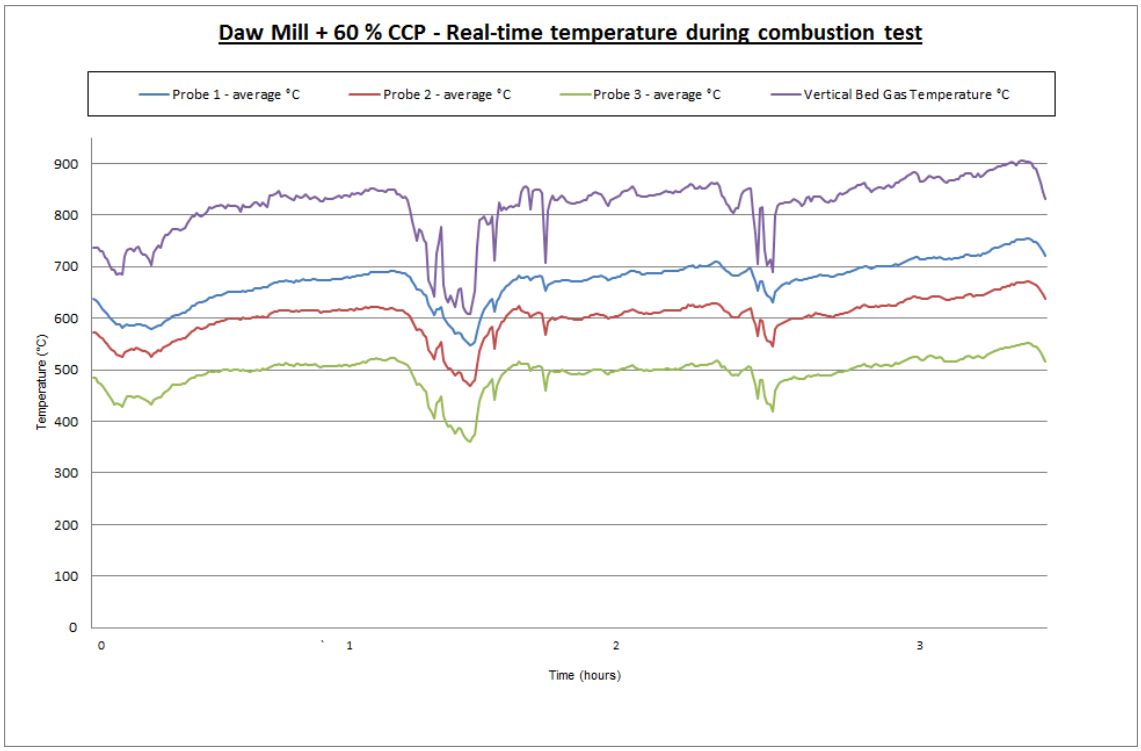
Daw Mill + 60 % CCP - Real-time temperature during combustion test
Probe 1 - average °C
Probe 2 - average °C
Probe 3 - average °C
Vertical Bed Gas Temperature °C
Temperature (°C)
900
800
700
600
500
400
300
200
100
0
0
1
2
3
Time (hours)

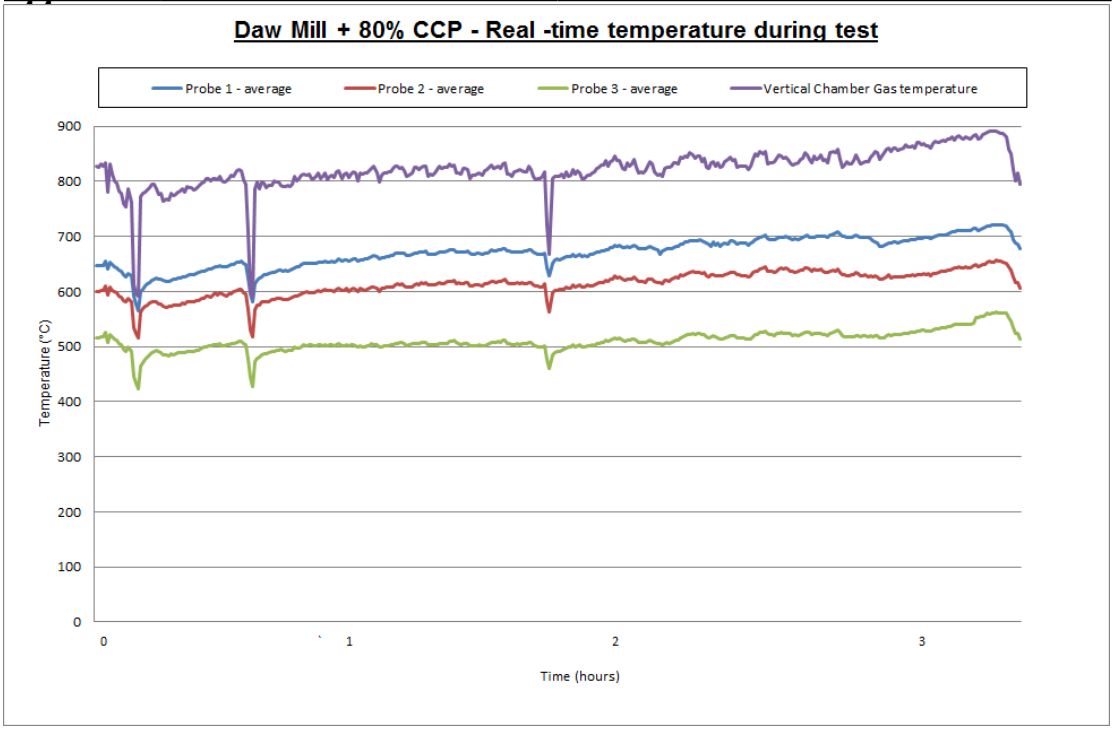
Daw Mill + 80% CCP - Real -time temperature during test
Probe 1 - average
Probe 2 - average
Probe 3 - average
Vertical Chamber Gas temperature
900
800
700
600
500
400
300
200
100
0
Temperature (°C)
0
1
2
3
Time (hours)

Appendix